

INCA333

Version 3.X

Manual

Gaithersburg, MD
2014

Content

1. List of Acronyms.....	4
2. Introduction	5
3. Theory basics	7
3.1. Definitions of Principal Quantities	7
3.2. Cavity Geometry	10
3.3. Viewing Conditions	11
3.4. Methods for Calculation of Effective Emissivities	12
3.5. Optical Properties of Materials for Blackbody Cavities	13
3.6. Three-Component (3C) BRDF Model	15
3.7. Fitting Parameters of 3C BRDF Model to the In-Plane BRDFs	20
3.8. Spectral DHR Splitting	22
3.9. Algorithm for Calculating Radiation Characteristics of Blackbody Radiators.....	24
4. Key Features of INCA333	28
5. Structure of INCA333	29
6. Units of Measurement.....	33
7. Working with INCA333.....	34
7.1. Working with INCA333 Databases.....	34
7.2. Working with INCA333 2D Graphs.....	36
7.3. Working with INCA333 3D Graphs.....	38
7.4. Activating INCA333. Evaluation vs. Full-Functioned Version	43
8. The BRDF Model Builder	46
8.1. Working with Monochromatic BRDF Model.....	46
8.2. Making the Model Wavelength-Dependent.....	47
8.3. BRDF Plotting	49
8.4. DHR Calculation	52
9. The FITTING Database.....	54
9.1. BRDF Fitting.....	54
9.2. Spectral DHR Splitting	59
9.3. BRDF Fitting and SDHR Splitting Report	61
10. The MATERIALS Database	62
11. The DATASETS Database	64
11.1. Creating New Dataset	64
11.2. Defining Cavity	65
11.3. Entering Temperature Distribution	66
11.4. Entering Viewing Conditions.....	69
11.5. Targeting	71
11.6. Entering Wavelengths and Performing Spectral Interpolation	72
12. Monte Carlo Calculations.....	75
13. The RESULTS Database	77
13.1. Viewing Results	77
13.2. Plotting Graphs	78

13.3. MCRT Calculation Report	79
14. References	80
15. Appendix. INCA333 Software License Agreement.....	85

1. List of Acronyms

Acronyms used in this Manual are shown in Table 1 below.

Table 1. Acronyms used in this Manual.

2D	Two-Dimensional
3C	Three-Component (BRDF model)
3D	Three-Dimensional
BB	Blackbody
BRDF	Bidirectional Reflectance Distribution Function
CPU	Central Processing Unit
DHR	Directional-Hemispherical Reflectance
EE	Effective Emissivity
FOV	Field-of-View
GB	Gigabyte
GUI	Graphical User Interface
K	Kelvin (<i>the basic SI unit of thermodynamic temperature</i>)
MB	Megabyte
MCRT	Monte Carlo Ray Tracing
MS	Microsoft
OS	Operating System
PC	Personal Computer
PR	Partial Reflectance
PSO	Particle Swarm Optimization
RAM	Random-Access Memory
RT	Radiance Temperature
SDHR	Spectral Directional-Hemispherical Reflectance
SI	International System of Units (<i>from French: Le Système international d'unités</i>)
SP3	Service Pack 3
SPR	Spectral Partial Reflectance
VC	Viewing Conditions

2. Introduction

The program INCA333 working under OS MS Windows® XP (with the SP3), Vista, 7, and 8 (in compatibility mode) is intended for numerical modeling of spectral radiation characteristics of isothermal and non-isothermal blackbody cylindrical cavities with inclined (tilted, slant) flat bottom and uses the three-component (3C) BRDF model [1, 2].

A cylinder with an inclined flat bottom and a flat annular diaphragm is the cavity shape which is widely used in optical radiometry and radiation thermometry as blackbody calibration sources [3–8] on parity with cylindrical cavity having outward or inward conical bottom. Both conical and tilted flat bottoms serve to prevent decrease in effective emissivity if the cavity internal surface has significant specular reflection that usually becomes predominant in the IR spectral range. However, a cylindrical cavity with a tilted flat bottom has an inarguable advantage in the simplicity of cavity fabrication and treatment of its internal surface. The European Standard [9] prescribes, among others, this shape for blackbody radiation sources intended for calibration of clinical ear thermometers.

INCA333 is applicable to design optimization, performance assessment, and metrological certification of blackbodies (BBs) used as standard reference sources in radiation thermometry (pyrometry), radiometry, photometry, for of optical sensors calibrations (e.g., in remote sensing), etc. According to the Kirchhoff law and the optical reciprocity principle, results obtained for effective emissivity of isothermal cavities can be also used for effective absorptivity of cavity detectors (including cryogenic) of optical radiation [10–12].

The program is based on the proprietary algorithm of the Monte Carlo ray tracing method (MCRT) implemented for a cylindrical cavity with an inclined flat bottom and a flat annular diaphragm, isothermal and nonisothermal, with arbitrary axial temperature distributions. The algorithm allows modeling the most common viewing conditions of such cavities. The different 3C BRDF models can be used for optical properties of each surface forming the cavity.

INCA333 allows employing experimentally determined optical properties of cavity wall. Initial experimental data are

- 1) BRDF measured in the plane of incidence at one wavelength λ_0 for up to 6 incidence angles. Measurements of BRDF require special equipment (see Refs. [13–31]).
- 2) Spectral directional-hemispherical reflectance (SDHR) measured at one incidence angle within a wavelength range $[\lambda_1, \lambda_2]$ which includes the wavelength λ_0 . Usually, these measurements can be conducted using conventional reflectometric accessories such as integrating spheres (see, e.g., [32–35]).

If experimental data are unavailable, INCA333 allows building *a priori* reflection models to perform parametric studies.

The minimal requirements for hardware and software are the following:

- CPU frequency 1.66 GHz
- Screen resolution 1600×1024
- RAM 3 GB
- Hard disk space 15 MB
- Video card 1 GB video RAM; OpenGL 2 compatible
- OS MS Windows[®] XP (with the SP3), Vista, 7, and 8 (in compatibility mode)

3. Theory basics

3.1. Definitions of Principal Quantities

A source of optical radiation whose radiation characteristics can be calculated on the basis of fundamental physical laws makes possible calibration of radiometers, spectroradiometers, radiation thermometers, etc. From theoretical point of view, a perfect blackbody (BB) is the most suitable object for this purpose. If its thermodynamic temperature is known, spectral characteristics of BB radiation at any wavelength can be computed with the help of Planck's law. However, a perfect BB is a physical abstraction that does not exist in real world. The perfect BB conditions are approximately realized inside an isothermal cavity with opaque walls. The radiation escaping cavity through a tiny opening imitates BB radiation very closely. In order to employ a BB as a standard reference source for optical radiometry and radiation thermometry, it is necessary to know how large are differences between radiation characteristics of a cavity and those of a perfect blackbody due to cavity geometrical parameters, optical properties of the wall material, and actual temperatures of cavity walls.

There are two different objects referred in literature as "blackbody":

1. A theoretical object that completely absorbs all radiant energy incident upon it. A BB emits maximal amount of radiant energy at given wavelength and given temperature in comparison with all other radiating bodies.
2. An artificial source of optical radiation designed to simulate characteristics of a perfect BB and used as a reference radiation source of calculable radiation characteristics.

In order to differentiate them, we shall use the term "perfect blackbody" for a theoretical object, keeping the term "blackbody" for an artificial source.

Quantitative measure of the difference in radiation characteristics between an artificial BB and a perfect one is the *effective emissivity* (EE). The qualifier "effective" is used due to the effect produced by multiple reflections. Unlike a flat sample, outgoing radiation of an element of a cavity wall consists not only of its own thermal radiation, but also of radiation falling from other surface elements and reflected by the element under consideration. The EE is determined by the cavity geometry, optical properties of the cavity walls, viewing conditions (VC), i.e., geometry of collecting the cavity radiation, and the temperature distribution over the radiating surface.

Generally speaking, EE is the ratio of a radiometric quantity (usually, radiance or spectral radiance) that characterizes a BB at a certain temperature to the same quantity of a perfect BB with the same temperature. However, real-world cavities are always nonisothermal. Temperature non-uniformity can change cavity radiation characteristics significantly. To avoid ambiguity in temperature assigned to the perfect blackbody in the EE definition, the *reference temperature* T_{ref} has to be introduced and assigned to the perfect BB. T_{ref} itself has no specific physical meaning; its choice, in general, is arbitrary.

Depending on the T_{ref} choice, the spectral EE of a nonisothermal BB can take any positive value, i.e., be greater than one. The spectral radiance of a BB do not change their values at any choice of T_{ref} . In practice, the temperature measured by a contact temperature sensor is commonly used for T_{ref} to keep EE of the nonisothermal BB comparable with those for the isothermal case. EE of a nonisothermal cavity depends on the wavelength even if the cavity internal surface has wavelength-independent optical characteristics.

The quantities characterizing BB radiation sources are usually defined for the non-refracting, non-absorbing, non-scattering, and non-emitting environment (i.e., vacuum at 0 K). It is also supposed that optical properties of cavity walls do not depend on temperature. Effect of background radiation will be considered in this Section later.

The primary characteristic of an artificial BB is the spectral local directional EE ε_e . It is defined by the following equation:

$$\varepsilon_e(\lambda, \xi, \omega, T_{ref}) = \frac{L_\lambda(\lambda, \xi, \omega)}{L_{\lambda,bb}(\lambda, T_{ref})}, \quad (1)$$

where L_λ is spectral radiance (in $\text{W} \cdot \text{m}^{-3} \cdot \text{sr}^{-1}$) of the radiation coming from a point on BB wall at a particular wavelength λ , with coordinates specified by the vector ξ , and the direction in which the radiation is emitted specified by the vector ω ; $L_{\lambda,bb}$ is spectral radiance of a perfect BB at a reference temperature T_{ref} and the same wavelength λ .

The numerator in Eq. (1) refers to the sum of own thermal radiation of the surface element and radiation that is falling from all possible directions and is reflected by this element in the direction considered. Denominator in Eq. (1) is expressed by the Planck law:

$$L_{\lambda,bb}(\lambda, T_{ref}) = \frac{c_1}{\pi \cdot \lambda^5 \left[\exp\left(\frac{c_2}{\lambda \cdot T_{ref}}\right) - 1 \right]}, \quad (2)$$

where $c_1 = 3.74177153 \cdot 10^{-16} \text{ W} \cdot \text{m}^2$ and $c_2 = 1.4387770 \cdot 10^{-2} \text{ m} \cdot \text{K}$ are the 1st and 2nd radiation constants, respectively [36].

Integration of Eq. (1) over a hemispherical solid angle transforms the spectral local directional EE $\varepsilon_e(\lambda, \xi, \omega, T_{ref})$ to the spectral hemispherical EE $\varepsilon_{e,h}(\lambda, \xi, T_{ref})$. According to Lambert's law, spectral

radiance of the perfect BB does not depend on the angle of observation and can be expressed through the spectral exitance M_λ (surface density of the emitted radiant power):

$$L_{\lambda,bb}(\lambda, T) = \frac{1}{\pi} M_{\lambda,bb}(\lambda, T). \quad (3)$$

The spectral hemispherical EE is defined by the following equation:

$$\varepsilon_{e,h}(\lambda, \xi, T_{ref}) = \frac{M_\lambda(\lambda, \xi)}{M_{\lambda,bb}(\lambda, T_{ref})} = \frac{M_\lambda(\lambda, \xi)}{\pi L_{\lambda,bb}(\lambda, T_{ref})}, \quad (4)$$

Depending on particular viewing conditions used for various types of radiometers, radiation thermometers, etc., one can define appropriate types of effective emissivities by averaging local directional effective emissivity over a visible part of cavity's internal surface and an appropriate solid angle. Some most practically important types of effective emissivities and corresponding types of viewing conditions for a cavity with inclined bottom are considered in Section 3.3.

Definitions (1) and (4) have been developed for a non-radiating background environment. However, real environment may have temperature greater than 0 K. Thermal radiation from surrounding environment falls onto the aperture of a BB cavity and can irradiate detector after multiple reflections inside the cavity. The simplest case of isotropic radiation of a perfect BB with the background temperature T_{bg} is usually considered. The effect of background radiation is taken into account by the second term in the Eq. (5).

$$\varepsilon_e(\lambda, \xi, \omega, T_{ref}, T_{bg}) = \varepsilon_e(\lambda, \xi, \omega, T_{ref}) + [1 - \varepsilon_e(\lambda, \xi, \omega)] \frac{\exp\left(\frac{c_2}{\lambda T_{ref}}\right) - 1}{\exp\left(\frac{c_2}{\lambda T_{bg}}\right) - 1}, \quad (5)$$

where $\varepsilon_e(\lambda, \xi, \omega, T_{ref}, T_{bg})$ is spectral EE of a nonisothermal BB taking into account background radiation; $\varepsilon_e(\lambda, \xi, \omega, T_{ref})$ does not include this correction; $\varepsilon_e(\lambda, \xi, \omega)$ is spectral EE of an isothermal BB. Correction for the background radiation can be neglected if $T_{bg} \ll T_{ref}$.

Radiance temperature (RT) T_s is defined as temperature of a perfect BB, for which the spectral radiance at the given wavelength λ has the same value as for thermal radiator under consideration. RT is sometimes called *brightness temperature* in such areas as remote sensing, astrophysics, etc. The RT T_s is defined by the equation:

$$L_\lambda(\lambda, \xi, \omega) = L_{\lambda,bb}(\lambda, T_s). \quad (6)$$

For an artificial BB, the radiance temperature can be expressed through the spectral EE:

$$T_s(\lambda, \xi, \omega) = c_2 \left\{ \lambda \ln \left[1 + \frac{\exp\left(\frac{c_2}{\lambda T_{ref}}\right) - 1}{\varepsilon_e(\lambda, \xi, \omega, T_{ref})} \right] \right\}^{-1}. \quad (7)$$

Eqs. (6) and (7) are also written for zero background radiation. Note that the RT does not depend on T_{ref} but depends on wavelength and VC.

3.2. Cavity Geometry

A sketch for the cavity geometry INCA333 deals with is depicted in Fig. 1.

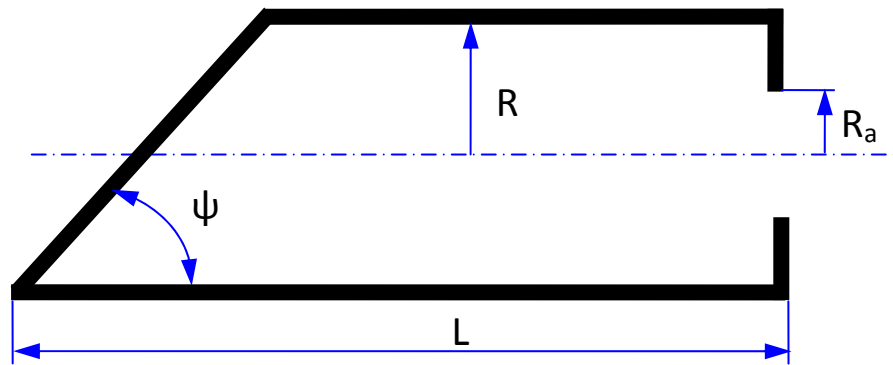


Fig. 1. A sketch for a cylindrical cavity with an inclined bottom.

Geometry of a cavity is completely determined by four parameters: cavity length L , radii of cylindrical part and aperture R and R_a , respectively, and the bottom inclination angle ψ . If $R_a = R$, the cavity is considered as a cavity without diaphragm. The following inequality must take place for the angle ψ :

$$\tan^{-1}\left(\frac{2R}{L}\right) \leq \psi \leq \frac{\pi}{2} . \quad (8)$$

INCA333 checks it and shows the warning message if this inequality is violated. Angle ψ is entered in degrees.

3.3. Viewing Conditions

Effective emissivities and radiance temperatures derived from them depend on *viewing conditions* (i.e., geometrical conditions of collecting the radiation by a measurement device). Effective emissivities can be obtained by averaging primary (local directional) effective emissivities over given spatial and angular domains. The types of viewing conditions which can be modeled in INCA333 are shown in Fig. 2.

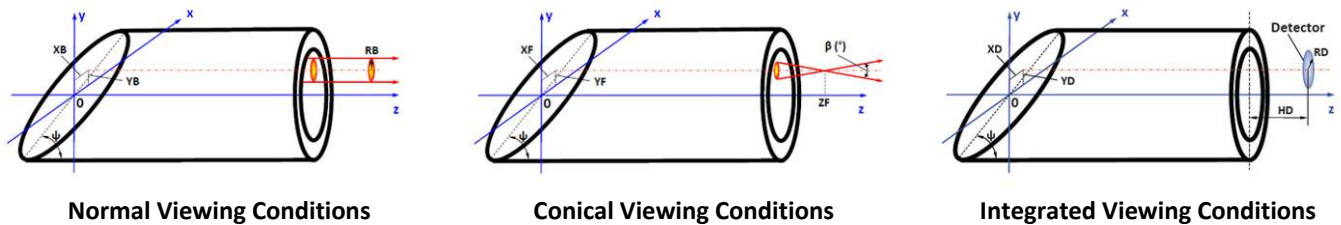


Fig. 2. Three types of viewing conditions modeled by INCA333.

Normal VC correspond to the collimated viewing beam parallel to the axis of the cylindrical part. Such viewing conditions are approximately implemented for the radiometric or pyrometric measurements with very long focal-length optics or for objective focused at infinity. Beam radius R_b can be determined by an external diaphragm. If $R_b \rightarrow 0$, the distribution of local normal EEs over the cavity aperture describes spatial uniformity of cavity radiation.

Conical VC reproduce the pinhole model mimicking the optical system that collects the cavity radiation onto the detector. For Conical viewing conditions, the beam axis is parallel the cavity axis. Case of convergent conical viewing beams is depicted in Fig. 2. To model divergent viewing beam, the apex of viewing cone must be placed behind the cavity bottom.

Integrated VC reproduce collecting of radiation emerging from a cavity by a circular detector (shown in blue) without optical system. Hemispherical VC (not shown in Fig. 2) can be considered as a special case of the Integrated VC when the RD coincides with the cavity aperture radius and $XD = YD = HD = 0$.

3.4. Methods for Calculation of Effective Emissivities

Direct measurements of EEs of BB radiation sources are often extremely difficult or even impossible. Sometimes, computational methods are the only way to determine EE. Moreover, calculation of EEs should be done at the blackbody design stage. Many computational methods have been developed to this end (see overviews [37-39]). These methods are based on the various physical and mathematical assumptions, have different areas of applicability and provide different degrees of accuracy. For *diffuse* cavities (i.e., cavities whose walls are considered as Lambertian emitters and reflectors) of simple shapes, series of papers by R. E. Bedford and C. K. Ma [40-42] established *de facto* standard technique for calculation of local hemispherical EEs which can be used subsequently to calculate EEs of diffuse cavities at any types of VC.

At present, the most comprehensive and flexible method for calculating radiation characteristics of blackbody radiators is the Monte Carlo method (see, e.g., Refs. [1, 2, 43-52]). It is based on the ray tracing algorithm that models radiation heat exchange among cavity walls and propagation of radiation from a blackbody to a radiation detector. The Monte Carlo method uses the ray (geometrical) optics approximation; such phenomena as polarization and diffraction are supposed to be negligible.

The vast majority of publications dealing with the Monte Carlo modeling of blackbodies concerns axisymmetric cavities. However, there are several works considered cylindrical cavities with an inclined bottom; for instance, the diffuse cavity with an inclined bottom is studied in Ref. [50], the specular-diffuse cavity is investigated in [51, 52].

EE calculations by the Monte Carlo method use the optical reciprocity principle and the technique of backward ray tracing. The history of a ray directed from the point of observation into a cavity is being traced until it leaves the cavity after reflections from the walls, or until its energy becomes less than the given value (flux threshold). The last point of reflection is considered as a birth point of a ray propagating in opposite direction. The spectral radiance acquired by a ray consists of the spectral radiance of the cavity wall's own thermal radiation (computed by Planck's law) at the point of the last reflection in the viewing direction and the sum of spectral radiances at the points of successive reflections computed along the ray trajectory and impaired by multiple reflections.

Averaging of spectral radiances over a large number n of ray trajectories allows estimating the EE and RT of a BB. Precision of the Monte Carlo calculations is proportional to $1/\sqrt{n}$. Usually, it is necessary to trace from 10^5 to 10^7 rays to achieve the EE accuracy of $10^{-4} \dots 10^{-6}$ (convergence of the computational process depends upon many factors and can be assessed by performing repeated numerical experiments).

Adequacy of the Monte Carlo ray tracing (MCRT) calculations depends equally to a great extent upon two factors. The first is the temperature distribution over the BB walls, especially over their directly viewable areas. Even the most precise BB calibration sources (fixed-point and heat-pipe blackbodies [53, 54]) may have non-negligible decrease in temperature toward their apertures. Usually, temperature of BBs is measured by contact methods only in several points (often, only in the bottom center). In this instance, one can evaluate the influence of temperature non-uniformity on the radiation characteristics of a BB by performing calculations with several feasible temperature distributions.

Second factor crucially affected EE is the angular behavior of the reflection model adopted for materials forming a cavity. The simplest (but very often insufficient) model is the diffuse model of reflection. The most powerful models must take into account bidirectional reflectance distribution function (BRDF) [55] that describes angular distributions of reflected radiation for every direction of incidence. Since the measurement data required for such a model is very often incomplete or absent at all, the specular-diffuse model of reflection proposed in 1960ths [56] and representing BRDF as a sum of the Lambertian (diffuse) and the perfect specular components is in common use up to date. However, BRDF for specular-diffuse model of reflection includes Dirac's delta-function in the expression for specular component what makes impossible fitting of model's parameters to measured BRDF. Moreover, separation of reflectance into the perfect diffuse (Lambertian) and perfect specular components cannot be done unambiguously. Besides, specular components of reflection for real-world materials of blackbody cavities have small but finite divergence what can lead to effects which cannot be predicted within the framework of the specular-diffuse model of reflection [1].

INCA333 uses three-component (3C) BRDF model [1, 2] and provides tools for fitting 3C model's parameters to BRDFs measured in the plane of incidence (so-called "in-plane BRDFs") and for splitting the spectral directional-hemispherical reflectance (SDHR) into three components – perfectly diffuse (Lambertian), glossy (having wide specular lobe), and quasi-specular (having narrow specular peak).

3.5. Optical Properties of Materials for Blackbody Cavities

The choice of material or coating for radiating BB cavities is determined by many parameters: operational temperature of a BB, required level of EE for the BB, cavity shape, and VC tat are used. BBs operating at low temperatures have radiating cavities internally coated with various black paints like those used for thermal detector of optical radiation [57-62]. High-temperature BBs usually made of graphite, pyrographite, ceramics, or other refractory materials [63, 64]. Cavities for intermediate temperature range frequently have oxidized metallic surface. The spectral range, in which the cavity operates, is determined primarily by the BB operating temperature. SDHR measured within some spectral range at a single incidence angle is the most accessible optical characteristic that can be measured with the help of standard measurement equipment (e.g., spectrophotometer with the integrating sphere or other reflectometric accessory).

Together with the spectral emissivity or spectral reflectance, the angular distribution of the radiation reflected from or emitted by a material is the matter of the first importance for the calculation of

radiation characteristics of BBs. This distribution is described by the BRDF. In the spherical coordinate system (see Fig. 3), BRDF, f_r [sr^{-1}], is defined [55] as

$$f_r(\lambda, \theta_i, \phi_i, \theta_v, \phi_v) = \frac{dL_{\lambda,v}(\lambda, \theta_i, \phi_i, \theta_v, \phi_v)}{dE_{\lambda,i}(\lambda, \theta_i, \phi_i)} = \frac{dL_{\lambda,v}(\lambda, \theta_i, \phi_i, \theta_v, \phi_v)}{dL_{\lambda,i}(\lambda, \theta_i, \phi_i) d\Omega_i}, \quad (9)$$

where θ and ϕ are the polar and azimuthal angles, respectively, L_λ is the spectral radiance of reflected radiation, E_λ is the spectral irradiance of incident radiation; $d\Omega$ is elementary solid angle; subscripts “i” and “v” refer to incidence and viewing directions, respectively.

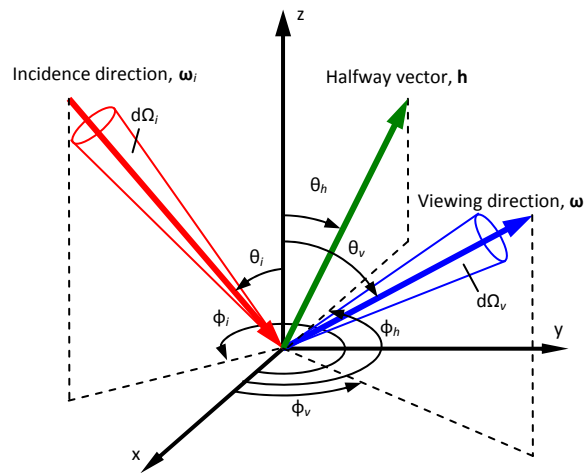


Fig. 3. Schematic for the BRDF definition.

It is supposed that fluorescence and translucency are absent. BRDF, as the function of 5 variables, comprehensively describes optical properties of a material. Without loss of generality, until Section 3.8, we will consider monochromatic radiation only and omit dependences on λ as well as the adjective “spectral”.

Physically plausible BRDF must obey the following two conditions:

1. Reciprocity principle which allows to interchange the incidence and the viewing directions:

$$f_r(\theta_i, \phi_i, \theta_v, \phi_v) = f_r(\theta_v, \phi_v, \theta_i, \phi_i). \quad (10)$$

2. Energy conservation law, which dictates that the DHR computed as the integral of the BRDF over the hemispherical solid angle, cannot be greater than unity for any incidence angle:

$$\rho(\theta_i) = \int_{\phi_v=0}^{2\pi} \int_{\theta_v=0}^{\pi/2} f_r(\theta_i, \phi_i, \theta_v, \phi_v) \sin \theta_v \cos \theta_v d\theta_v d\phi_v \leq 1 \quad \text{for any } \theta_i \quad (11)$$

Unfortunately, BRDF of materials and coatings used for radiating surfaces of BBs are studied insufficiently. Very often, BRDF is measured only in the plane of incidence and for several incidence angles only. Although some materials are used in BBs operating at elevated temperatures, BRDF measurements are usually conducted at ambient temperature. The use of published data is problematic due to many uncontrolled parameters of the material such as roughness, granularity, treatment, etc., which vary significantly from sample to sample. Obtaining reliable data requires individual investigation of each specific material.

For MCRT calculations, it is necessary to know the BRDF values at any combination of incidence and viewing directions. Habitual incompleteness of BRDF measurements leads to necessity of introducing BRDF models, usually, in the form of analytical functions. A number of such models were developed for computer graphics, digital image synthesis, and remote sensing during two last decades (the extensive bibliography can be found, for instance, in [65-72]). These models can be subdivided onto physically-based (i.e., describing real physical phenomena such as a reflection of optical radiation from randomly rough surfaces or volumetric scattering in turbid media), empirical (which are no more than mathematical formulae with a set of tunable parameters), and semi-empirical models, which are in-between two first categories.

Physically-based models cannot be too sophisticated; they better describe behavior of materials exhibiting only one type of scattering (e.g., scattering on the surface roughness or subsurface scattering) and provide reasonable predicting of optical characteristics of such materials outside the angular range of measurement. However, real-world materials seldom or never exhibit scattering conditioned by only one physical phenomenon. For instance, reflection of infrared radiation from a metallic substrate covered with a black paint is conditioned by scattering on the paint's rough surface, volumetric scattering within a paint layer, reflection from metallic substrate, and so forth.

A well-chosen approximating function and a set of tuning parameters can ensure excellent fitting of empirical model to the measured BRDF but there is no guarantee for physical plausibility of these results for all possible incidence and viewing angles.

The best approach must combine two above-mentioned methodologies.

3.6. Three-Component (3C) BRDF Model

As can be seen from Figs. 4 and 5 presenting BRDF measured at ambient temperatures for a black coating and graphite sample (see also [57-62, 64]), most BRDFs can be represented as the sum of three components: near-Lambertian (diffuse), almost specular (quasi-specular), and glossy (having wider

forward-scattering lobe). The names of components are not concerned with physical phenomena they determine but refer to their shapes only. Only isotropic BRDF models depending on $\phi = |\phi_i - \phi_v|$ instead of ϕ_i and ϕ_v are considered.

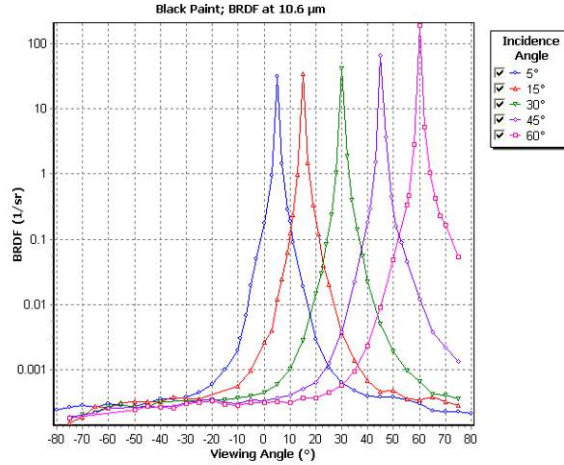


Fig. 4. Logarithmic plot for BRDFs of a black paint with predominantly specular reflection measured at ambient temperature and wavelength of 10.6 μm .

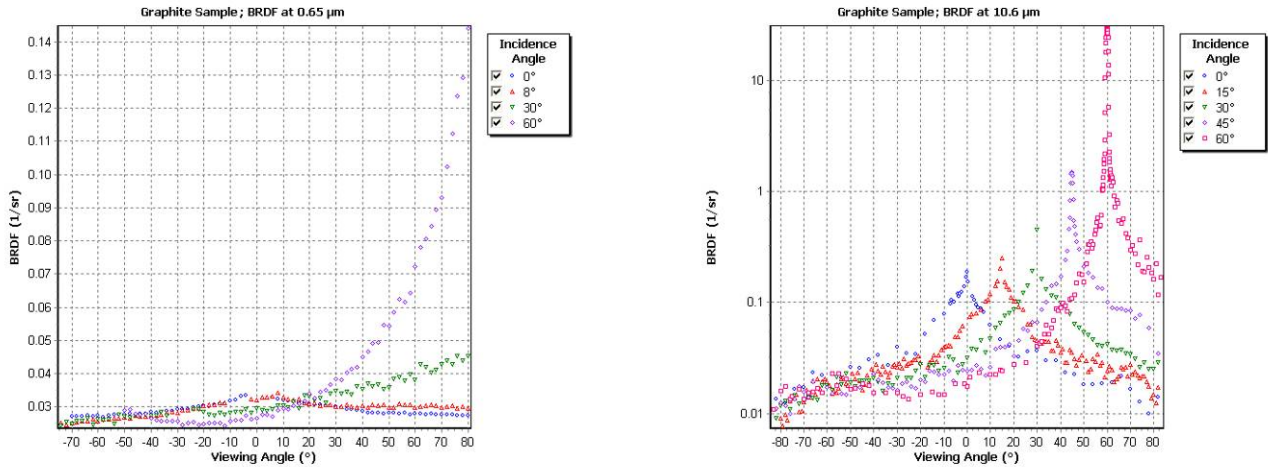


Fig. 5. BRDFs of graphite sample measured at ambient temperature; left plot is for 0.65 μm , right plot (logarithmic) is for 10.6 μm .

The Three-component (3C) BRDF model $f_{r,3C}$ introduced in [1] can be represented by the linear combination of diffuse $f_{r,d}$, quasi-specular $f_{r,qS}$, and glossy $f_{r,g}$ components:

$$f_{r,3C} = k_d f_{r,d} + k_{qs} f_{r,qs} + k_g f_{r,g}, \quad (12)$$

where k_d , k_{qs} , and k_g are non-negative and

$$k_d + k_{qs} + k_g = 1. \quad (13)$$

Diffuse component might be caused by multiple scattering on the surface roughness, or by volumetric scattering inside a translucent coating etc. Diffuse component corresponds to reflected radiation more or less uniformly scattered within the hemispherical solid angle. Lambertian reflection (also known as ideal diffuse or perfectly diffuse reflection) is the extreme case of diffuse reflection when $f_{r,d} = \text{const}$.

Quasi-specular component has small but finite divergence unlike specularly reflected ray in the case of perfectly specular reflection.

Glossy component is similar to the specular component but so wider that it forms rather specular lobe than peak.

The schematic representation of 3C BRDF model is shown in Fig. 6.

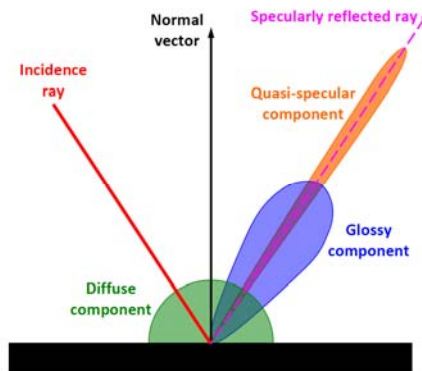


Fig. 6. Schematic representation of 3C BRDF model.

For the diffuse component, the Lambertian BRDF is used:

$$f_{r,d} = \frac{R_d}{\pi}, \quad (14)$$

where R_d is the partial diffuse reflectance that defines the directional-hemispherical reflectance (DHR) ρ_d of the diffuse component.

For the specular and glossy components, the isotropic version of the model, proposed in [73] for rough surfaces, is adopted:

$$f_r(\theta_i, \theta_v, \phi) = \frac{R(\theta_h)}{\pi\sigma} \exp\left[-\left(\frac{\tan \theta_h}{\sigma}\right)^2\right] \frac{2[1 + \cos \theta_i \cos \theta_v - \sin \theta_i \sin \theta_v \cos \phi]}{(\cos \theta_i \cos \theta_v)^4}, \quad (15)$$

where σ is the roughness parameter, θ_h is the halfway angle (see Fig. 3 and explanation below).

This BRDF model is based on the microfacet model of reflection [74] that represents rough surface as a set of randomly oriented perfectly specular tiny facets. Specular reflectance R , of microfacet depends on the angle θ_h of the incidence onto the microfacet. This *halfway angle* is formed by the surface normal and the *halfway vector* $\mathbf{h} = (\boldsymbol{\omega}_v - \boldsymbol{\omega}_i) / (2\|\boldsymbol{\omega}_v - \boldsymbol{\omega}_i\|)$ (see Fig. 3).

It is assumed that microfacet normals have Gaussian distribution with zero mean value and standard deviation σ . BRDF lobe becomes wider with the growth of σ . Elementary physical reasoning suggests that if $R(\theta_h) \equiv 1$, the DHR of a microfacet model must equal 1 for all incidence angles. However, DHR of all microfacet models, which neglect multiple reflections among microfacets, deviate from 1 for such a case; the greater roughness the greater this deviation. Last term in Eq. (15) is constructed to minimize the deviation of DHR from 1 at $R(\theta_h) \equiv 1$. Deviations become significant only for large σ and large θ_i . Since the reflectances of materials of blackbody cavities are essentially low, uncertainty due to neglecting multiple reflections for the DHR calculation by integration of BRDF (12) is essentially very small.

The original model [73] uses Schlick's approximation [75] of Fresnel's reflection law for unpolarized radiation:

$$R_{Sch}(\theta_h) = \begin{cases} R + (1-R)(1 - \cos \theta_h)^5, & \text{if } R > 0 \\ 0, & \text{if } R = 0 \end{cases} \quad (16)$$

where R is the partial specular reflectance (specular reflectance of a microfacet at the normal incidence).

Eq. (16) is slightly modified as compared with the original Schlick's formula to correct the approximation behavior for $R = 0$ and $\theta_i > 0$. For non-dielectrics, Eq. (16) gives greater deviations from Fresnelian reflectance at large θ_h . However, large θ_h values are typical for very rough surfaces when the effect of multiple reflections among microfacets overrides error of Schlick's approximation. Eq. (15) is used for both quasi-specular and glossy components; it is allowed that $0.0001 \leq \sigma_{qs} \leq 0.01$ for the quasi-specular

component and $0.01 < \sigma_g \leq 1$ for the glossy component. In-plane BRDFs of glossy component plotted in the Cartesian coordinate system according to Eqs. (15) and (16) for $R_g = 0.1$, $\sigma_g = 0.1$, and six values of θ_i (0° , 15° , 30° , 45° , 60° , and 75°) are shown in Fig. 7. The negative values of viewing angles θ_v correspond to backscattering.

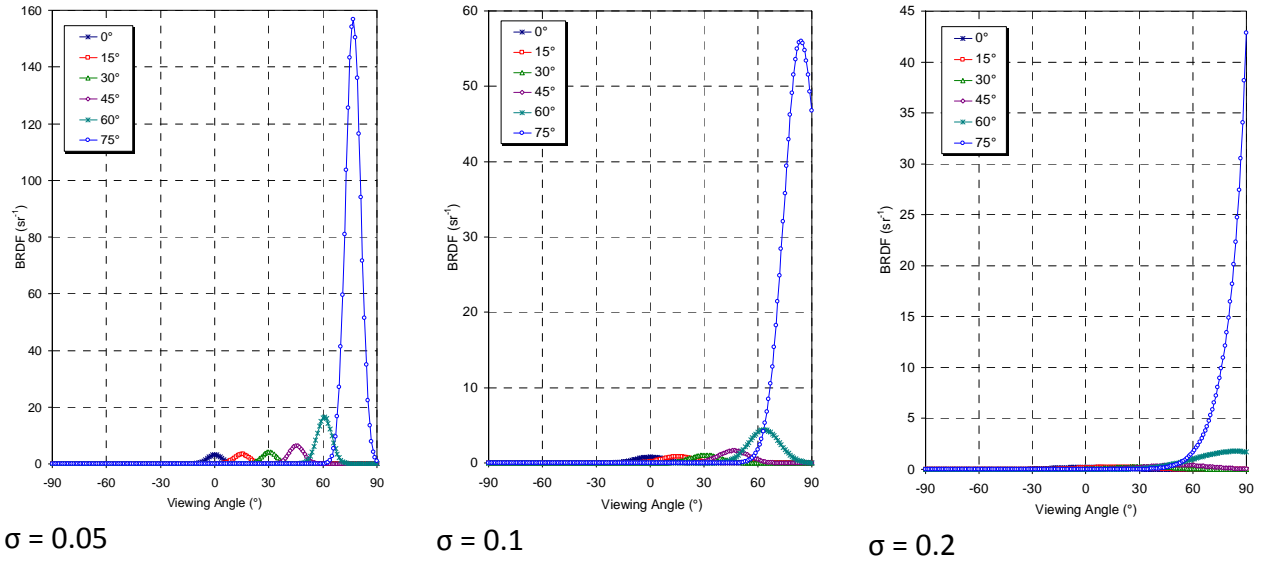


Fig. 7. In-plane BRDFs for the glossy components for $R_g = 0.1$; $\sigma_g = 0.05, 0.1$, and 0.2 .

The 3D plots of glossy BRDFs expressed in relative units for $R_g = 0.1$ and $\sigma_g = 0.05, 0.1$, and 0.2 are presented in the spherical coordinate system in Fig. 8 for 45° of incidence.

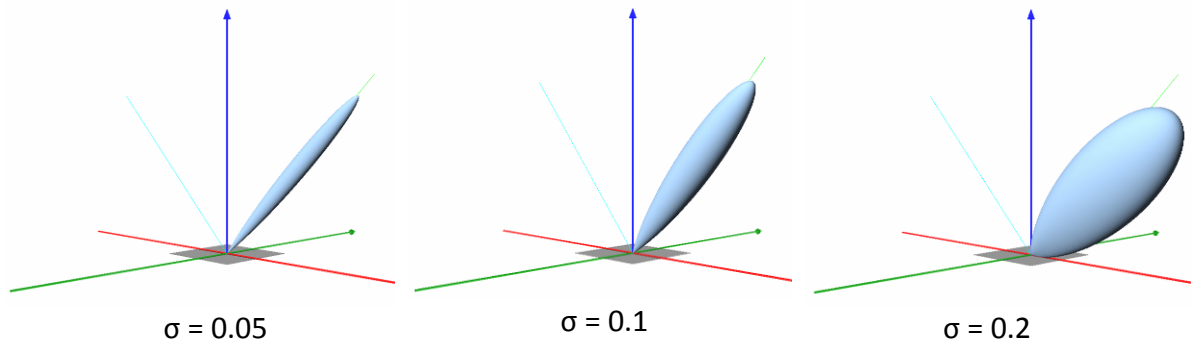


Fig. 8. The three-dimensional plots in the spherical coordinate system of glossy BRDFs expressed in relative units for $R_g = 0.1$ and $\sigma_g = 0.05, 0.1$, and 0.2 for 45° of incidence.

Although the model expressed by Eq. (15) is developed for randomly rough surfaces, it was found that it satisfactorily approximates glossy lobes of other nature.

DHR of the 3C BRDF model can be represented in the form

$$\rho_{3C}(\theta_i) = \rho_d + \rho_{qs}(\theta_i) + \rho_g(\theta_i), \quad (17)$$

where every summand is the DHR of the appropriate component:

$$\rho_d = k_d \int_{\phi=0}^{2\pi} \int_{\theta_v=0}^{\pi/2} f_{r,g}(R_d, \theta_i, \theta_v, \phi) \sin \theta_v \cos \theta_v d\theta_v d\phi = k_d R_d, \quad (18)$$

$$\rho_{qs}(\theta_i) = k_s \int_{\phi=0}^{2\pi} \int_{\theta_v=0}^{\pi/2} f_{r,qs}(R_{qs}, \sigma_{qs}, \theta_i, \theta_v, \phi) \sin \theta_v \cos \theta_v d\theta_v d\phi, \quad (19)$$

$$\rho_g(\theta_i) = k_g \int_{\phi_v=0}^{2\pi} \int_{\theta_v=0}^{\pi/2} f_{r,g}(R_g, \sigma_g, \theta_i, \theta_v, \phi) \sin \theta_v \cos \theta_v d\theta_v d\phi. \quad (20)$$

We call R_d , R_{qs} , and R_g *partial reflectances* (PRs) of corresponding components.

3.7. Fitting Parameters of 3C BRDF Model to the In-Plane BRDFs

The 3C model of reflection has 8 parameters: $k_d, R_d, k_{qs}, R_{qs}, \sigma_{qs}, k_g, R_g$, and σ_g . Three of them are interrelated as it is shown in Eq. (13). Besides, the following conditions must be fulfilled:

$$0 \leq k_d, R_d, k_{qs}, R_{qs}, k_g, R_g \leq 1, \quad (21)$$

$$0.0001 \leq \sigma_{qs} \leq 0.01, \quad (22)$$

$$0.01 < \sigma_g \leq 1. \quad (23)$$

Mathematically, we deal with the problem of constrained optimization and have to find 8 values of the 3C model parameters which minimize distances between computed and measured BRDFs according to some goodness-of-fit criterion. Multiple numerical experiments did not help in isolating a unified criterion for all variety of BRDF shapes. For smooth BRDFs with the moderate dynamic range, the L_2 metric ensures the best fitting results. The objective function $F(k_d, R_d, k_{qs}, R_{qs}, \sigma_{qs}, k_g, R_g, \sigma_g)$ for the metric L_2 equals

$$F = \sum_{k=1}^{n_i} \sum_{j=1}^{n_{v,k}} [f_{r,m}(\theta_{i,k}, \theta_{v,jk}) - f_r(\theta_{i,k}, \theta_{v,jk})]^2, \quad (24)$$

where f_r and $f_{r,m}$ are computed and measured in-plane BRDF, respectively, n_i is the number of incidence angles, $n_{v,k}$ is the number of viewing angles in the BRDF measured at k^{th} incidence angle $\theta_{i,k}$, $\theta_{v,jk}$ is the j^{th} viewing angle for the BRDF measured for $\theta_{i,k}$.

It was found that for very non-uniform BRDFs with a large dynamic range (for instance, for almost uniform BRDF with a narrow specular peak), the C metric for relative deviations is more suitable:

$$F = \begin{cases} 0, & \text{if } f_{r,m}(\theta_{i,k}, \theta_{v,jk}) = f_r(\theta_{i,k}, \theta_{v,jk}) = 0, \text{ otherwise} \\ \max_{k=1, \dots, n_i} \max_{j=1, \dots, n_{v,k}} \left\{ \frac{|f_{r,m}(\theta_{i,k}, \theta_{v,jk}) - f_r(\theta_{i,k}, \theta_{v,jk})|}{f_{r,m}(\theta_{i,k}, \theta_{v,jk}) + f_r(\theta_{i,k}, \theta_{v,jk})} \right\} \end{cases} \quad (25)$$

The objective functions defined by Eqs. (24) and (25) have multiple minima but only one of them is the deepest. Therefore we have to deal with multimodal objective functions and, correspondingly, with the global optimization problem. For such problems, the solution usually depends on a starting point. It was assumed that there is no a priori information which would allow us to select a “good” starting point needed to detect the global minimum among several local minima. The particle swarm optimization (PSO) method [76] was chosen to solve this problem due to the following two main reasons. First, PSO only requires knowledge of lower and upper allowed values for each variable instead of its “good” zero approximations. Second, PSO is capable (at least, in principle) to solve global optimization problems.

PSO is a stochastic, derivative-free, iterative optimization method that imitates random movement of “particles” in the multidimensional search-space. The movements of the particles are determined by their individual best known positions as well as the best known position for a swarm as a whole. Although PSO does not guarantee locating the global minimum, the probability of its detection is high at the optimal tuning of the algorithm. INCA333 uses the algorithm described in Ref. [77] conjugated with the normalization of parameters k_d , k_{qs} , and k_g for calculation of $f_{r,3C}$ after successive iterations. Normalization is performed according to Eq. (13). Multiple re-starts strategy is used to avoid stagnation and convergence to wrong solutions (local minima).

Maximal number of iterations (particle movements in the swarm), which can be executed without restarts equals $n_{iter} = 10^4$ in INCA333. Default number of restarts $n_{restarts} = 20$; user can vary this number

between 1 and 100. Increase in number of restarts increases the probability of achieving the best fit but also increases computation time. To initiate restart, one of two criteria must be fulfilled:

- 1) Objective function did not decrease during $\gamma \cdot n_{iter}$, where $0 < \gamma \leq 1$ is the *Stagnation Length*
- 2) Radius of the hypersphere circumscribed in the 8-dimensional space of 3C model parameters is reduced by the factor of *Swarm Contraction* in comparison with the initial radius of the swarm. Swarm Contraction can take values 10^{-2} , 10^{-3} , 10^{-4} , 10^{-5} , 10^{-6} , 10^{-7} , 10^{-8} , and 10^{-9} ; the default value equals 10^{-4} .

The final solution is made by the set of parameters corresponding to the minimal value of the objective function. For defaults settings taking in INCA333 and overwhelming majority of BRDFs considered, the probability of finding the global minimum estimated by numerical experiments exceed 99.7%.

The approach described in this Section allows not only fitting the 3C model parameters to the measured 2D (in-plane) BRDF but also to recover 3D (hemispherical) BRDF and compute the DHR of a material at any incidence angle using numerical integration.

3.8. Spectral DHR Splitting

In the previous Sections, only the case of monochromatic radiation was considered. Such an approach makes sense because BRDF is frequently measured at one or only a few wavelengths (usually, wavelengths of laser radiation). However, spectral EEs and RTs of BB radiators often should be computed for a continuous spectral range (actually, for sufficiently dense discrete set of wavelengths). An algorithm for making the 3C model wavelength-dependent is proposed in [2].

If we have SDHR of a material measured at the incidence angle $\theta_{i,0}$ within the spectral range from the wavelength λ_{\min} to the wavelength λ_{\max} and BRDF of the same material measured for the wavelength $\lambda_0 \in [\lambda_{\min}, \lambda_{\max}]$, one can suppose that:

- (a) The relative shape of BRDF remains the same for all $\lambda \in [\lambda_{\min}, \lambda_{\max}]$ if the scattering type does not change abruptly within the spectral interval $[\lambda_{\min}, \lambda_{\max}]$. For the 3C BRDF model, this means that parameters $k_d, k_{qs}, k_g, \sigma_{qs}$, and σ_g remain constant within spectral range considered, but partial reflectances R_d, R_{qs} , and R_g are wavelength-dependent (*spectral partial reflectances, SPRs*).
- (b) Relative contribution of partial DHR ρ_d, ρ_{qs} , and ρ_g of each component in the SDHR ρ does not change within the spectral interval considered, that is ratios $\gamma_d = \rho_d^* / \rho^*(\theta_{i,0})$, $\gamma_{qs} = \rho_{qs}^* / \rho^*(\theta_{i,0})$, and $\gamma_g = \rho_g^* / \rho^*(\theta_{i,0})$ do not depend on wavelength for all $\lambda \in [\lambda_{\min}, \lambda_{\max}]$. Here, asterisked values are obtained using the 3C BRDF model with best fit values of parameters and Eqs. (18)-(20).

If condition (b) fulfills, one can calculate the SDHR at $\theta_{i,0}$ of components for any $\lambda \in [\lambda_{\min}, \lambda_{\max}]$:

$$\rho_d(\lambda) = \gamma_d \rho(\lambda, \theta_{i,0}), \quad (26)$$

$$\rho_{qs}(\lambda, \theta_{i,0}) = \gamma_{qs} \rho(\lambda, \theta_{i,0}), \quad (27)$$

$$\rho_g(\lambda, \theta_{i,0}) = \gamma_g \rho(\lambda, \theta_{i,0}), \quad (28)$$

Comparison of Eqs. (26) – (28) with Eqs. (18) – (20) leads to the following independent equations for SPRs R_d , R_{qs} , and R_g for every $\lambda \in [\lambda_{\min}, \lambda_{\max}]$:

$$\gamma_d \rho(\lambda, \theta_{i,0}) = k_d R_d(\lambda), \quad (29)$$

$$\gamma_{qs} \rho(\lambda, \theta_{i,0}) = k_{qs} \int_{\phi=0}^{2\pi} \int_{\theta_v=0}^{\pi/2} f_{r,qs}(R_{qs}(\lambda), \sigma_{qs}, \theta_{i,0}, \theta_v, \phi) \sin \theta_v \cos \theta_v d\theta_v d\phi, \quad (30)$$

$$\gamma_g \rho(\lambda, \theta_{i,0}) = k_g \int_{\phi=0}^{2\pi} \int_{\theta_v=0}^{\pi/2} f_{r,g}(R_g(\lambda), \sigma_g, \theta_i, 0, \theta_v, \phi) \sin \theta_v \cos \theta_v d\theta_v d\phi. \quad (31)$$

Eq. (29) has infinite set of solutions; any solution can be chosen because only the SDHR $\rho(\lambda, \theta_i)$ is a measurable value; γ_d is the result of calculation according to $\gamma_d = \rho_d^* / \rho^*(\theta_{i,0})$; therefore, any product $k_d R_d(\lambda)$ is acceptable. Eqs. (30) and (31) are nonlinear and can be solved numerically for every λ from the given wavelength set. INCA333 uses Brent's method [78] to find the roots of Eqs. (30) and (31) and multidimensional adaptive quadratures [79] for integration over the hemispherical solid angle.

We will refer to the approach and the algorithm described in this Section as *Spectral DHR Splitting*. If BRDF is measured at several wavelengths $\lambda_{0,k}$, $k = 1, \dots, n_0$ within spectral interval $[\lambda_{\min}, \lambda_{\max}]$, this wavelength range can be split into n_0 subranges containing $\lambda_{0,k}$. It is supposed that two above-mentioned conditions are fulfilled for each spectral subrange.

3.9. Algorithm for Calculating Radiation Characteristics of Blackbody Radiators

Calculation of the EEs of isothermal cavities using the MCRT method can be performed using the Kirchhoff law for the cavity's EE and effective absorptance [80]. However, Kirchhoff's law cannot be applied to nonisothermal cavities due to thermodynamic equilibrium violation. At the same time, the Helmholtz reciprocity principle remains in force and allows employing the backward ray tracing [81]. The MCRT method requires averaging of spectral radiances of a large amount of rays launched from the points and in the directions determined by the VC. INCA333 employs the importance sampling [82] technique to generate randomly reflected ray according to the given BRDF.

A large number n of rays have to be launched into a cavity; their start points and directions are generated randomly, according to the viewing conditions which have to be modeled. The statistical weight $w_{0k} = 1$ is assigned to the k -th ray before tracing. Before each reflection, the type of reflection is chosen with the help of pseudo-random number u uniformly distributed from 0 to 1. If $u \leq k_d$, a random ray is generated according to the Lambertian BRDF; otherwise, if $u \leq k_d + k_{qs}$, reflection is quasi-specular; otherwise it is glossy.

Importance sampling for diffuse component can be done using well-known method [83]:

$$\begin{cases} \sin^2 \theta_v = u_\theta \\ \phi_v = 2\pi u_\phi \end{cases}, \quad (31)$$

where u_θ and u_ϕ are two random numbers from a uniformly distributed set between 0 and 1, θ_v and ϕ_v are the polar and azimuthal angles of a reflected ray in the local spherical coordinate system with the origin at the point of reflection and z-axis coincident with the surface normal.

INCA333 uses an alternative, faster method that produces Cartesian coordinates of the unit vector directed along the reflected ray. The pair of uniformly distributed random numbers u_x and u_y are generated and accepted if $u_x^2 + u_y^2 < 1$, otherwise the new pair of u_x and u_y are generated. Cartesian coordinates of the unit reflection vector ω_v in the local coordinate system are computed as

$$\begin{cases} \omega_{vx} = 2u_x - 1 \\ \omega_{vy} = 2u_y - 1 \\ \omega_{vz} = +\sqrt{1 - \omega_x^2 - \omega_y^2} \end{cases}. \quad (33)$$

The statistical weight $w = R_d$ is assigned to the diffusely reflected ray.

The sampling procedure described in Ref. [73] was applied to quasi-specular and glossy components. First, spherical coordinates of the halfway vector \mathbf{h} (see Fig. 3) are computed using random numbers u_θ and u_ϕ :

$$\begin{cases} \theta_h = \tan^{-1}(-\sigma \ln u_\theta) \\ \phi_h = 2\pi u_\phi \end{cases}, \quad (34)$$

Second, spherical coordinates are transformed to Cartesian coordinates:

$$\begin{cases} h_x = \sin \theta_h \cos \phi_h \\ h_y = \sin \theta_h \sin \phi_h \\ h_z = \cos \theta_h \end{cases} \quad (35)$$

When coordinates of the halfway vector \mathbf{h} are found, one can compute coordinates of the viewing vector $\boldsymbol{\omega}_v$ specularly reflected from the microfacet with the normal \mathbf{h} for the given incidence vector $\boldsymbol{\omega}_i$:

$$\begin{cases} \omega_{vx} = \omega_{ix} - 2(\boldsymbol{\omega}_i \cdot \mathbf{h})h_x \\ \omega_{vy} = \omega_{iy} - 2(\boldsymbol{\omega}_i \cdot \mathbf{h})h_y \\ \omega_{vz} = \omega_{iz} - 2(\boldsymbol{\omega}_i \cdot \mathbf{h})h_z \end{cases} \quad (36)$$

According to the sampling procedure proposed in Ref. [73], the statistical weight

$$w = \frac{2R_{qs,g}(\theta_h)}{1 - \omega_{iz}/\omega_{vz}} \quad (37)$$

is assigned to the quasi-specular or glossy reflected ray.

Thus, after each reflection, the statistical weight is multiplied by the factor that is determined by the sampling procedure:

$$w_{j,k} = w_{j-1,k} \times \begin{cases} R_d(\lambda) & \text{for diffuse reflection} \\ \frac{2R_{qs}(\lambda, \theta_{i,j-1,k})}{(1 + \cos \theta_{i,j-1,k} / \cos \theta_{v,j-1,k})} & \text{for quasi - specular reflection,} \\ \frac{2R_g(\lambda, \theta_{i,j-1,k})}{(1 + \cos \theta_{i,j-1,k} / \cos \theta_{v,j-1,k})} & \text{for glossy reflection} \end{cases} \quad (38)$$

where $\theta_{i,jk}$ and $\theta_{v,jk}$ are the incidence and viewing (reflection) angles, respectively; the index “j” denotes the number of reflection.

The ray is traced until it escapes the cavity or until its statistical weight becomes less than predefined threshold value (10^{-12} in INCA333). Backward ray tracing considers the last reflection point as the emission point of the ray propagated in the opposite direction, i.e. toward the observer. At the j -th reflection point, the spectral radiance of the backward propagated k -th ray comprises the radiation emitted and reflected at this point and can be expressed by the recurrence relation:

$$L_{\lambda,j,k}(\lambda) = (1 - w_{j+1,k}) L_{\lambda,bb}(\lambda, T_{j+1,k}) + w_{j+1,k} L_{\lambda,j+1,k}, \quad (39)$$

where $L_{\lambda,bb}$ is the spectral radiance of the perfect blackbody expressed by Planck's law, $T_{j+1,k}$ is the temperature of a cavity surface at the point of the $j+1$ -th reflection of the k -th ray.

The spectral radiance of the k -th backward propagated ray leaving the cavity can be written as

$$L_{\lambda,k}(\lambda) = [1 - w_{1,k}(\lambda)] L_{\lambda,bb}(\lambda, T_{1,k}) + \sum_{j=2}^{m_k} [1 - w_{j,k}(\lambda)] L_{\lambda,bb}(\lambda, T_{j,k}) \prod_{l=1}^{j-1} w_{l,k}(\lambda), \quad (40)$$

where m_k is the number of reflections in the k -th ray trajectory. Finally, the estimator for the spectral directional EE of a cavity at a wavelength λ is

$$\varepsilon_e(\lambda, T_{ref}) = \frac{1}{n L_{\lambda,bb}(\lambda, T_{ref})} \sum_{k=1}^n L_{\lambda,k}(\lambda). \quad (41)$$

For an isothermal cavity, $T_{jk} = T_{ref}$ for all $j = 1, \dots, m_k$ and $k = 1, \dots, n$. Simple transformations lead to

$$\begin{aligned} \varepsilon_e(\lambda, T_{ref}) &= \frac{1}{n L_{\lambda,bb}(\lambda, T_{ref})} \sum_{j=1}^n \left[(1 - w_{j,1}) L_{\lambda,bb}(\lambda, T_{ref}) + \right. \\ &\quad \left. + \sum_{k=2}^{m_j} (1 - w_{j,k}) L_{\lambda,bb}(\lambda, T_{ref}) \prod_{l=1}^{k-1} w_{j,l} \right] = \\ &= \frac{1}{n} \sum_{j=1}^n \left[(1 - w_{j,1}) + \sum_{k=2}^{m_j} (1 - w_{j,k}) \prod_{l=1}^{k-1} w_{j,l} \right] = \\ &= 1 - \frac{1}{n} \sum_{j=1}^n \prod_{l=1}^{m_j} w_{j,l} = \varepsilon_e(\lambda) \end{aligned} \quad (42)$$

Thus, Eqs. (40) and (41) are transformed into the equation derived in Ref. [1] for an isothermal cavity using the approach based on the Kirchhoff law.

Effect of background temperature can be taken into account analytically by substitution of effective emissivity values computed according to Eqs. (40) and (41) into Eq. (5). The RT can be computed using Eq. (7). Calculations for each wavelengths are performed successively, wavelength-by-wavelength.

4. Key Features of INCA333

- Modeling of a cylindrical cavity with a flat inclined bottom with or without a flat annular diaphragm
- Modeling of isothermal or nonisothermal cavities with arbitrary one-dimensional (along Z axis) temperature distribution specified for up to 1001 points
- Successive (wavelength-by-wavelength) calculation of effective emissivities and radiance temperatures for up to 501 wavelengths
- Possibility to build 3C BRDF model from scratch or to fit its parameter to in-plane BRDFs measured at up to 6 incidence angles for one wavelength
- Possibility to separate the spectral directional-hemispherical reflectance measured at one incidence angle into the components of 3C reflection model to make it wavelength-dependent
- Calculation of effective emissivities of isothermal and nonisothermal cavities and radiance temperatures for given temperature distribution
- Possibility to take into account the contribution of a background radiation
- Three types of VC each having up to 4 variable parameters (Normal, Conical for divergent and convergent viewing beams, and Integrated)
- Successive calculations for up to 201 viewing conditions of the same type
- Built-in expandable databases for:
 - Geometrical parameters, reflection models for materials, temperature distribution, and viewing conditions for blackbody radiators (the DATASETS database)
 - Measured BRDFs and SDHRs, results of BRDF fitting and SDHR splitting (the FITTING database)
 - Wavelength-dependent 3C BRDF models of materials and coatings (the MATERIALS database)
 - MCRT results, i.e., spectral effective emissivities and radiance temperatures (the RESULTS database)
- Interpolation of spectral data stored in the MATERIALS database on the wavelength set specified in the DATASETS database
- Automatically generated reports in ASCII format
- Editable, exportable, and printable 2D graphs representing:
 - Scaled cross-section of a cavity
 - Viewing conditions
 - Measured and fitted BRDFs; measured SDHRs and results of their spectral splitting
 - Dependence of material's SPRs on wavelength
 - Temperature distributions along Z axis
 - Dependences of effective emissivities on the wavelength
 - Dependences of effective emissivities on one variable parameter of VC
- Possibility to save 2D graph data in text file or as MS Excel spreadsheet
- 3D interactive and editable plots of 3C BRDF models in spherical coordinate system
- Possibility to save 3D graph data in text file
- Possibility to save in file or copy to clipboard 2D and 3D graphs as bitmap

5. Structure of INCA333

The functional scheme of the INCA333 is shown in Fig. 9. The **DATASETS** database (*inca333.dbs* file in the *DB* folder) contains initial data on geometry, materials, and temperatures of blackbodies. Measured BRDFs and SDHRs as well as fitting and spectral splitting results are saved in the **FITTING** database (*inca333fit.dbs* file in the *DB* folder). The **BRDF Fitting and SDHR Splitting** Unit performs fitting 3C BRDF model parameters to the measured BRDFs and computes SPRs of the model using spectral splitting of measured SDHRs. Data on materials optical properties (parameters of wavelength-dependent 3C models) are saved in the **MATERIALS** database (*inca333mat.dbs* file in the *DB* folder). The fitting and splitting results should be exported from the **FITTING** to the **MATERIALS** database to be used in the MCRT calculations of radiation characteristics of blackbodies. **Preprocessing** unit extracts all necessary initial data from the **DATASETS** and **MATERIALS** databases, checks data self-consistency, and performs preliminary calculations. Then the **Monte Carlo Ray Tracing** unit executes stochastic modeling and writes the results to the **RESULTS** database (*inca333res.dbs* file in the *DB* folder). The **2D Visualization** unit displays Cartesian plots for functions of one variable (cross-sections of cavities, temperature distributions, in-plane BRDFs, various spectral dependences, etc.) The **3D Visualization** unit displays hemispherical BRDF plots in spherical coordinates. The **BRDF Model Builder** allows creating 3C BRDF models from scratch if experimental data are unavailable or deficient.

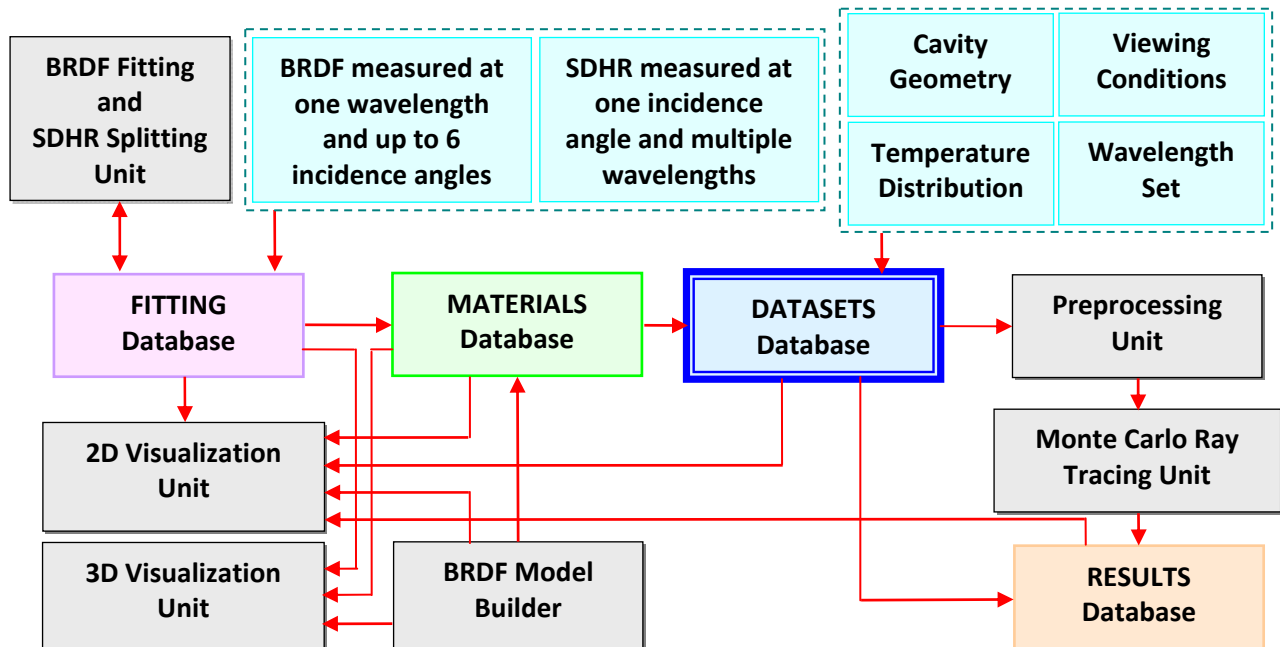


Fig. 9. Functional scheme of the INCA333.

INCA333 doesn't require installation. The zip-archive with the Evaluation Version can be downloaded for free from www.virial.com. *INCA333* folder can be placed at any convenient place of the hard drive. The folder *INCA333* has the following structure:

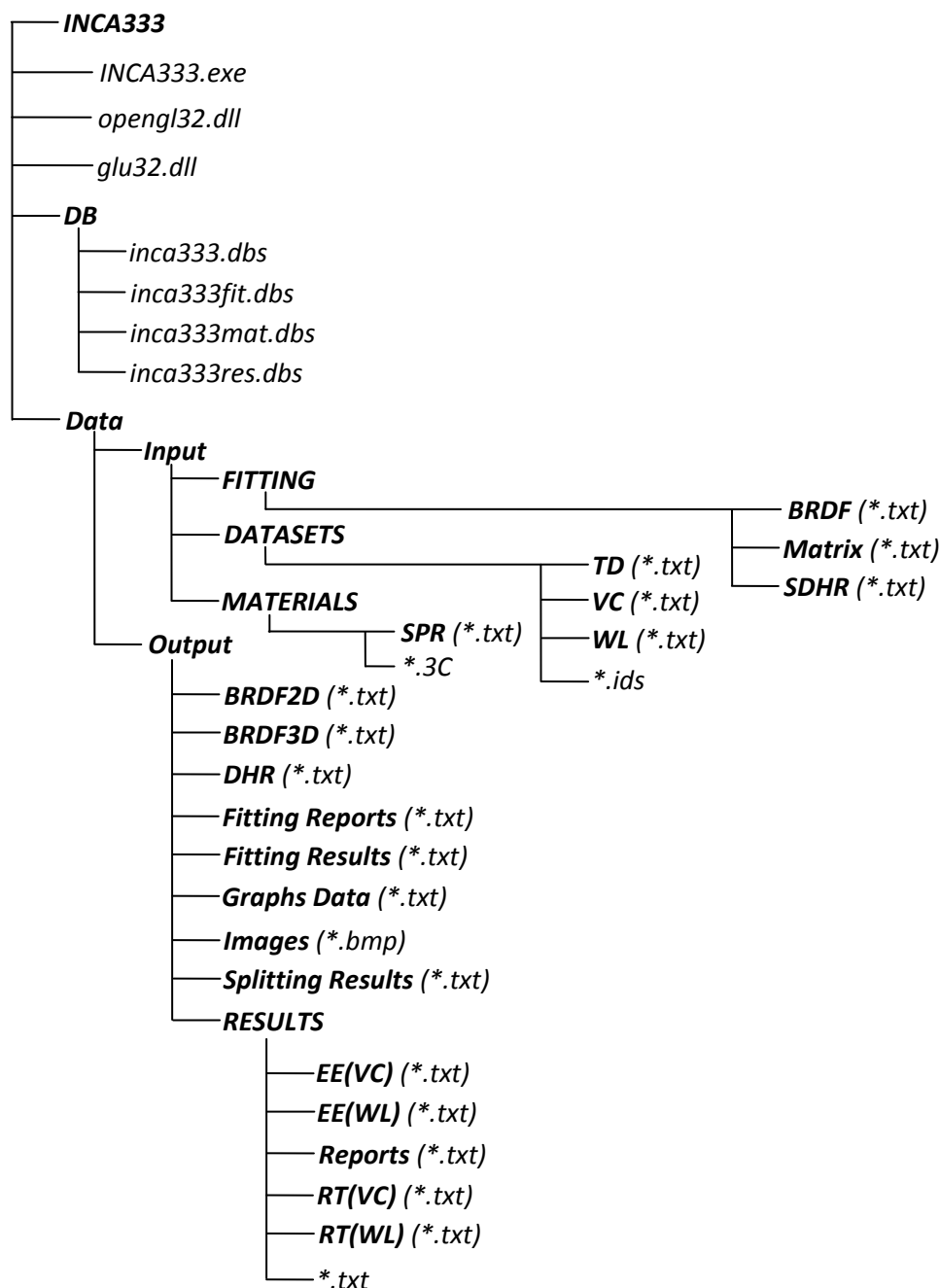


Figure 10. Structure of *INCA333* folder.

Most of the files in the subfolders **Input** and **Output** are text (ASCII) files. They can be opened and edited in any text editor, e.g., Windows Notepad. Data from some INCA333 tables can be saved as text files in the **Input** subfolder (see detail in Table 2).

Table 2. Content of subfolders of the **Data** folder.

Subfolder	Input	Output	Content
<i>INCA333\Datasets\TD</i>	✓	✓	Temperature distribution data
<i>INCA333\Datasets\VC</i>	✓	✓	Viewing conditions data
<i>INCA333\Datasets\WL</i>	✓	✓	Wavelength sets
<i>INCA333\MATERIALS\SPR</i>	✓	✓	Spectral partial reflectances
<i>INCA333\Data\Input\FITTING\BRDF</i>	✓	✗	BRDFs for one incidence angle
<i>INCA333\Data\Input\FITTING\Matrix</i>	✓	✗	BRDFs for multiple incidence angles with shared viewing angles
<i>INCA333\Data\Input\FITTING\SDHR</i>	✓	✗	Spectral directional-hemispherical reflectances
<i>INCA333\Data\Output\BRDF2D</i>	✗	✓	2D BRDF data
<i>INCA333\Data\Output\BRDF3D</i>	✗	✓	3D BRDF data
<i>INCA333\Data\Output\DHR</i>	✗	✓	Directional-hemispherical reflectances obtained by numerical integration of 3C BRDF models
<i>INCA333\Data\Output\Fitting Reports</i>	✗	✓	Fitting reports
<i>INCA333\Data\Output\Fitting Results</i>	✗	✓	Fitting results: measured and fitted BRDFs
<i>INCA333\Data\Output\Graphs Data</i>	✗	✓	Data saved from graphs plotted in separate window
<i>INCA333\Data\Output\Images</i>	✗	✓	Bitmaps of 2D and 3D graphs
<i>INCA333\Data\Output\RESULTS</i>	✗	✓	All results of Monte Carlo modeling: effective emissivities and radiance temperatures
<i>INCA333\Data\Output\RESULTS\EE(VC)</i>	✗	✓	Effective emissivities vs. variable parameter of viewing conditions for one wavelength
<i>INCA333\Data\Output\RESULTS\EE(WL)</i>	✗	✓	Effective emissivities vs. wavelength for one values of variable parameter of viewing conditions
<i>INCA333\Data\Output\RESULTS\Reports</i>	✗	✓	Full report of Monte Carlo modeling: initial data and results
<i>INCA333\Data\Output\RESULTS\RT(VC)</i>	✗	✓	Radiance temperatures vs. variable parameter of viewing conditions for one wavelength
<i>INCA333\Data\Output\RESULTS\RT(WL)</i>	✗	✓	Radiance temperatures vs. wavelength for one values of variable parameter of viewing conditions

The *.3C binary files contain 3C BRDF models and intended for data exchange between INCA333 and other programs that use the 3C BRDF model.

The *.ids binary files contains entire record of the **DATASETS** database, i.e., all initial data for Monte Carlo modeling except data that stored in the **MATERIALS** database. They allow to transfer data prepared with INCA333 running on one PC to another PC and use them with another instance of INCA333 providing that records for cavity wall materials will be also transferred using *.3C files.



- Only one instance of INCA333 can be run on one PC.
- To preserve functionality of the program do not change the content and mutual arrangement of INCA333 subfolders and files.
- All records in INCA333 databases and data files are supplied with the INCA333 are for exemplification purposes only and cannot be used as initial data for solving your specific tasks.

6. Units of Measurement

INCA333 uses the International System of Units (SI). Table 3 shows the units of physical quantities that INCA333 uses.

Table 3. Units of measurement used in INCA333.

Quantity	Unit	Comments
Linear dimensions	Arbitrary	All the cavity and viewing conditions linear dimensions must be expressed in the same units
Wavelength	Micrometer	$1\ \mu\text{m} = 10^{-6}\ \text{m}$
Angular dimensions	Degree, °	$1^\circ = 0.0174532925\ \text{rad}$
Solid angles	Steradian, sr	SI derived unit: 1 steradian is defined as the solid angle subtended at the center of a unit sphere by a unit area on its surface
Temperature	Kelvin, K	Conversion formulas: $[\text{K}] = [^\circ\text{C}] + 273.15$; $[\text{K}] = ([^\circ\text{F}] + 459.67) \times 5/9$

7. Working with INCA333

7.1. Working with INCA333 Databases

The common mode of data representation of INCA333 databases is a spreadsheet or a table. A table may be single, or be linked with other table(s). In the last case, the main table is referred to as master table, and its depended tables are called detail tables. For instance, in the **MATERIALS** database, each record of the master table contains fields for material name, date and time of a record creation, weights of each component, parameters σ_{qs} and σ_g for quasi-specular and glossy components, respectively.

The detail table contains fields for wavelength and SPRs R_d , R_{qs} , and R_g for diffuse, quasi-specular, and glossy components, respectively. Some editable fields can be associated with the stand-alone controls. Non-editable (read-only) fields have yellow-colored background. "Date and Time" field in **DATASETS** database is an example of such a field. It is filling in automatically when a new record is created. All the fields except two text fields ("Comments" and "Report") in the **RESULTS** database are non-editable.

To manipulate data in a table, use keyboard commands or the special control – the Database Navigator (see Fig. 11). Use <Tab> and arrow keys, mouse, or other pointing device for moving between cells of the table.

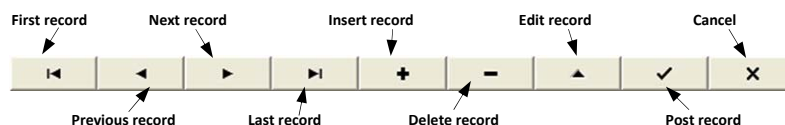


Fig. 11. The database navigator.

To add a new record to a table, use one of the following methods:

- Click *Insert Record* in the Database Navigator;
- Press *Insert* key;
- Press ↓ if you are in the last row of the table.

To delete a current record:

- Click *Delete Record* in the Database Navigator or
- Press *Delete* key.

When a record in the master table is deleted, all records in detail table(s) associated with deleted record of the master table will be also deleted.

To edit a record, click *Edit Record* in the appropriate database navigator or directly enter the value in the input field. Editable fields can be edited by entering corresponding values, or setting switches, or choosing values from drop-down lists. Usually, changes made in an edited or newly added record are saved in database after exiting the data grid or stand-alone control. However, to make sure that changed values are saved, one can click *Post Edit* button of the database navigator. Until changes are saved, one can restore previous values in the edited field by pressing *Esc* key or by clicking *Cancel* in the database navigator.

Some fields cannot be left empty. If you leave them blank, the INCA333 may react by a message **Field “...” must have a value**. In this case, press “OK” button below the message then click *Cancel* or *Delete* of the appropriate database navigator.

“Comments” fields store arbitrary text information that can be useful for your records identification. Master tables of the **DATASETS**, **FITTING**, **MATERIALS**, and **RESULTS** databases allow performing incremental search in the first column by using the input field “Find” at the top of the table. Search is performed as long as symbols are entered. Records in all master tables may be arranged by several fields. To switch sorting mode, use “Sort by” radio-buttons at the top of the master table.

Four database files (*inca333.dbs*, *inca333fit.dbs*, *inca333mat.dbs*, and *inca333res.dbs*) are stored in the *INCA333\DB* folder. One can move some or all of them to another place (for example, for archiving purposes). If INCA333 cannot find some database file, a new empty one will be created after notification message. Since cavity data, including names of materials are saved in *inca333.dbs* while optical properties for these materials are saved in *inca333mat.dbs*, the user should watch the compatibility of these files. If some material assigned to a cavity wall is absent in MATERIALS database, the message **Material “...” created “...” not found** will appear before calculations.

All data contained in a table can be loaded from or saved in text (ASCII) file by clicking **Load** or **Save** buttons. To delete more than one record, use **Erase** button. Clicking it calls the window shown in Fig. 12.

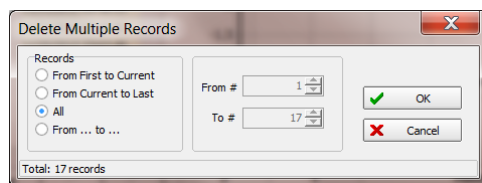


Fig. 12. Deleting multiple records.

The same window is used for partial erasing of more than one record, specifically, when it needed to erase materials assigned to several surfaces, or temperatures assigned to several temperature nodes.

7.2. Working with INCA333 2D Graphs

2D graphs for functions of one variable are used in INCA333 for several purposes:

- To show cavity shape, positions of points in which temperatures are defined, and for targeting that allows to check up correctness of viewing conditions specified
- To display temperature distribution along Z axis
- To plot measured and fitted in-plane BRDFs and fitting residuals
- To watch BRDF fitting process
- To plot dependences of DHR and its components (computed by numerical integration of 3C BRDF models) on wavelength and incidence angle
- To plot SPRs of 3C model against wavelength
- To display results of interpolation/extrapolation of SPRs extracted from **MATERIALS** database for the wavelength set that is used for Monte Carlo calculations
- To plot computed spectral effective emissivities and radiance temperatures vs. wavelength and vs. variable parameter of viewing conditions

INCA333 allows plotting a magnified fragment of the graph: holding left mouse button depressed, drag the cursor right and downwards to zoom (see Fig. 13) and left and upwards to unzoom.

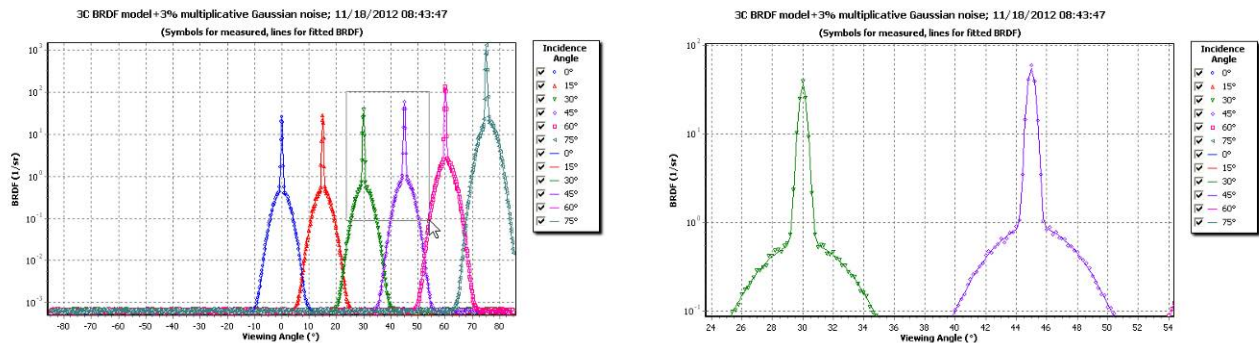


Fig. 13. Use of zoom: graph before (left) and after zoom (right).

To displace curves relative to graph axes, hold the left mouse button depressed and move cursor. To restore graph original position, draw a rectangle of arbitrary size by moving from the bottom right corner to the top left one while left mouse button remains pressed.

The graphs for in-plane BRDFs have the checkbox **Logarithmic BRDF Scale** on the lower panel. Check or uncheck it to switch between linear and logarithmic scale for the left axis of a graph.

Clicking [Show in Separate Window](#) on the lower panel re-plots graph in a separate sizable window (Fig. 14) that provides access to the Graph Editor, allows to save data in text file, copy to clipboard and save in file graph's bitmap.

Click **Edit Graph** to call the Graph Editor that provides comprehensive access to the properties of the graph via intuitive GUI. The Graph Editor gives the possibility to edit individual curves (series) and all major elements of the graph (points, axes, legend, title, etc.), copy to clipboard, save in the file, print the graphs, copy and save series values in formats of text (ASCII) file, MS Excel spreadsheet, HTML and XML tables (see screenshots in Figs. 15 - 17).

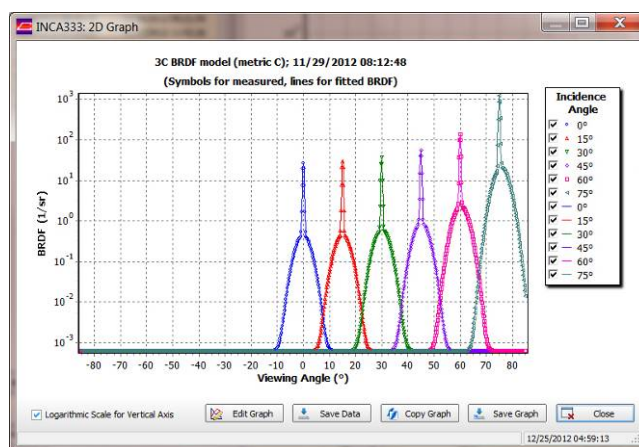
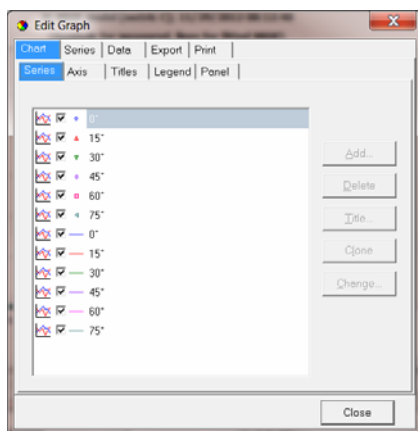
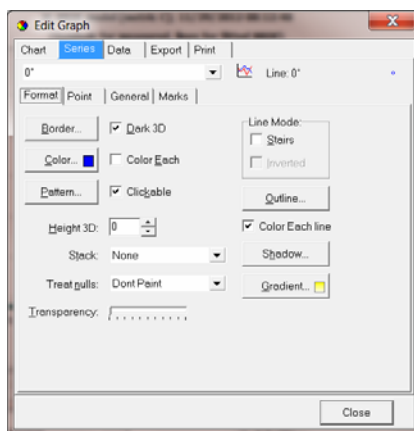


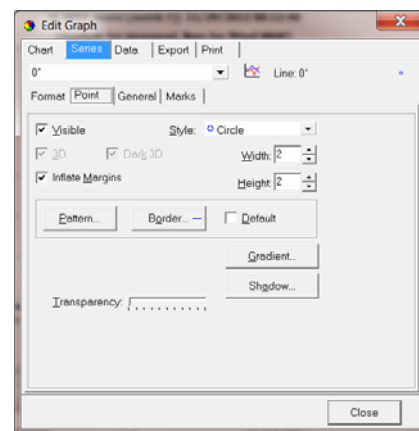
Fig. 14. Plotting graph in the separate window.



Access to individual series
(curves)

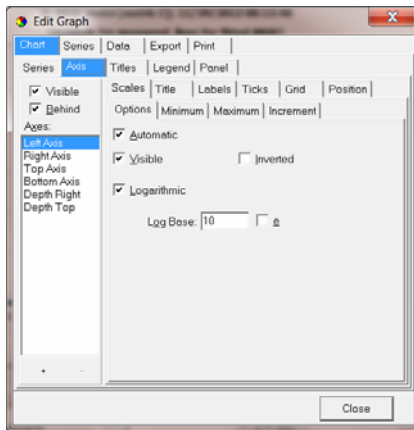


Formatting series

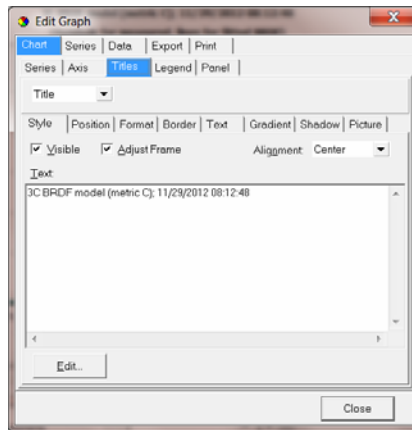


Formatting points

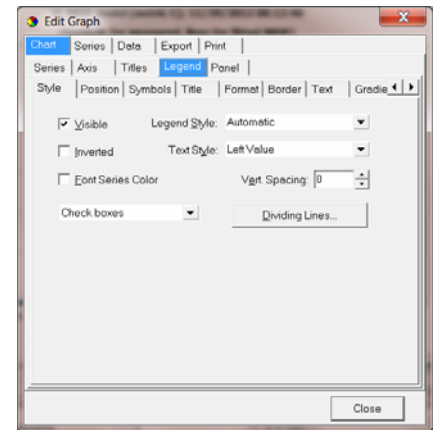
Fig. 15. Editing appearance of individual series (curves).



Editing graph axes

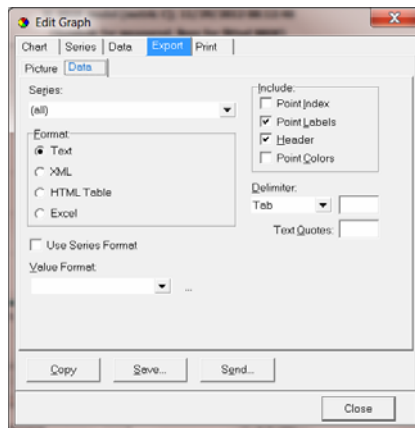


Editing graph title

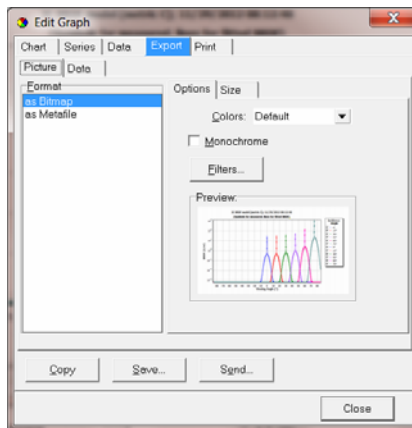


Formatting graph legend

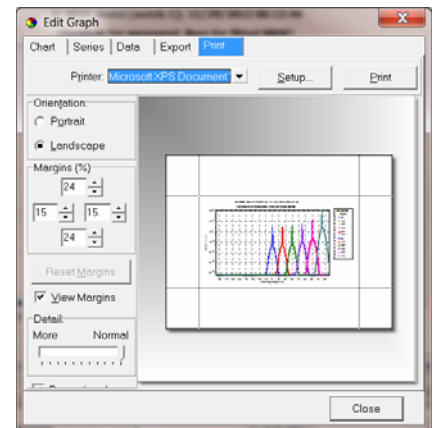
Fig. 16. Editing graph axes, title, and legend.



Data Export



Graph copying and saving



Graph printing

Fig. 17. Exporting capabilities of the Graph Editor.

7.3. Working with INCA333 3D Graphs

Three-dimensional (3D) graphs in INCA333 are intended for visualization of 3C BRDF model plotted in spherical coordinate system. It is supposed that $\phi_v = 180^\circ$ that is projection of the direction of incidence coincides with the x axis. Clicking **Plot 3D BRDF** button opens the window shown in Fig. 18.

Plots of 3D BRDF are interactive: user can change the incidence angle for real-time re-plotting. All controls placed on the tabbed page View instantly change the plot. When the checkbox "Normalize Plot" is checked, 3D BRDF at any incidence angle is scaled up by dividing by its maximum at the same angle; otherwise, dividing is performed by the maximum at normal incidence for all BRDFs. Fig. 19 demonstrates difference in these methods of normalization.

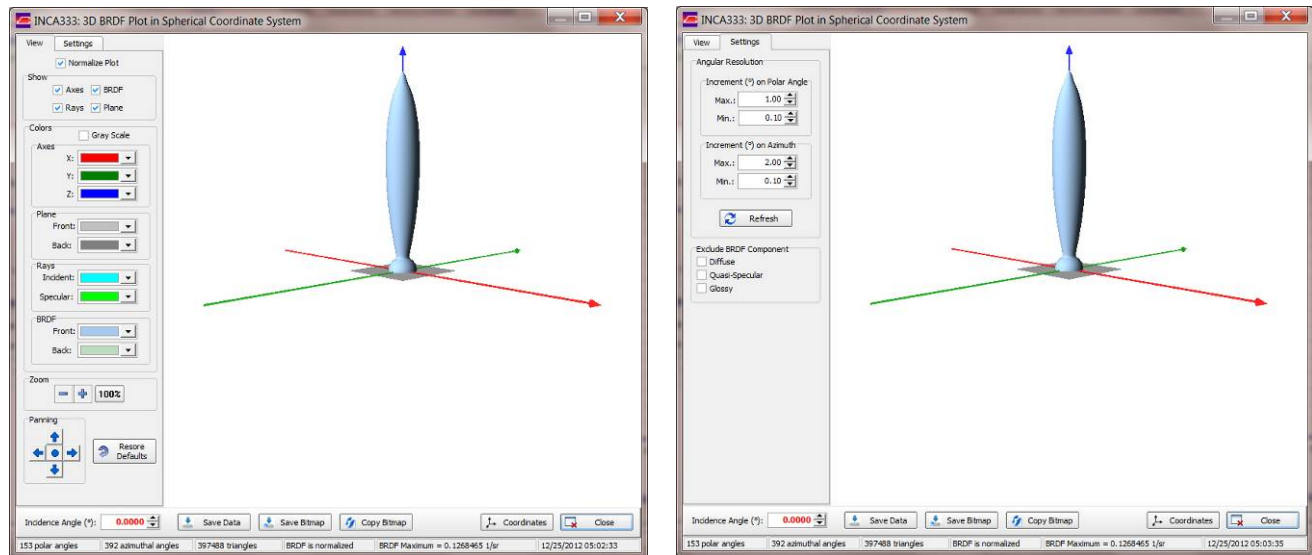


Fig. 18. 3D (hemispherical) BRDF plotted in spherical coordinates.
 Right-hand screenshot: tabbed page **View** is active;
 left-hand screenshot: tabbed page **Settings** is active.

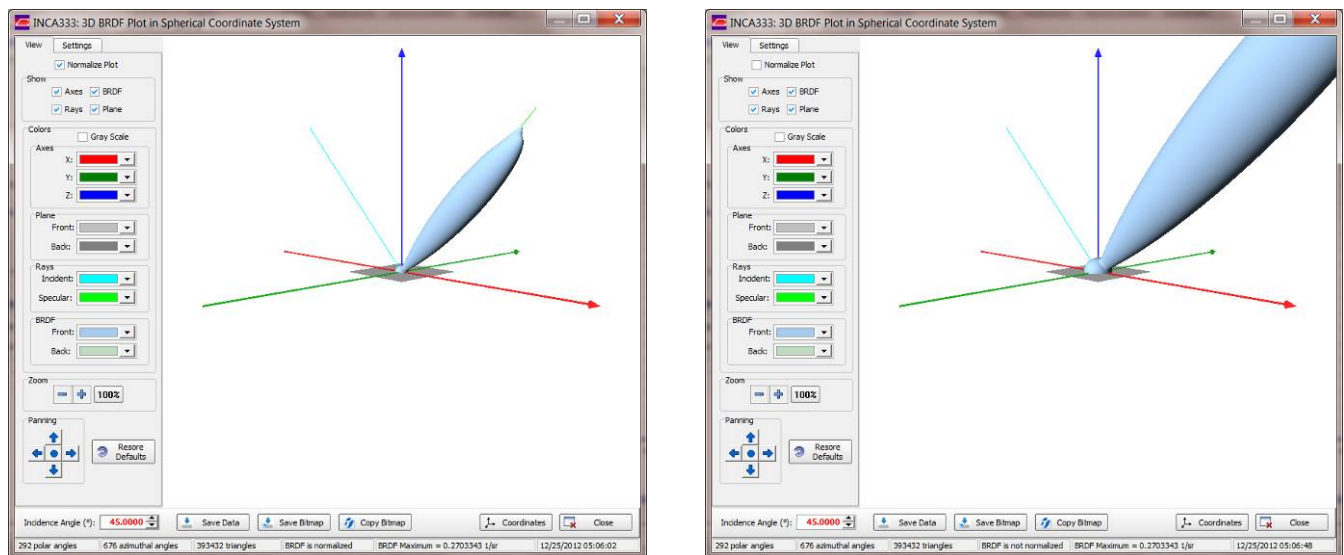


Fig. 19. 3D plots of the same 3C BRDF model using different normalization methods (checked/unchecked **Normalize Plot**).

If the checkbox “Normalize Plot” is checked, maximal value of the normalized BRDF equals 1 for any incidence angle. Uncheck this checkbox to watch angular behavior of the 3C BRDF model using the same scale of BRDF values for all incidence angles (see an example in Fig. 20).

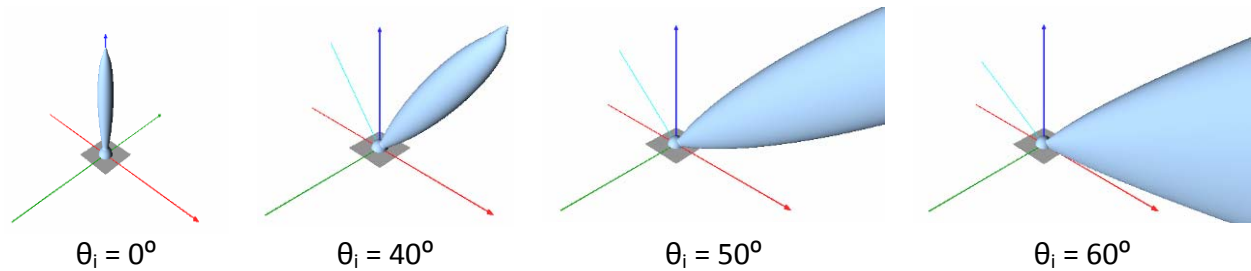


Fig. 20. 3C BRDF plots for fourth incidence angles θ_i at unchecked “Normalize Plot”.

The tabbed page “View” contains controls for changing visibility and colors of all 3D plot elements, zoom and pan tools. To restore the initial view click **Restore Defaults** button.

User can rotate the plot around three axes by moving mouse cursor over the image while mouse left button is pressed. Fig. 21 shows an example of such a modified view.

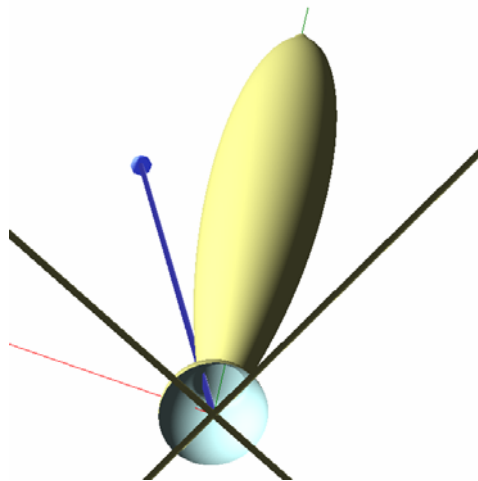


Fig. 21. An example of modified view of 3D BRDF.

If quasi-specular component of the 3C BRDF is too narrow to be plotted with the default angular resolution, the following notification message is appeared:

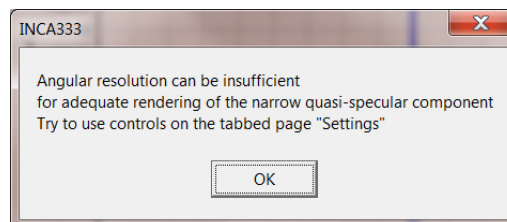


Fig. 22. Notification of possible insufficient angular resolution.

INCA333 employs non-uniform triangulation of the hemisphere to improve quality of 3D BRDF rendering. Nodes are arranged more densely toward the direction of specular reflection (see Fig. 23).

Angular resolution (and, therefore, rendering quality) is defined by values of minimal ($\Delta\theta_{v,\min}, \Delta\phi_{\min}$) and maximal ($\Delta\theta_{v,\max}, \Delta\phi_{\max}$) increments that can be varied in ranges specified in Table 4. User can try to change minimal and maximal increments then click **Refresh**. It should remember that the increase in the number of nodes leads to substantial reduction of rendering speed.

If increased angular resolution did not give the desired results, one can try to plot BRDF without quasi-specular component by setting $R_{qs} = 0$. Any component of the 3C BRDF model can be excluded from plot (and restored if necessary) using checkboxes in the tabbed page **Settings**. An example is shown in Figs. 23 and 24.

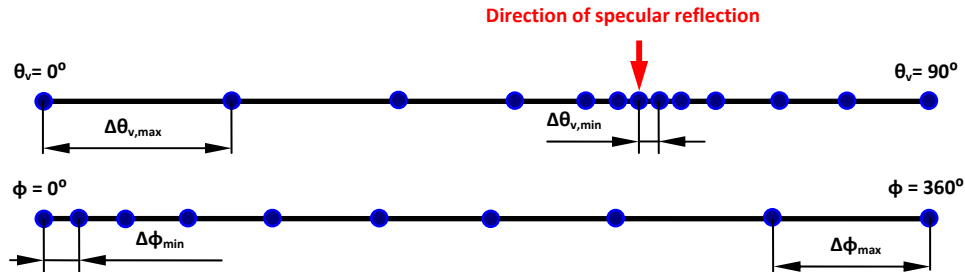


Fig. 23. Non-uniform arrangement of nodal points of hemispherical grid.

Table 4. Angular increment ranges.

		From	To
Polar angle	Min. increment (°)	0.05	1
	Max. increment (°)	0.5	10
Azimuth	Min. increment (°)	0.05	1
	Max. increment (°)	2	10

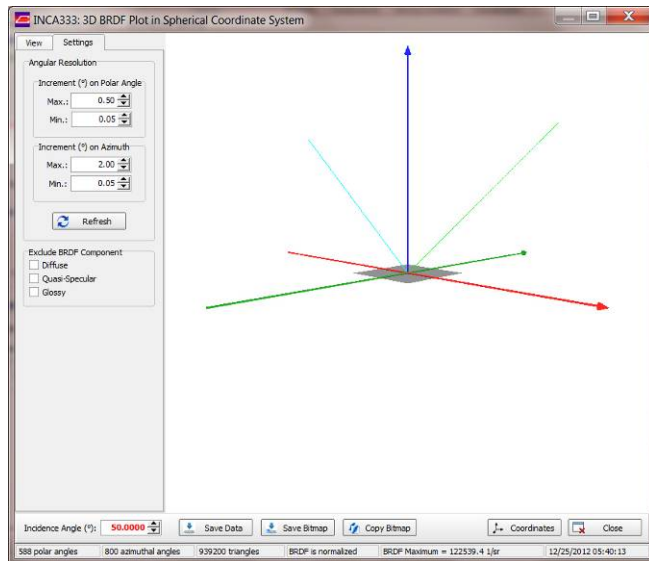


Fig. 24. BRDF cannot be plotted at maximal angular resolution due to very narrow quasi-specular peak.

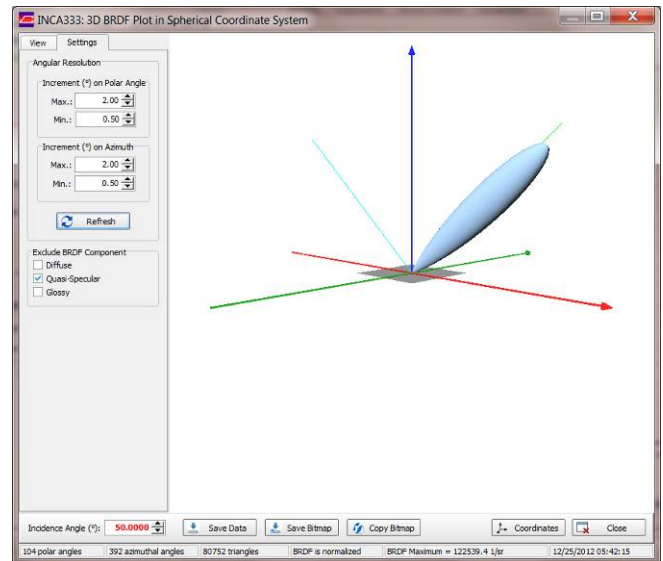


Fig. 25. The same BRDF plotted without quasi-specular component at the default resolution.

The following buttons provide exporting capabilities for 3D BRDF:

Save Data saves 3D BRDF data in text file (see examples in *Data\Output\BRDF3D*);

Save Bitmap saves image in *.bmp file (see examples in *Data\Output\Images*);

Copy Bitmap copies image to clipboard.

To see coordinate system, click **Coordinates** (see Fig. 26).

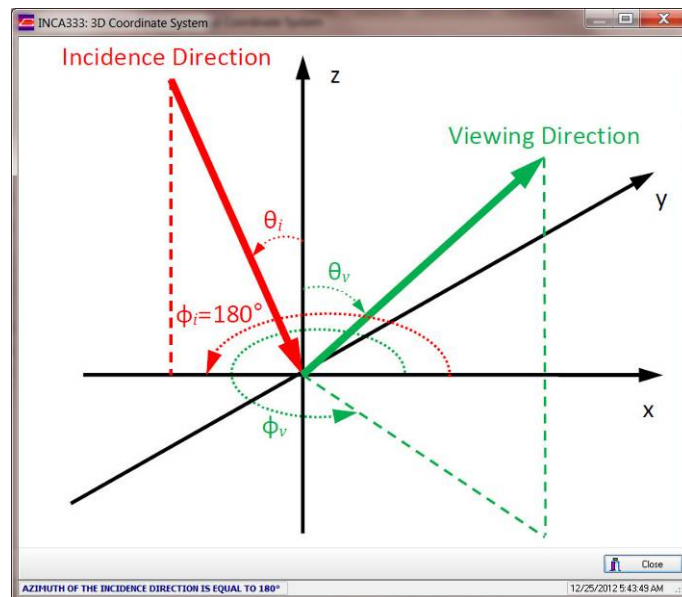


Fig. 26. Window displaying the Cartesian and spherical coordinate systems used for 3D BRDF plots.

7.4. Activating INCA333. Evaluation vs. Full-Functioned Version

In distinct of full-functioned program, the evaluation version does not allow to enter new or drastically modify existing records in **DATASETS**, **MATERIALS**, and **FITTING** databases. Instead, the Evaluation version allows to learn INCA333 working principles, to investigate examples included in databases and data files, plot graphs, etc. The evaluation version of INCA333 can be downloaded for free from www.virial.com. To obtain activation key and activate INCA333 you have to purchase the license. Activation transforms the evaluation version into full-functioned program.

Download the evaluation version. It does not require installation. Just unzip INCA333.zip and place INCA333 folder to convenient place on your hard drive. Open the folder *INCA333* and run *INCA333.exe*. The main window will appear (see the left-hand screenshot in Fig. 27). If the license is purchased, INCA333 can be activated by clicking **Activate** button. The Activation window will appear (see Fig. 28).

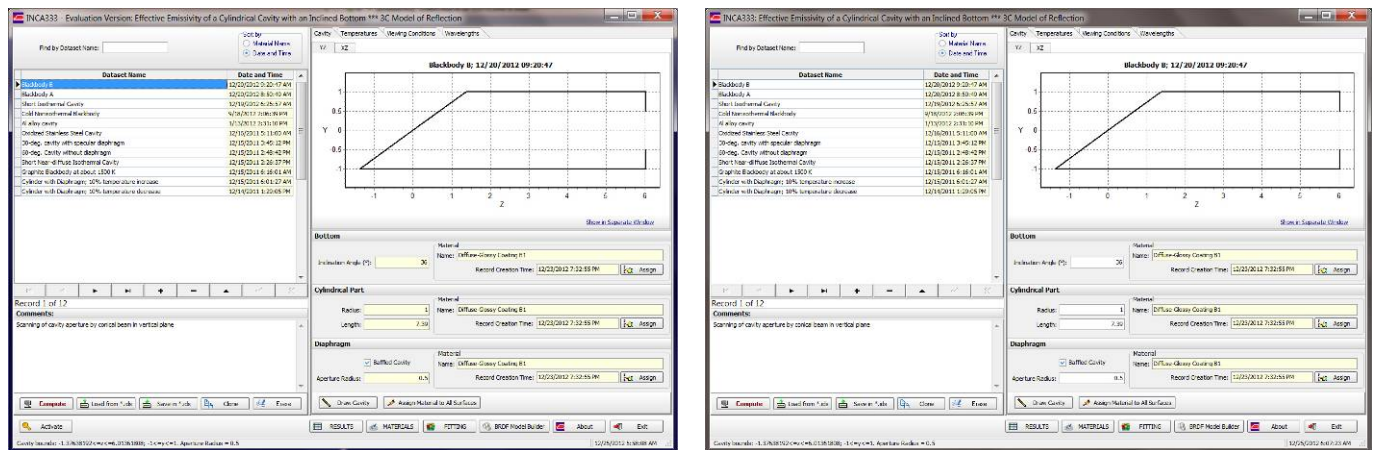


Fig. 27. INCA333 main window before (left-hand screenshot) and after (right-hand screenshot) activation.

Enter the activation key and click **OK**.

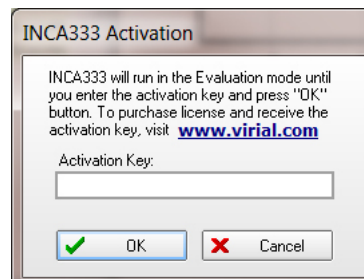


Fig. 28. INCA333 Activation window

To finalize activation, read and accept the INCA333 Software License Agreement (Fig. 29). One can read this document in the Appendix. The screenshot of the activated INCA333 main window is shown in the right-hand screenshot in Fig. 27.

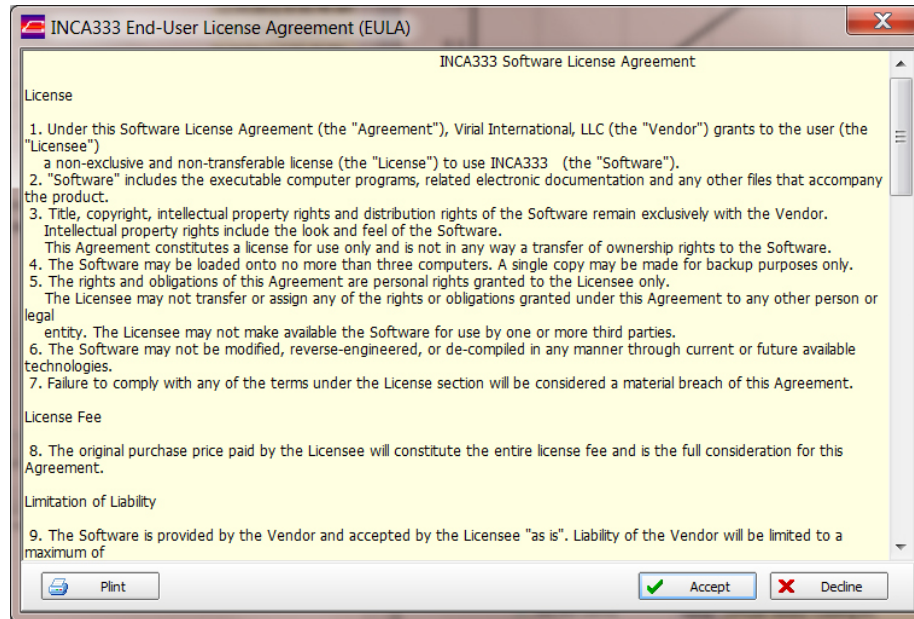


Fig. 29. INCA333 activation must be finalized by accepting the end-user license agreement.

That's all. Now, you can start solving your tasks with INCA333. We recommend to adhere the following workflow:

1. If experimental BRDF data are available, fit parameters of 3C BRDF model to BRDF data measured at one wavelength and at 2 to 6 incidence angles. The more incidence angles the more reliable fitting results. If there are no experimental BRDF data available, use BRDF Model Builder to build the 3C BRDF model from scratch, e. g., on the basis of some indirect information about reflection properties of a material.
2. If experimental SDHR data are available, perform spectral splitting of the SDHR measured at one incidence angle to determine SPRs R_d , R_{gs} , and R_g for every wavelength for which SDHR is measured. If you haven't measured SDHR data, perform spectral DHR splitting at one wavelength for which your model was created.
3. Export your model's data to the MATERIALS database.
4. Repeat steps 1 – 3 for all materials used for cavity walls.
5. Enter new dataset name (and optional comments) to the DATASETS database.
6. Enter geometrical parameters of the cavity.
7. Assign materials to each surface forming the BB.
8. Select which BB you'll model: isothermal or nonisothermal.
9. Enter reference and background temperatures (skip this step for the isothermal BB).

10. Enter positions of temperature points and on the cavity generatrix (skip this step for the isothermal BB).
11. Assign temperatures for the temperature points (skip this step for the isothermal BB).
12. Select the type of viewing conditions for which MCRT should be performed.
13. Enter geometrical parameters of viewing conditions.
14. Perform targeting to check correctness of viewing conditions specified.
15. Enter wavelengths (1 to 501) for which MCRT should be performed.
16. Check interpolation quality of the SPRs for each material used in your dataset; change wavelength set if necessary.
17. Perform MCRT with moderate values of accuracy parameter (e.g., for 10,000 rays traced) to evaluate the necessary values of rays and time required to trace them.
18. Perform Monte Carlo calculations with the accuracy enough for your goals.
19. Browse results of calculations in the **RESULTS** database, plot dependences of EE (and RT, for non-isothermal cavity) on wavelength and/or on variable viewing conditions parameter.
20. If necessary, save results and report in text files.

8. The BRDF Model Builder

8.1. Working with Monochromatic BRDF Model

If experimental data for BRDF is incomplete or absent, you still can build the 3C BRDF model based on some indirect information about angular properties of material's reflection. Such a model might be useful at the blackbody design stage for material selection as well as for parametric investigation of dependences of blackbody radiation characteristics on angular reflection properties of cavity walls. To open the BRDF Model Builder, click **BRDF Model Builder** button on the bottom panel of the main INCA333 window (Fig. 27). Fig. 30 shows the BRDF Model Builder; it has two tabbed pages: "Monochromatic 3C BRDF Model" and "Spectral DHR Splitting".

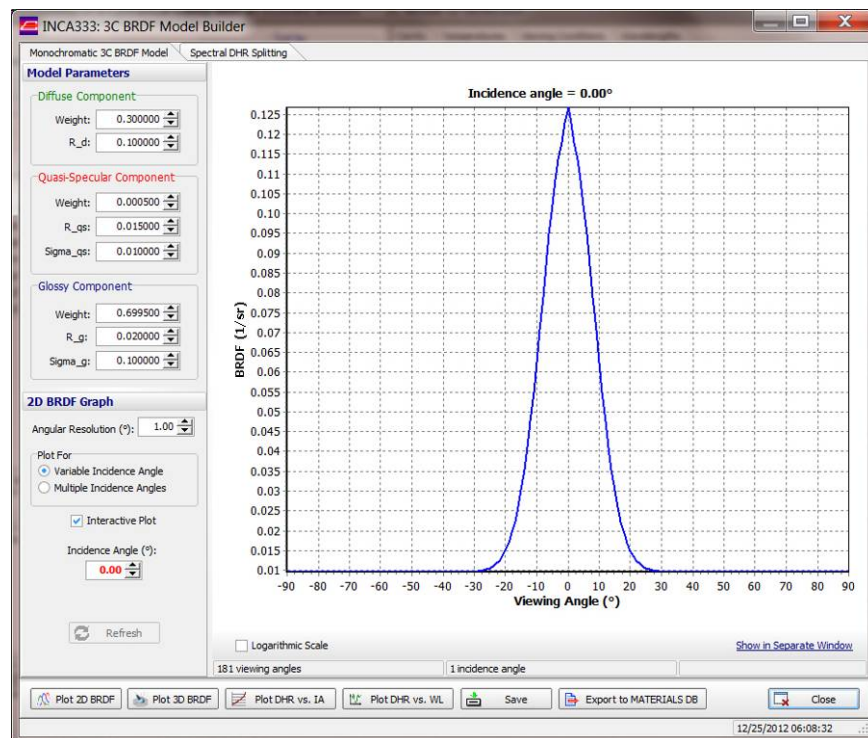


Fig. 30. The BRDF Model Builder: the **Monochromatic 3C BRDF Model** tabbed page is selected; 2D BRDF is plotted for one incidence angle

The left-hand panel of the "Monochromatic 3C BRDF Model" tabbed page contains controls for entering parameters of monochromatic 3C BRDF model and plotting its 2D graphs. Switches **Plot For** allow to choose between plotting for one and for up to 6 incidence angles in one graph. In the first case, if the **Interactive Plot** checkbox is checked, graph will be re-plotted immediately, as soon as angular resolution, incidence angle or any parameter of the model is changed. If **Interactive Plot** is unchecked, user has to click **Refresh** button additionally. The last option can be more convenient when all three

components have non-zero weights since their normalization is performed just after changing one of their values.

To plot 2D BRDF for multiple incidence angles, select **Multiple Incidence Angle** in the **Plot For** switch; enter minimum, maximum, and number of incidence angles, then click **Refresh** (see Fig. 31). Component weights will be also normalized automatically before plotting.

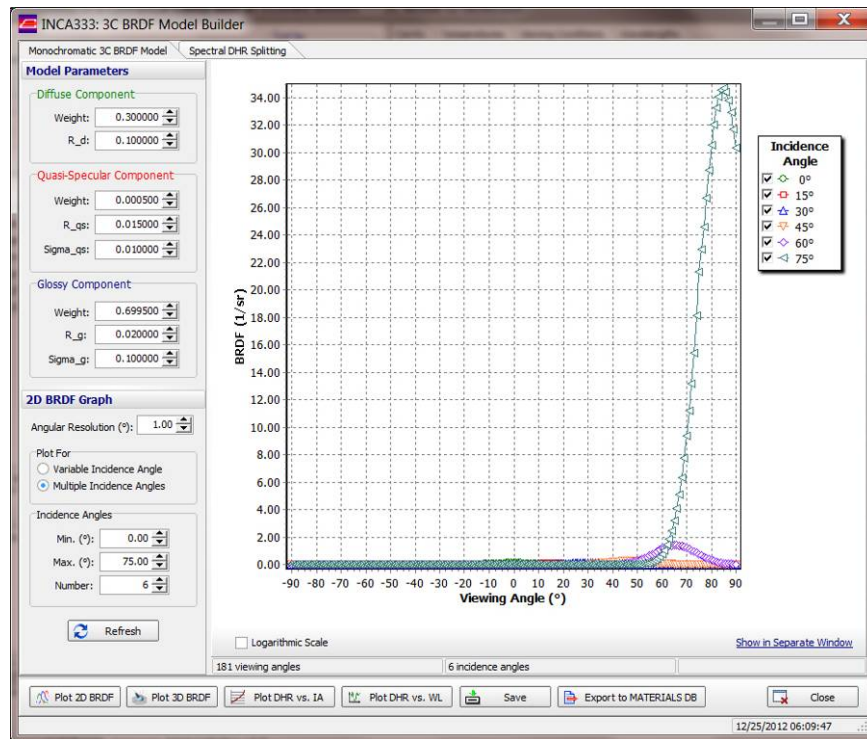


Fig. 31. The BRDF Model Builder: the **Monochromatic 3C BRDF Model** tabbed page is selected; 2D BRDF is plotted for 6 incidence angles

8.2. Making the Model Wavelength-Dependent

Method of SDHR separation into components of the 3C model (SDHR splitting) is described in Section 3.8. Application of spectral splitting to the SDHR measured within some finite wavelength range makes the 3C BRDF model wavelength-dependent. To transform the monochromatic model onto wavelength-dependent one, select the tabbed page "Spectral DHR Splitting" (see Fig. 32). Click **Load** to open a text file containing SDHR. A fragment of such a file is shown in Fig. 33. First line comprises the value in degrees of the incidence angle at which SDHR was measured; the text starting from "//" is considered as comments and will be ignored; next lines consist of wavelength in μm and SDHR itself separated by at least one space or <Tab> symbol. These values will be loaded into two first columns of the table and plotted in the graph (see Fig. 31). Examples of similar files can be found in the subfolder **Data\Input\Fitting\SDHR**.

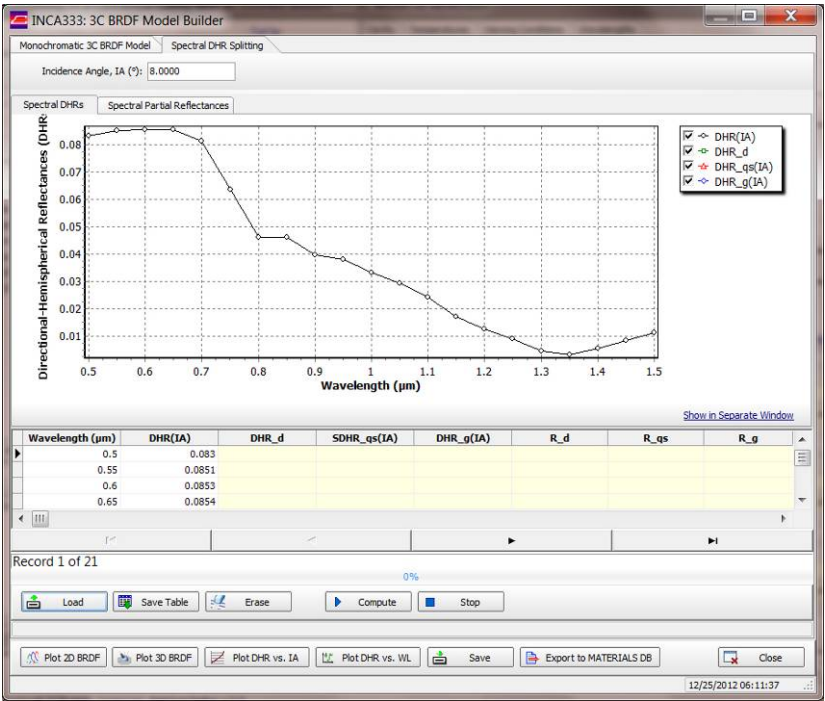


Fig. 32. The BRDF Model Builder; the **Spectral DHR Splitting** tabbed page is selected.

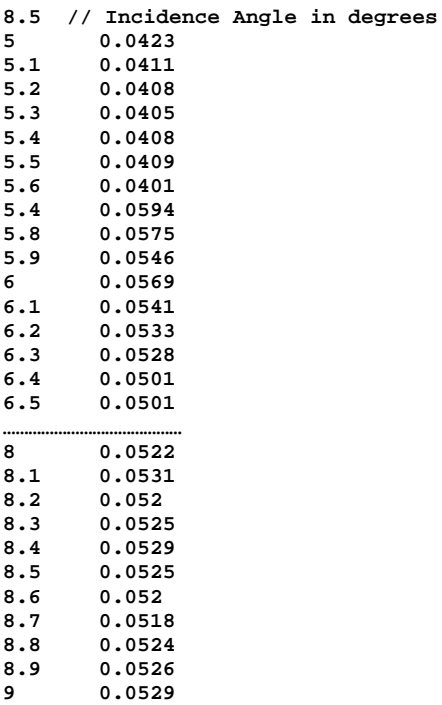


Fig. 33. A fragment of text file containing SDHR.

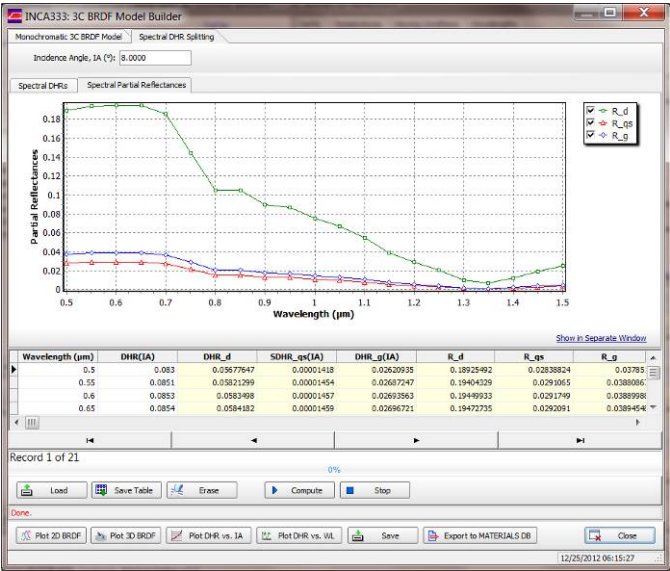
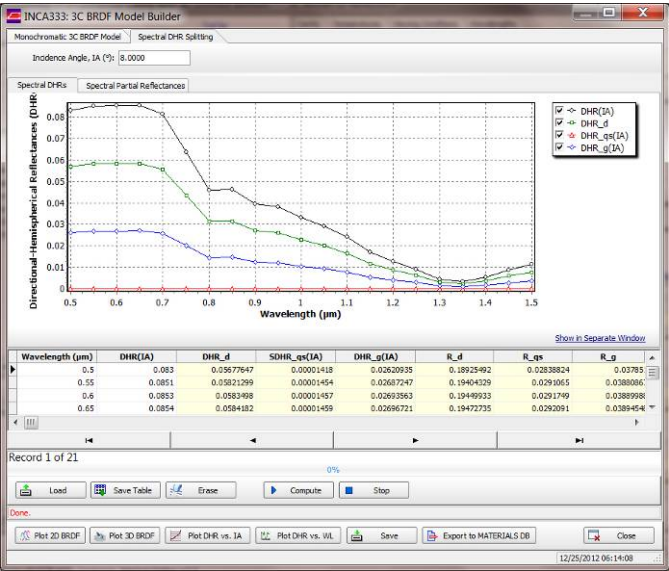


Fig. 34. Results of the spectral splitting.

Click **Compute** button. The SDHR loaded will be split wavelength-by-wavelength onto partial SDHRs $\rho_d(\lambda, \theta_{i,0})$, $\rho_{qs}(\lambda, \theta_{i,0})$, and $\rho_g(\lambda, \theta_{i,0})$, where $\theta_{i,0}$ is the incidence angle which appeared in the input field

at the top in Fig. 32. Simultaneously, SPRs $R_d(\lambda)$, $R_{qs}(\lambda)$, and $R_g(\lambda)$ will be computed, entered into the table, and plotted. Fig. 34 shows the results of spectral splitting. Calculations can be interrupted at any time by clicking **Stop** button.

Since k_d , k_{qs} , and k_g are related by Eq. (13) and inequality (21), for every BRDF model there is certain range of SDHR values for which a solution exists, that is values of BRDF and SDHR must be self-consistent. Otherwise, SPRs cannot be found within interval $[0, 1]$, i.e. physically plausible solution does not exist. The following notification will appear in such a case:

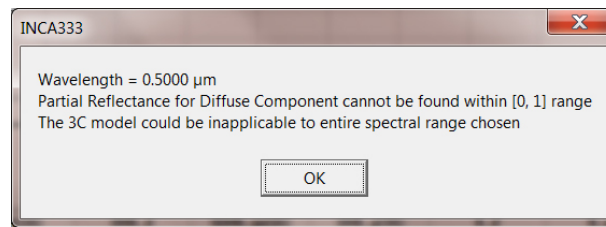


Fig. 35. Notification of inconsistency of 3C BRDF model and SDHR.

Results of calculation (entire table) can be saved in text file by clicking **Save Table** button. The complete 3C BRDF model can be save in MATERIALS database by clicking **Export to MATERIALS DB**. Before exporting, the Material Name will be requested (Fig. 36). On can use any sequence of up to 100 symbols.

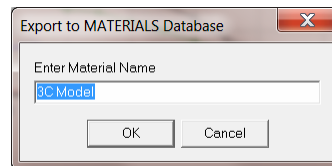


Fig. 36. Request for the name under which the 3C Model will be stored in MATERIALS database.

BRDF Model Builder does not store modeling results, thence the user should take care to export results to **MATERIALS** database or save (by clicking **Save**) in a binary *.3C file the model he built.

8.3. BRDF Plotting

When it is necessary to plot 2D BRDF for a specific wavelength (for a specific record in the table at the bottom of the tabbed page **Spectral DHR Splitting**, see Fig. 34), click **Plot 2D BRDF**. The window shown in

Fig. 37 will appear. The actual wavelength is indicated in the white panel of the status bar. For description of functions for buttons in the lower panel see Section 7.2.

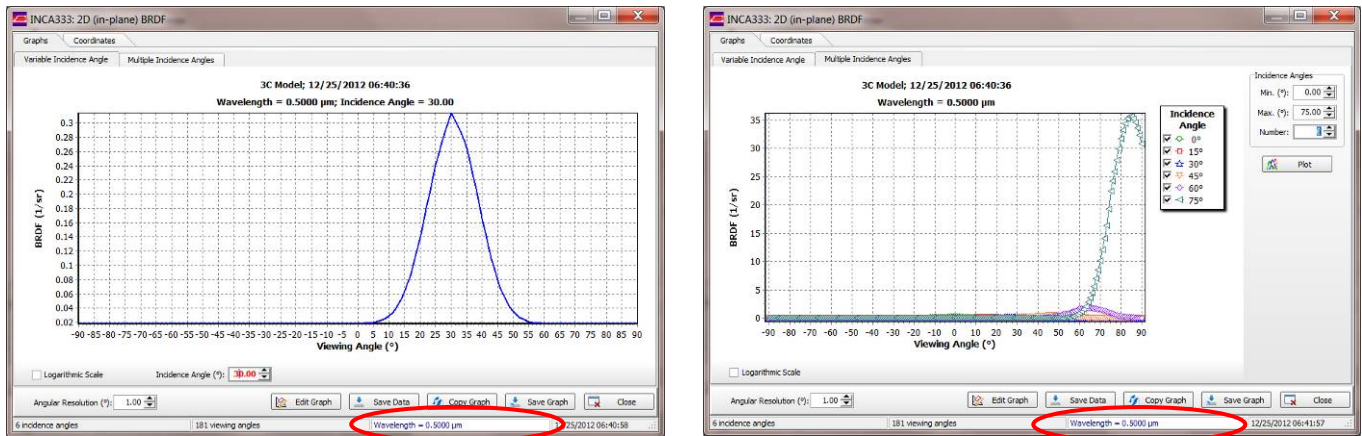


Fig. 37. 2D graphs plotted for $\lambda = 0.5 \mu\text{m}$ (circled in red).

If SPRs are not calculated (corresponding fields in the table are empty), BRDF will be plotted for monochromatic model (see Fig. 38); generally, plots will be the same and can be handled in the same manner as those in Figs. 30 and 31.

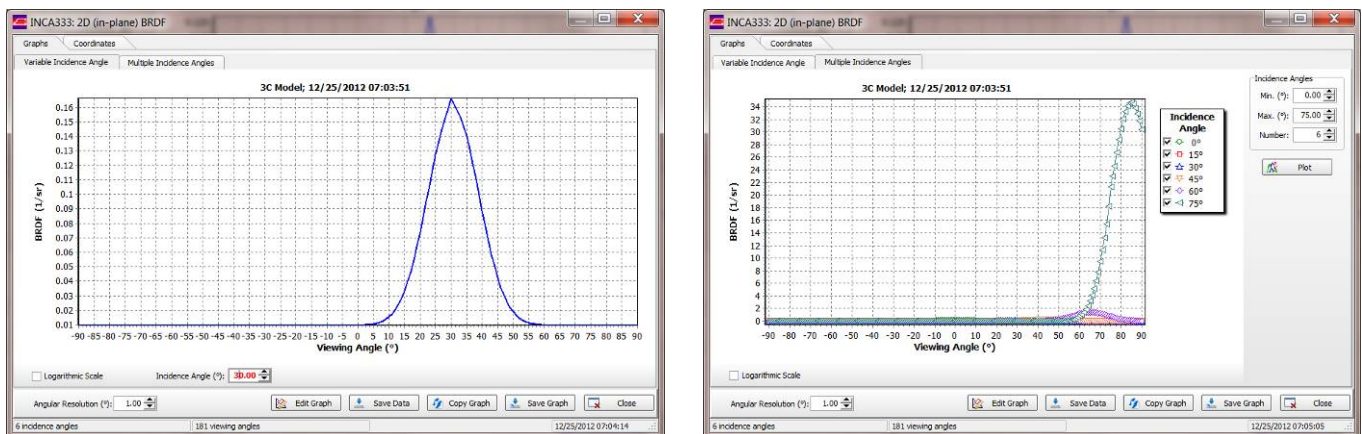


Fig. 38. 2D graphs plotted for monochromatic model (wavelength is not specified).

The tabbed page **Coordinates** shows 2D Cartesian and polar coordinate systems and explains viewing angle signs (see Fig. 39).

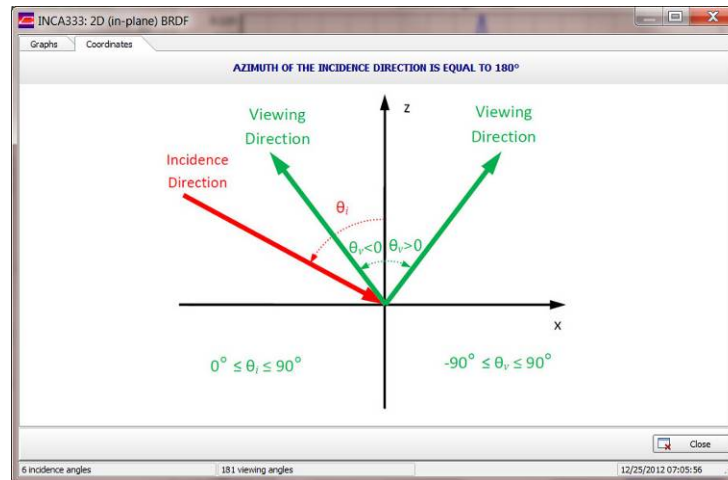


Fig. 39. 2D Cartesian and polar coordinate systems.

To plot 3D BRDF for a specific wavelength, click Plot **3D BRDF**. The only difference of the windows appeared from that shown in Fig. 18 is the white panel showing actual wavelength (see Fig. 40).

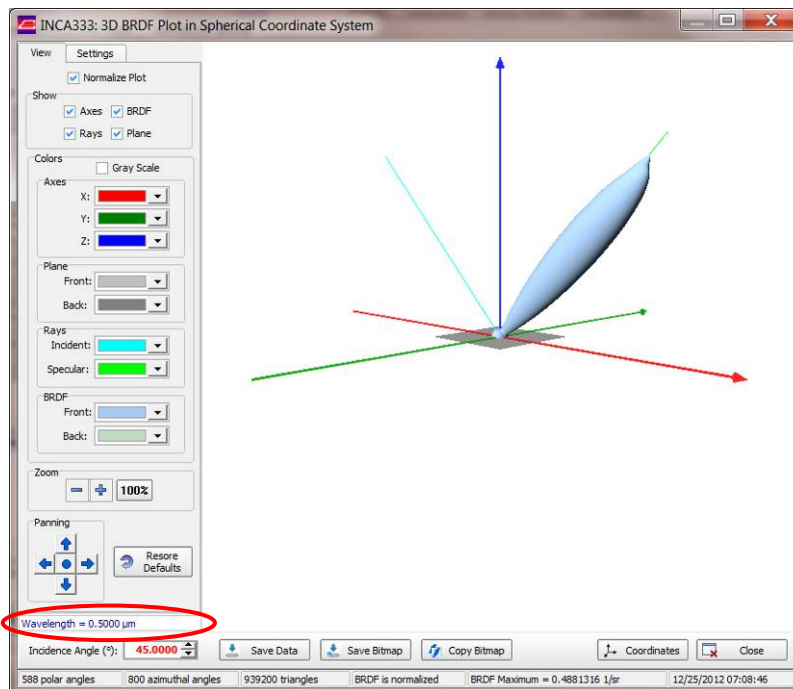


Fig. 40. 3D BRDF plot for $\lambda = 0.5 \mu\text{m}$ (circled in red).

8.4. DHR Calculation

BRDF Model Builder provides a possibility to compute dependence of DHR on incidence angle at a given wavelength by clicking **Plot DHR vs. IA** button (see Figs. 30-32, 34). Like in the case of BRDF plotting, wavelength at which DHR is computed is corresponding to the current record in the SDHR table. If this table is empty, or spectral splitting is not performed yet, DHR will be computed for the monochromatic BRDF model for which wavelength does not defined. Figs. 41 and 42 show the window for calculating DHR vs. incidence angle before and after calculations.

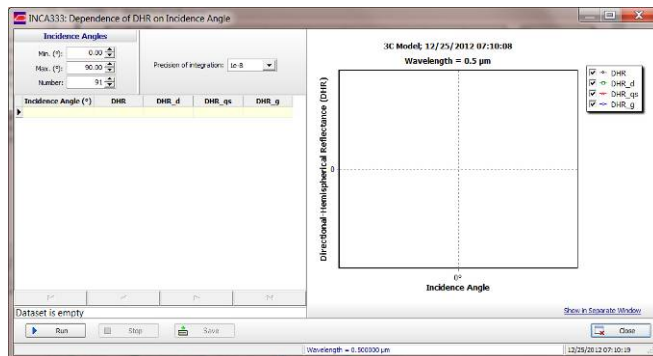


Fig. 41. Window for calculating DHR vs. incidence angle before calculations.

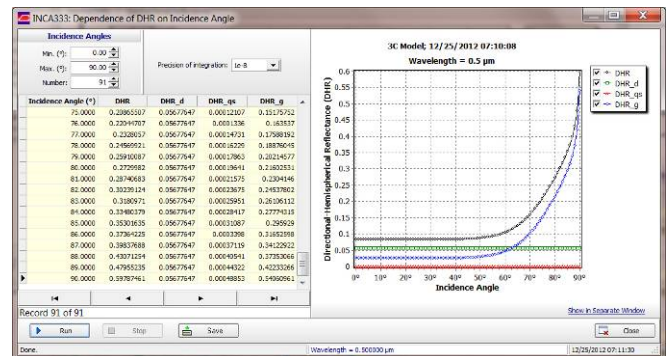


Fig. 42. Window for calculating DHR vs. incidence angle after calculations.

User has to enter min. and max. incidence angles and their number as well as allowable relative error of adaptive integration (or remain unchanged their default values). Calculations start by clicking **Run** button and will be performed for incidence angles uniformly distributed between their min. and max. values. Computed DHR and their components will be shown in the table and plotted (see Fig. 41). Calculations can be interrupted at any time by clicking **Stop**. Results can be saved as a text file by clicking **Save**. Examples of such files can be found in the **Data\Output\DHR** folder.

If spectral splitting is done, one can compute SDHR and its components for a given incidence angle as a function of wavelength. Click **Plot DHR vs. WL** button (see Figs. 30-32, 34) to open the window shown in Fig. 43. If there are no spectral splitting data, the message “No spectral data found” will be displayed.

Enter the incidence angle for which SDHR has to be computed and allowable relative error of adaptive integration (or remain unchanged their default values) and click **Run**. Fig 44 shows the window for calculating DHR vs. wavelength after performing calculations. Like in the previous case, calculations can be interrupted at any time by clicking **Stop**. Results can be saved as a text file by clicking **Save**. Examples of such files can be found in the same **Data\Output\DHR** folder.

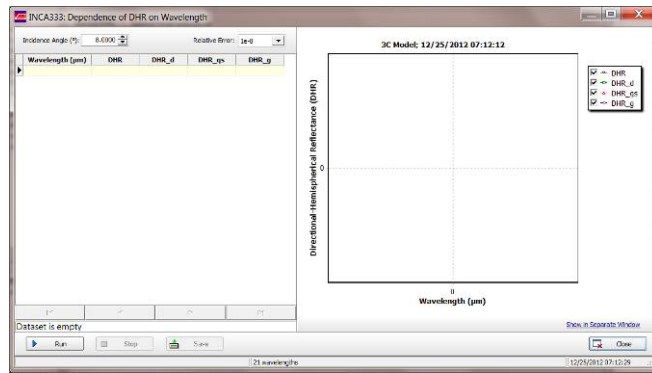


Fig. 43. Window for calculating DHR vs. wavelength before calculations.

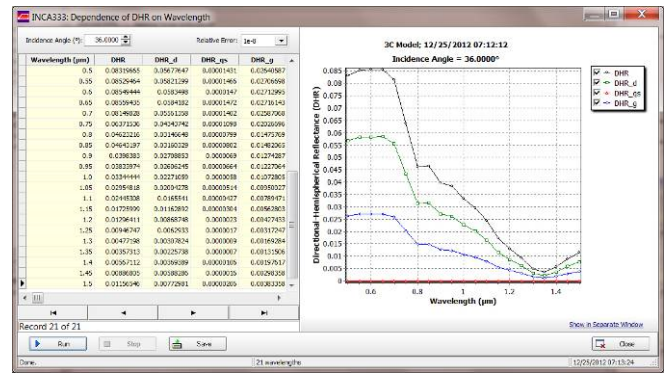


Fig. 44. Window for calculating DHR vs. wavelength after calculations.

9. The FITTING Database

9.1. BRDF Fitting

To open the FITTING database with its own tools for BRDF fitting and spectral DHR splitting, click FITTING button in the main INCA333 window (Fig. 27). The FITTING database window will be opened (Fig. 45).

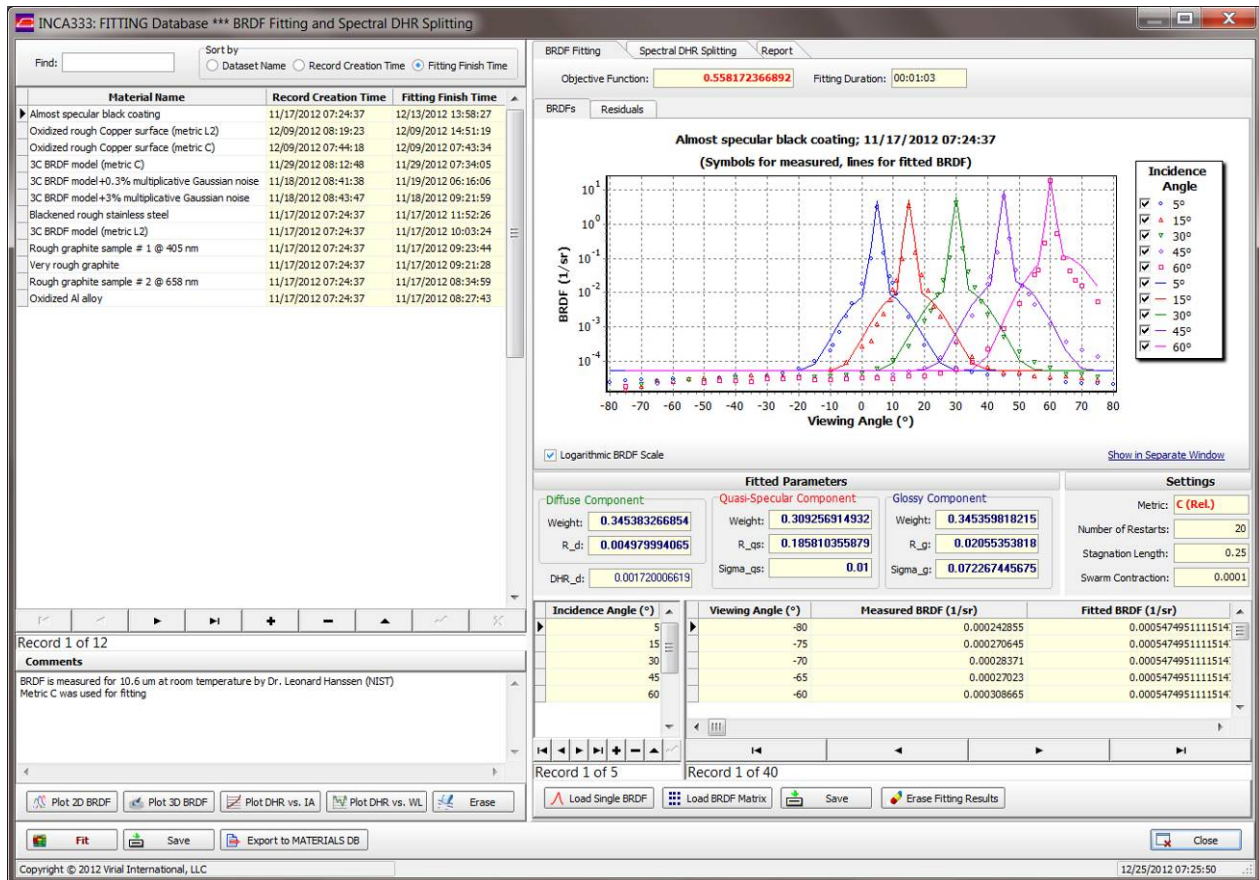


Fig. 45. The FITTING database window; the tabbed page “BRDF Fitting” is selected.

To create a new record click **Insert Record (+)** button of the Database Navigator under the table in the left panel and enter the name of material (up to 100 symbols) in the first column. Optionally, one can enter in the text field “Comments” some additional text information which can be useful for further identification of your task. The next step is to enter experimental BRDF data.

There are two possibilities to enter measured BRDF data from text files of two different formats. The first way is to enter BRDF for each incidence angle successively, angle-by-angle, by clicking **Load Single**

BRDF. This way must be used if BRDFs for different incidence angles contain different sets of viewing angles. The text files of the format shown in Fig. 46 must be prepared:

```

5 // Incidence angle (deg.)
-80 0.000242855
-75 0.000270645
.....
-55 0.000284425
-50 0.00028157
-45 0.000320945
-40 0.000364755
.....
-10 0.0020117
-9 0.003
-7 0.0068
-5 0.02
-3 0.05
0 0.178
3 0.95154
5 30.8345
7 1.43985
9 0.28840315
.....
30 0.00065106
35 0.000474505
40 0.000396925
.....
75 0.000226735
80 0.000217455

```

Fig. 46. A fragment of text file that contains BRDF for one incidence angle.

The first line must contain the incidence angle in degrees; the text beginning from “//” is a comment and can be omitted. In next lines, the first column contains viewing angle in degrees; negative viewing angles correspond to backscattering (see Fig. 39). The second column contains BRDF values in sr^{-1} . Columns must be separated by at least one space or <Tab> symbol. Such a file can be prepared in any text editor, e.g. Microsoft® Notepad, or using Microsoft® Office Excel and saving spreadsheet as Text (Tab-delimited) file. Text files must be prepared for each incidence angle. Some examples can be found in the **Data\Input\FITTING\BRDF** folder.

The second way is to enter BRDFs for all incidence angles at once by clicking **Load BRDF Matrix**. In this case, the set of viewing angles must be the same for all incidence angles. BRDF can be represented as a rectangular matrix having $n_i + 1$ columns and n_v rows, where n_i and n_v are numbers of incidence and viewing angles, respectively. The first line of the file must contain the number of incidence angles; the second line contains incidence angles in degrees. Next lines comprise of viewing angle in degrees and BRDFs in sr^{-1} for each incidence angle separated by at least one space or <Tab> symbol. A fragment of such a text file is shown in Fig. 48. The text beginning from “//” is optional and can be omitted; it will be ignored when the file is reading. Several examples of such files can be found in the **Data\Input\FITTING\Matrix** folder. The data loaded will be saved in the FITTING database, displayed in the graph, and shown in the table for each incidence angle.

```

3 // Number of incidence angles
6.00000 30.50000 60.75000 // Incidence angles in degrees
-78.000000 7.17034571290718E-0003 4.41403593868017E-0003 5.08488016203046E-0003
.....
-30.000000 2.61244092941532E-0002 6.23390404507518E-0003 3.71623015962541E-0003
.....
0.000000 2.80166030219057E-0001 2.64115063473582E-0002 9.43411141633987E-0003
.....
15.000000 8.57154841527054E-0002 1.05795558542013E-0001 1.74595601856709E-0002
.....
30.000000 2.61244092941532E-0002 3.74778434634209E-0001 4.93410490453243E-0002
.....
60.000000 8.14418229106762E-0003 4.90448214113712E-0002 1.10970735549927E+0000
.....
78.000000 7.17034571290718E-0003 2.86295469850302E-0002 5.05613118410110E-0001

```

Fig. 47. A fragment of text file that contains BRDF matrix.

To start fitting, click **Fit** button. The **BRDF Fitting Monitor** window will appear (Fig. 48). Its right part contains two graphs: the upper is for real-time displaying measured and fitted BRDFs and the lower for displaying residuals. The red arrow in Fig. 48 shows the splitter that allows to change relative sizes of both graphs (by dragging splitter using the mouse or other pointing device) or to collapse one of graphs completely (by clicking the left or right segment of the splitter).

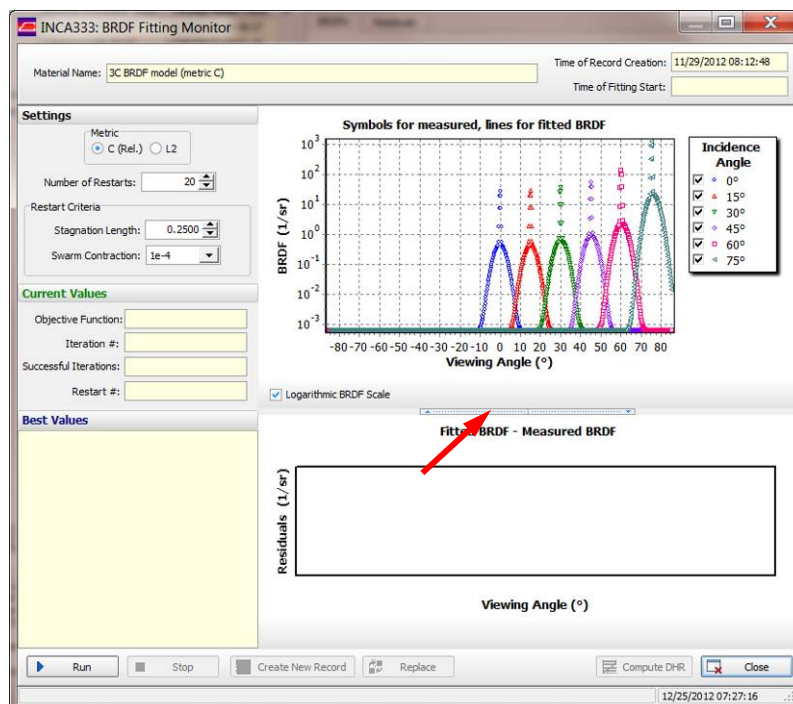
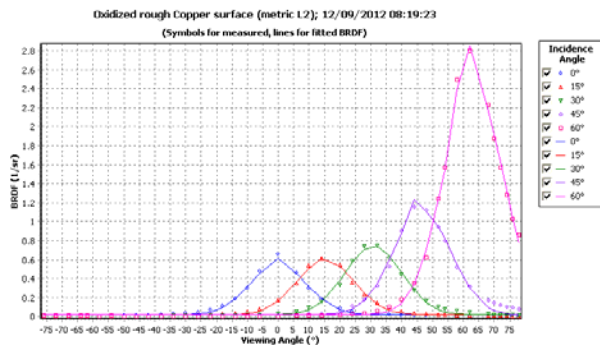


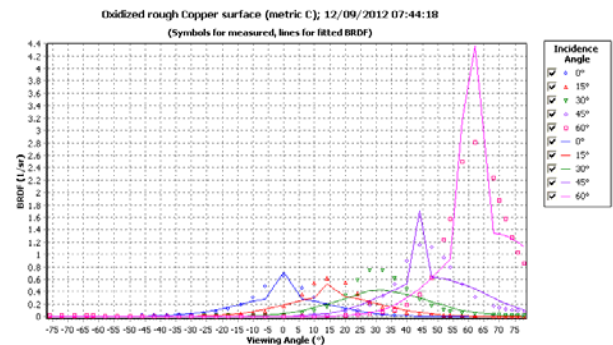
Fig. 48. The BRDF Fitting Monitor window. The red arrow points at the splitter.

First, the metric (see Eqs. (24) and (25)), which will be used for fitting has to be chosen. Due to variety in shape of BRDFs for various materials, it is hard to exactly predict which metric (L_2 or C) is more appropriate in certain case; however one can formulate a common rule which is illustrated by two examples below.

For smooth BRDF curves with moderate dynamic range, metric L_2 gives the best result while the result obtained with the metric C is unsatisfactory (Fig. 49).



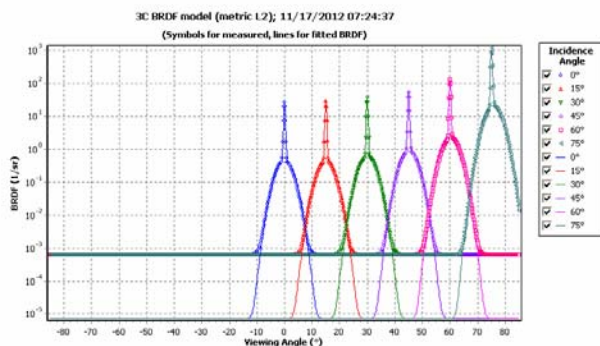
Metric L_2 – good fitting quality



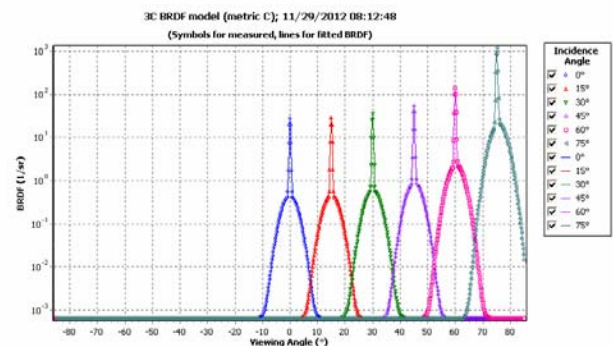
Metric C – poor fitting quality

Fig. 49. Fitting performed for the same smooth BRDF using metrics L_2 and C .

For unsmooth BRDFs, especially for BRDFs whose dynamic ranges are of several orders of magnitude (this concerns BRDFs having sharp specular and glossy peaks against low diffuse component), the metric L_2 , as a rule, gives the worst fitting results in comparison with metric C because it tends to average the BRDF values (see Fig. 50).



Metric L_2 – poor fitting quality



Metric C – good fitting quality

Fig. 50. Fitting performed for the same sharp BRDF using metrics L_2 and C .

As it was already mentioned in Section 3.7, INCA333 uses multiple restarts strategy to avoid false convergence to local minima of the objective function and prevent stagnation (state when the PSO algorithm cannot find the better solution during a large number of iterations). The fitting reliability is defined by the Number of Restarts, the Stagnation Length and the Swarm Contraction, which default values user can vary widely. However, only for experienced users we can recommend changing these parameters.

Click **Run** to start fitting. User can watch the fitting process numerically (current values the objective function, model parameters and DHR of the diffuse component, iteration number, number of successful iterations and number of restarts) and in two graphs; they will be re-plotted as soon as the next better solution is found (see Fig. 51). To interrupt fitting at any time, click **Stop**.

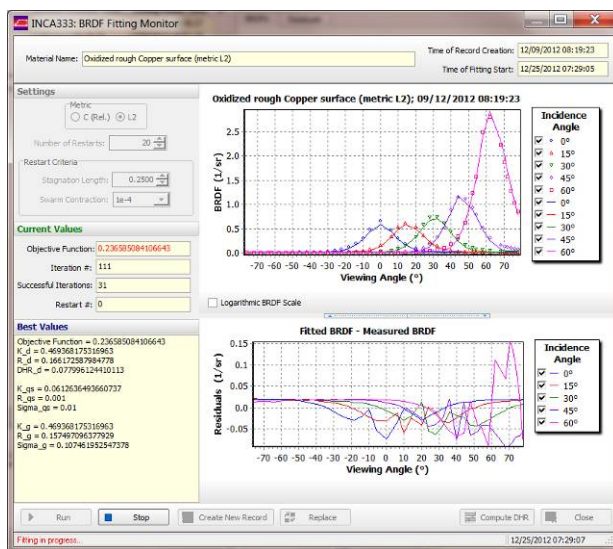


Fig. 51. The Fitting Monitor window: fitting is in progress.

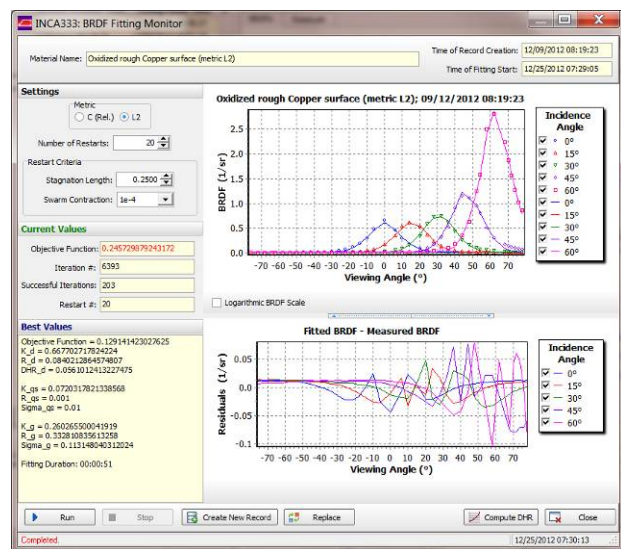
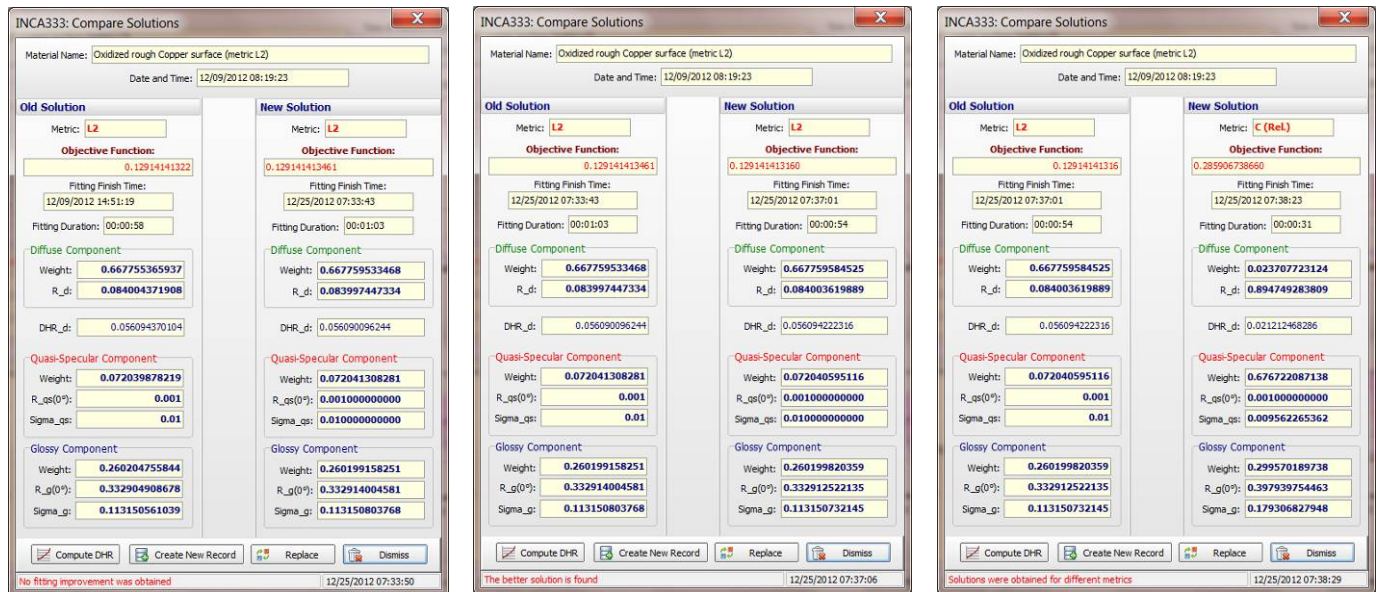


Fig. 52. The Fitting Monitor window: fitting is done.

Fig. 52 shows the BRDF Fitting Monitor for the fitting finished. When fitting is completed or interrupted, user has a possibility to compare new solution with the old one stored (if any) in the FITTING database. Three possible cases are shown in Fig. 53. User should decide to save new solution in the FITTING database by replacing the old one, or to dismiss the new solution.

Usually, the best choice for the first case (No fitting improvement was obtained) is clicking **Dismiss**. For the second case (The better solution is found) user can choose between **Create New Record** and **Replace**. To make a choice in the third case when old and new solutions were obtained for different metrics, we recommend to choose **Dismiss**. User will be able to save new solution in the FITTING database later, after additional thorough comparison of new solution with old one.



No fitting improvement was obtained

The better solution is found

Solutions were obtained for different metrics

Fig. 53. Three possible cases of comparing new and old solutions.

The **Compare Solutions** window will be closed at any choice but user still can save new the solution in the **FITTING** database by clicking **Create New Record** or **Replace** in the **BRDF Fitting Monitor** window (see Fig. 52). Besides, **Compute DHR** buttons of both **BRDF Fitting Monitor** and **Compare Solutions** windows allow computing the dependence of DHR on the incidence angle for the fitted model.

The fitted BRDF and model's parameters can be erased by clicking **Erase Fitting Results** button in the **FITTING** database window (Fig. 45). After an affirmative answer to confirmation request, erased data cannot be restored. The measured and fitted BRDFs can be saved in text file using the **Save** button. Examples of these files can be found in **Data\Output\Fitting Results** folder.

9.2. Spectral DHR Splitting

Method of SDHR splitting is described in Section 3.8; its use in the **FITTING** database is analogous to that described in Section 8.3. Open the tabbed page "Spectral DHR Splitting" of the **FITTING** database window (see Fig. 54). If the spectral DHR separation for the current material was not performed yet, both graphs and the table beneath them will be empty. To enter SDHR from the text file click **Load**. The text file must be prepared as it was shown in Fig. 33; examples can be also found in the folder **Data\Input\FITTING\SDHR**.

Purpose, functions, and operating modes of buttons **Load**, **Save Table**, **Erase**, **Compute**, **Stop**, **Plot 2D BRDF**, **Plot 3D BRDF**, **Plot DHR vs. IA**, and **Plot DHR vs. WL** are no different from the corresponding

buttons in BRDF Model Builder described in Section 8. Fig. 55 shows the **FITTING Database** window after SDHR splitting.

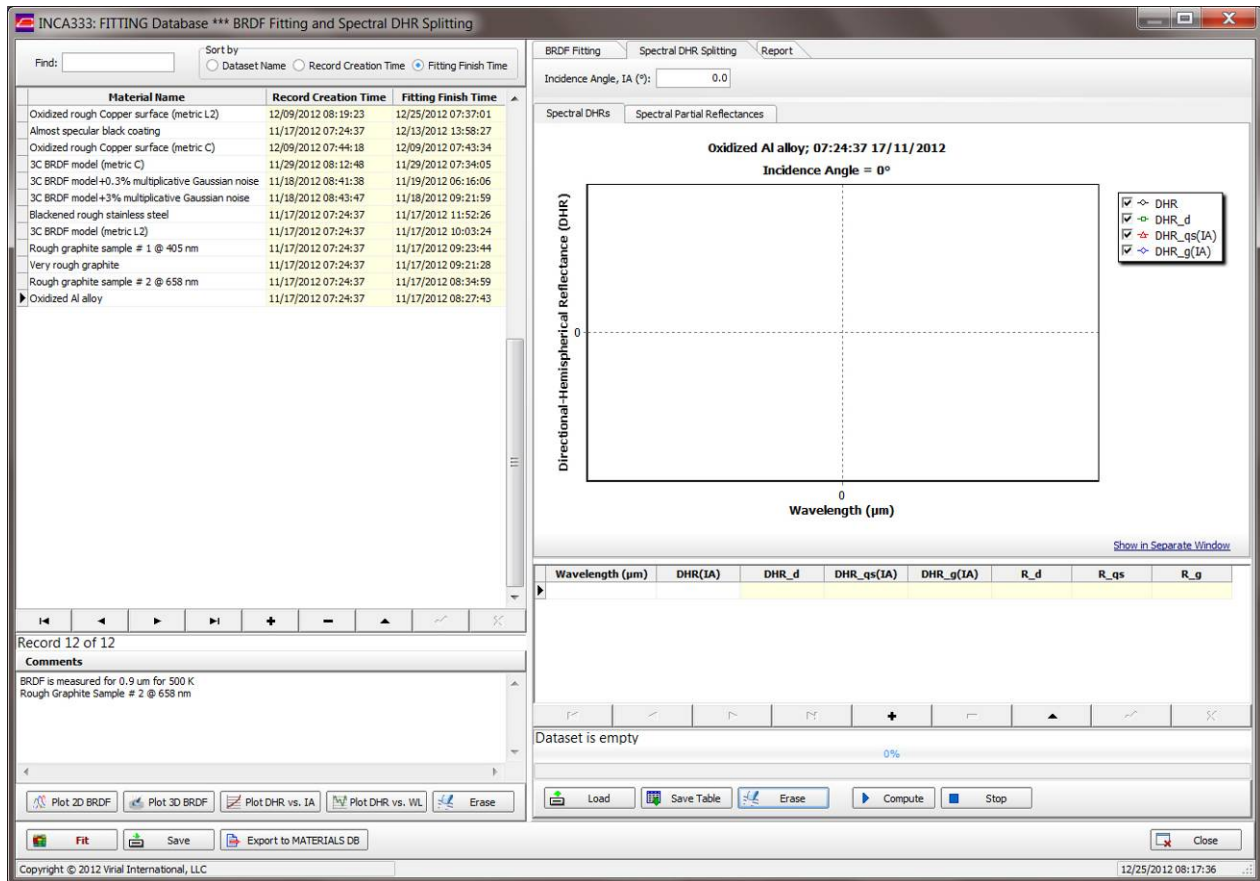


Fig. 54. The **FITTING** database window: the “Spectral DHR Splitting” tabbed page before splitting.

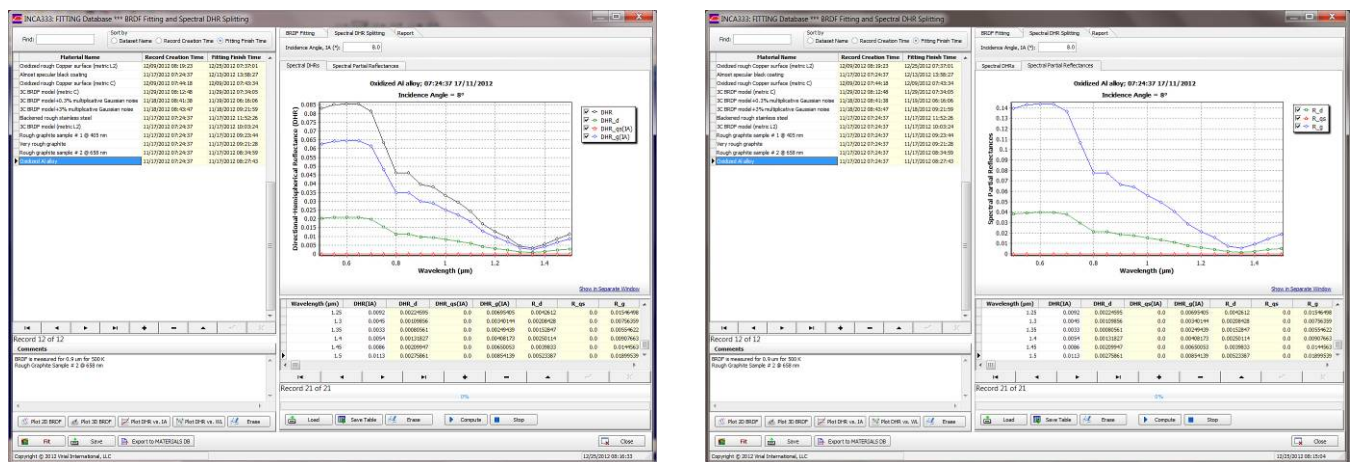


Fig. 55. The **FITTING** database window: the “Spectral DHR Splitting” tabbed page after splitting: left – tabbed page “Spectral DHRs”; right – tabbed page “Spectral Partial Reflectances”.

9.3. BRDF Fitting and SDHR Splitting Report

When the BRDF fitting ends, all initial data, settings, and results are saved in the **FITTING** database as a large text field called “Report”. Additional data are appended to its end when the SDHR ends. “Report” is a read-only field (see Fig. 56) however one can make it editable if uncheck the checkbox **Read Only**.

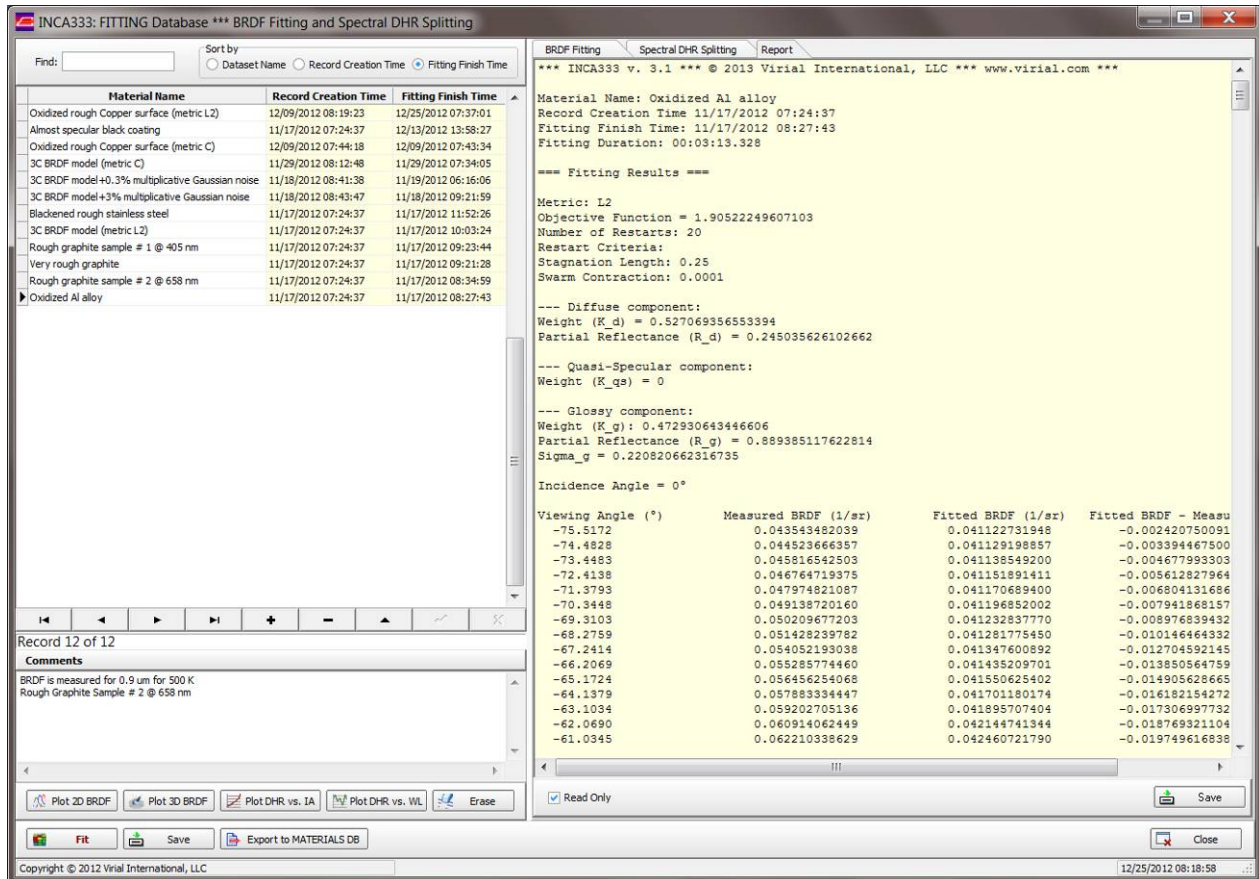


Fig. 56. The tabbed page “Report” of the **FITTING** database window.

The Report can be saved in text file by clicking the Save button. Examples of such text files can be found in the **Data\Output\Fitting Reports** folder.

10. The MATERIALS Database

To open the MATERIALS database window, click **MATERIALS** button placed in the group “Databases”, in the left panel of the main INCA333 window (Fig. 27). The window shown in Fig. 57 will appear.

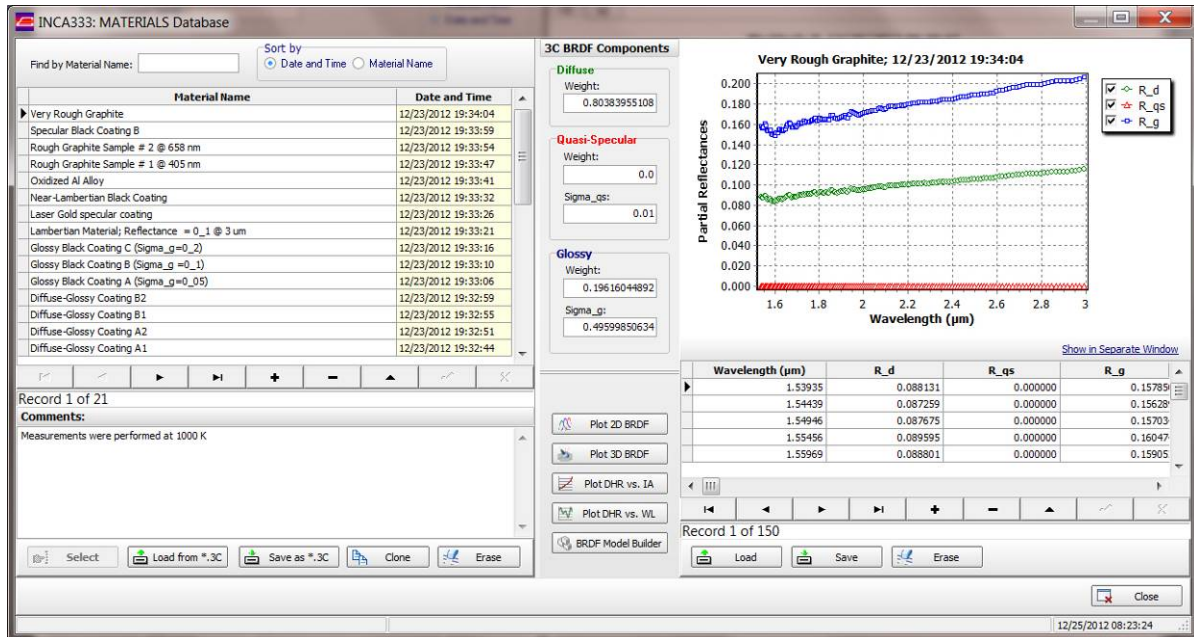


Fig. 57. The **MATERIALS** database window.

The **MATERIALS** database can be opened also at the assigning of materials to the cavity surfaces (see Section 11.2). In this instance, the button Select in the lower left panel will be enabled.

There are five ways to add new material to the **MATERIALS** database:

- 1) Exporting 3C model from the **FITTING** database (see Section 9).
- 2) Exporting 3C model from **BRDF Model Builder** (see Section 8).
- 3) Loading 3C model from binary *.3C file using **Load from *.3C** button.
- 4) Creating a copy of already existing record by clicking the **Clone** button and modifying some parameters; cloning is especially convenient for parametric studies of BB radiation characteristics.
- 5) Entering all data manually.

The binary files of *.3C format can be created by the **BRDF Model Builder** and using **Save as *.3C** button of the **MATERIALS** database itself. Files of this format are convenient for data exchange between INCA333 programs working on different PCs. Manual data entering is less convenient and can be recommended only for simplest 3C models, e.g., consisted of one component only.

In order to make some partial changes in the Material record, one can create a copy of the existing Material by clicking **Clone** button. The new material name will be requested:

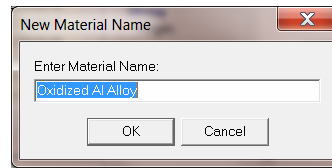


Fig. 58. Request of new material name.

One can keep the name of original record for its copy; records will differ in dates of their creation.



Be careful when change data in the **MATERIALS** database manually: all the 3C BRDF model parameters and SPRs must be self-consistent, i.e. must not produce SDHRs greater than 1.

The SPRs contained in the right table can be saved in and load from text file using **Save** and **Load** buttons, respectively. Examples of such files can be found in **Data\Input\MATERIALS\SPR** folder.

Purpose, functions, and operating modes of buttons **Erase**, **Plot 2D BRDF**, **Plot 3D BRDF**, **Plot DHR vs. IA**, and **Plot DHR vs. WL** are no different from the corresponding buttons in BRDF Model Builder described in Section 8.

11. The DATASETS Database

11.1. Creating New Dataset

The **DATASETS** database stores all initial data for BB cavity modeling except data for cavity wall materials which is stored in **MATERIALS** database. The DATASETS database is associated with the main INCA333 window (see Fig. 59) which consists of the left part with the table of datasets (and optional comments) and the tabbed pages at right. We recommend to enter initial data in the same order in which the tabbed pages are ordered.

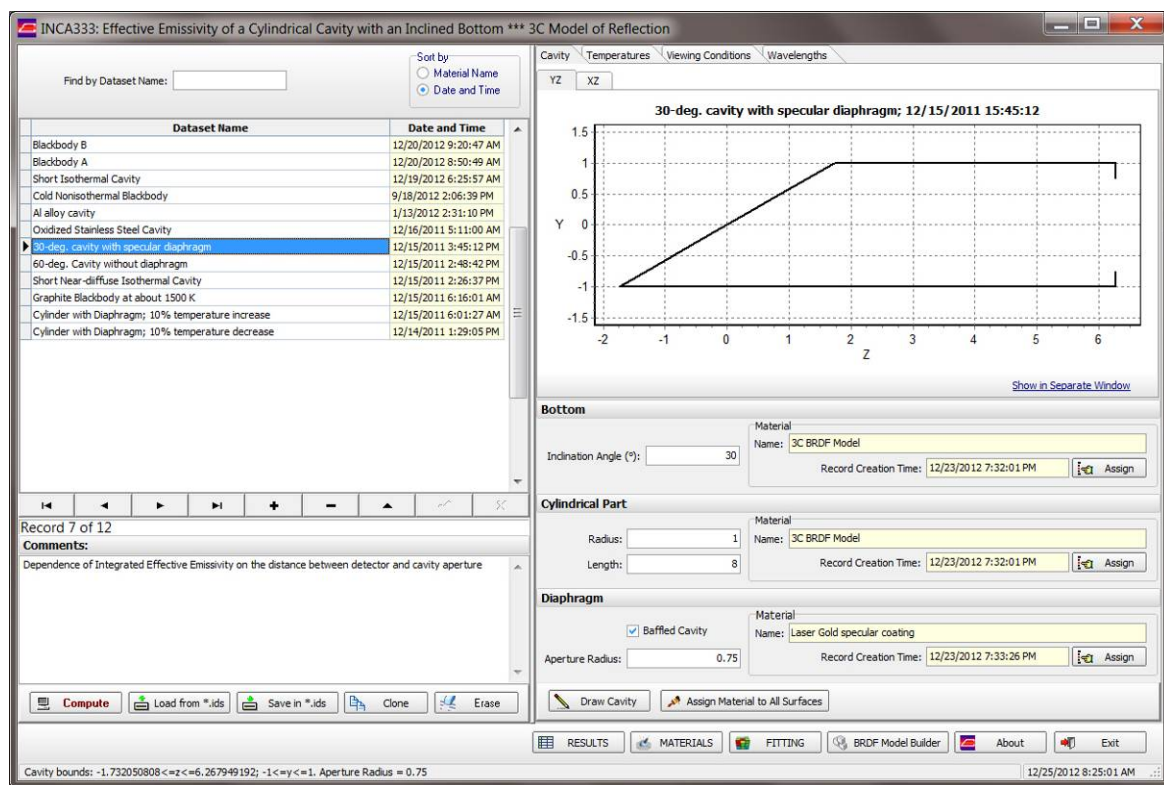


Fig. 59. The DATASETS database window; the tabbed page "Cavity" is active.

To create new record (dataset), click **Insert Record (+)** button of the database navigator below the left table. Enter the dataset name (up to 100 arbitrary symbols) then click **Post Edit**. Optional comments can be entered at any stage of dataset creation or editing.

User can make a copy of existing dataset by clicking **Clone**. This possibility is convenient when only a part of initial data should be modified.

Entire dataset can be saved as binary *.ds file by clicking **Save as *.ds** and loaded from *.ds file by clicking **Load from *.ds**. This possibility is provided for dataset exchanging between SPEEP323 copies working on different PCs.

11.2. Defining Cavity

To define cavity geometry, enter the bottom inclination angle in degrees; radius and length of cylindrical part, and aperture radius, if cavity has a diaphragm (see Fig. 60). If the cavity has no diaphragm, uncheck **Baffled Cavity** checkbox; in this case, the aperture radius is equal to the radius of the cylindrical part. When entering of cavity geometry is completed, click **Draw Cavity** button to draw scaled sections of the cavity in YZ and XZ planes (Fig. 61).

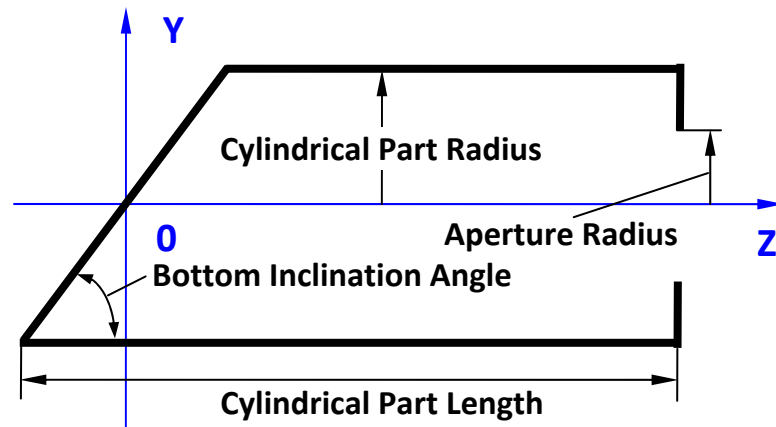


Fig. 60. Cavity geometry.

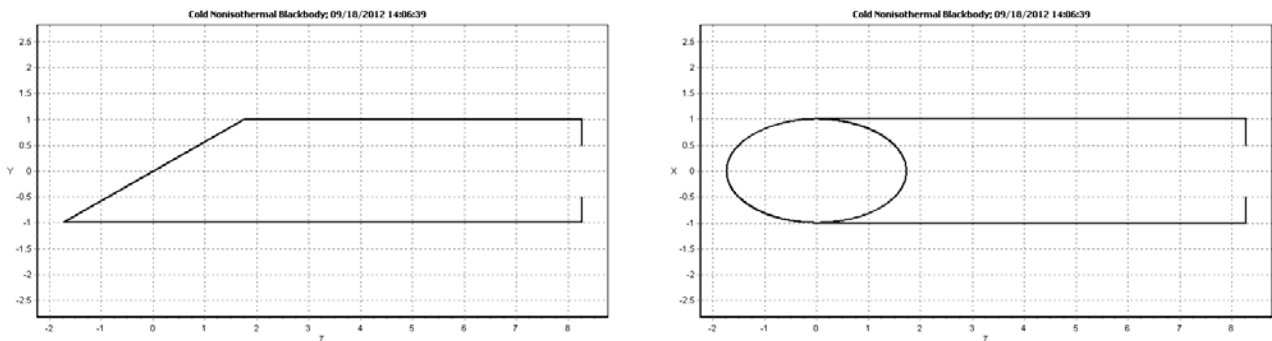


Fig. 61. Scaled drawing of a cavity in YZ and XZ planes

To assign material to one surface, click **Assign** button for the bottom, cylindrical part, and diaphragm (if any). The **MATERIALS** database window will be opened. Double-click the material selected, or select material, then click **Select** button. The material chosen together with the date and time of this material's record creation will be entered into the appropriate fields. One can assign material to all surfaces by clicking **Assign Material to All Surfaces** button.

11.3. Entering Temperature Distribution

INCA333 allows computing EE of isothermal and nonisothermal cavities. Open the tabbed page "Temperatures" (Fig. 62) and choose **Isothermal** or **Nonisothermal** in the group "Cavity Surface" of radio-buttons. If **Nonisothermal** is chosen, the reference **Tref (K)** and background **Tbg (K)** temperatures have to be entered. For the **Isothermal** case (Fig. 63), temperatures should not be entered; T_{bg} is supposed to be 0 K, and RT will not be computed.

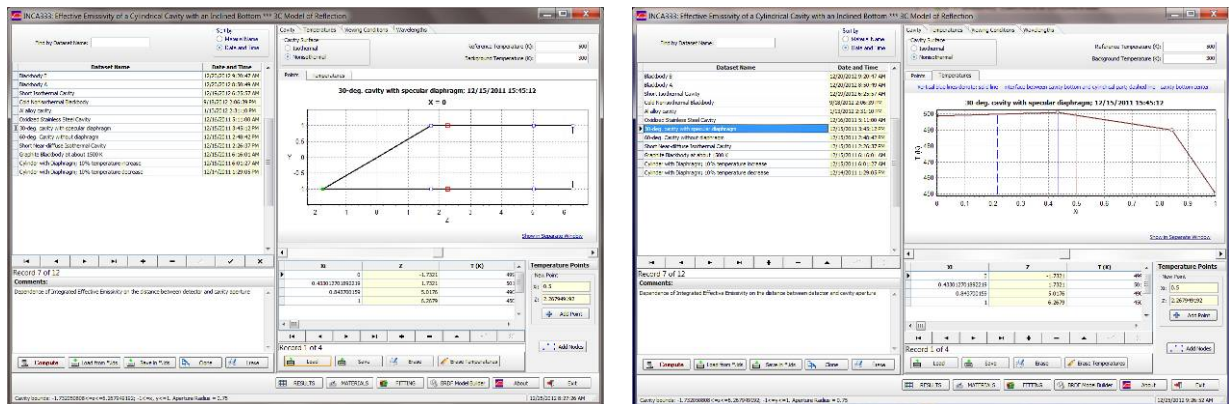


Fig. 62. The tabbed page "Temperatures":
the left screenshot shows positions of temperature points on the cavity generatrix;
the right screenshot shows the temperature distributions plot.

The next step consists of the input of points on the cavity generatrix in which temperatures will be defined. INCA333 allows specifying the one-dimensional temperature distribution, i.e. cavity temperature that varies along Z axis. Temperature of a diaphragm is supposed to be equal to the temperature of the adjacent points of the cylindrical part. In order to provide self-consistent representation of temperature distributions for cavities of various geometrical parameters, the uniform coordinate ξ (X_i) is introduced. It coincides with the Z axis but passes from the deepest point of the cavity, where $\xi = 0$, to the cylindrical part edge, where $\xi = 1$. It is possible to enter X_i in the first column of the table; the coordinate Z will be calculated automatically for the geometrical parameters of the current cavity record and entered in the appropriate non-editable column of the table.

In parity of the manual entering, INCA333 offers several ways to enter points where temperature should be specified.

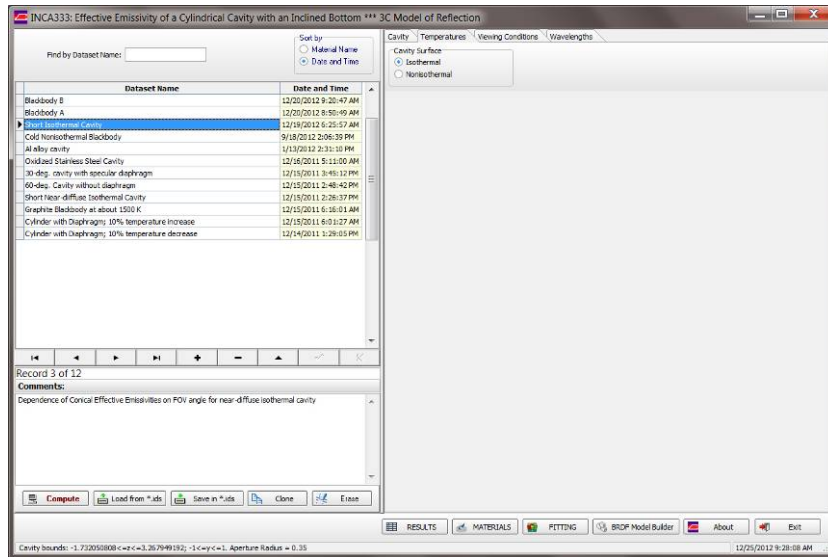


Fig. 63. The tabbed page “Temperatures” for an isothermal cavity.

To enter new temperature point, move the slider show in Fig. 64. Its movement is synchronized with the movement of two red square markers in the cavity section drawing; values of X_i and Z are displayed in the appropriate fields to the left of the table. After choosing suitable place of temperature point, click **Add Point** button. New point will be entered into table and will appear as a small blue square on the drawing. The green filled marker denotes the current record in the table.

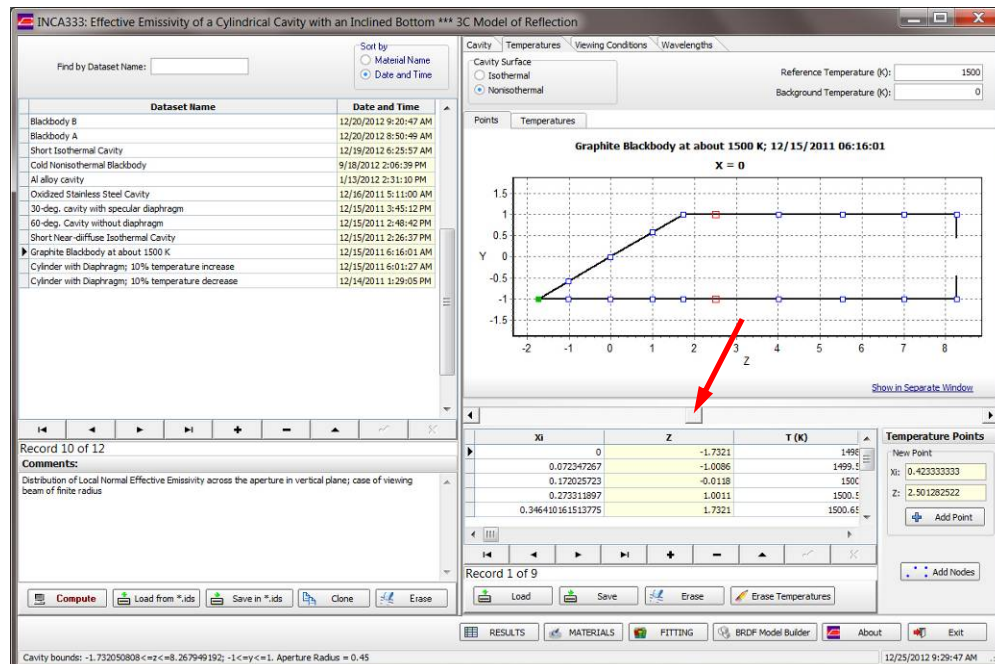


Fig. 64. Interactive input of a new temperature point. The red arrow points the slider.

Use **Add Nodes** button to employ all generatrix nodes as points where temperatures will be defined (see Fig. 65).

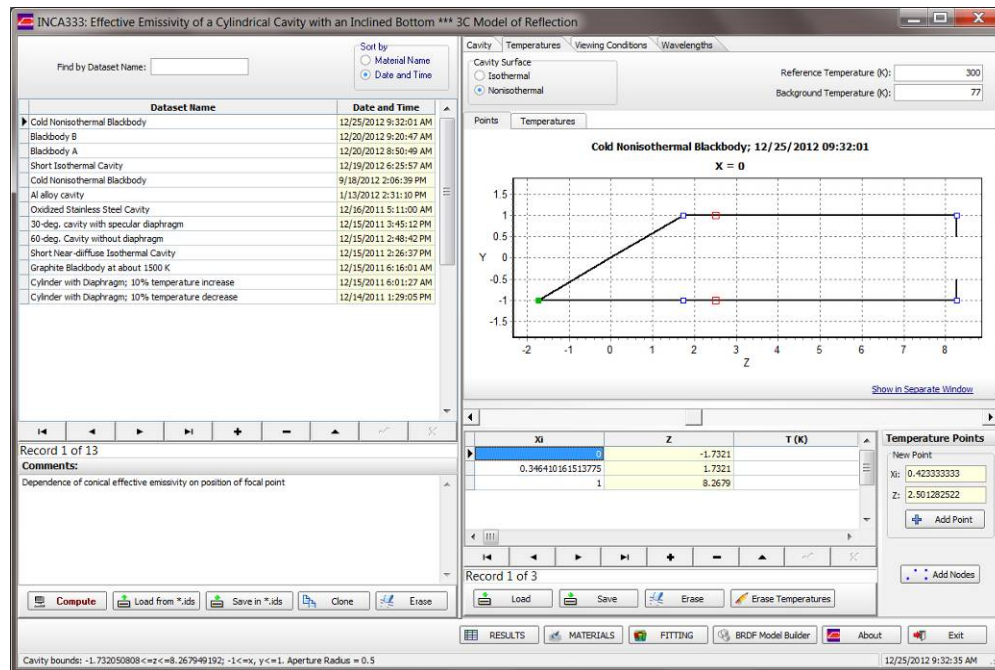


Fig. 65. Use of generatrix nodes as temperature points.

Load and **Save** buttons are intended for loading from and saving in text file the temperature distribution. Fig. 66 presents an example of the content of such a file. Starting from the second line, the first column represents Xi values, five other columns correspond to five temperature distributions. Other examples can be found in **Data\Input\DATASETS\TD** folder.

Xi	T (K)
0.0000000000000E+0000	1.4980000000000E+0003
7.2347267000000E-0002	1.4995000000000E+0003
1.7202572300000E-0001	1.5000000000000E+0003
2.7331189700000E-0001	1.5005000000000E+0003
3.46410161513775E-0001	1.5006500000000E+0003
5.7416267900000E-0001	1.4970000000000E+0003
7.2727272700000E-0001	1.4930000000000E+0003
8.7400319000000E-0001	1.4880000000000E+0003
1.0000000000000E+0000	1.4800000000000E+0003

Fig. 66. An example of text file which contains temperature distribution.

The **Erase** button allows deleting multiple temperature points. The **Erase Temperatures** calls the window analogous to that shown in Fig. 12 and allows erasing several or even all temperatures at once but keeps temperature points unchanged.

Note that the temperature distributions composed for one cavity can be applied to other cavities, but temperature points will be displaced.

11.4. Entering Viewing Conditions

INCA333 provides 3 types of different viewing conditions, but only one certain type can be used in one run of a modeling code. However, one can use up to 201 combinations of geometrical parameters that define the given type of viewing conditions.

Type of Viewing Conditions (Normal, Conical, and Integrated) can be chosen by clicking radio-buttons of the group in the upper left part of the tabbed page “Viewing Conditions” (see Fig. 67).

Simultaneously with the switching radio-buttons, the table at the bottom of tabbed page changes columns corresponding to geometrical parameters of selected Viewing Condition type. These parameters are shown in the pictures (see Fig. 2) displayed in the top right part of the tabbed page.

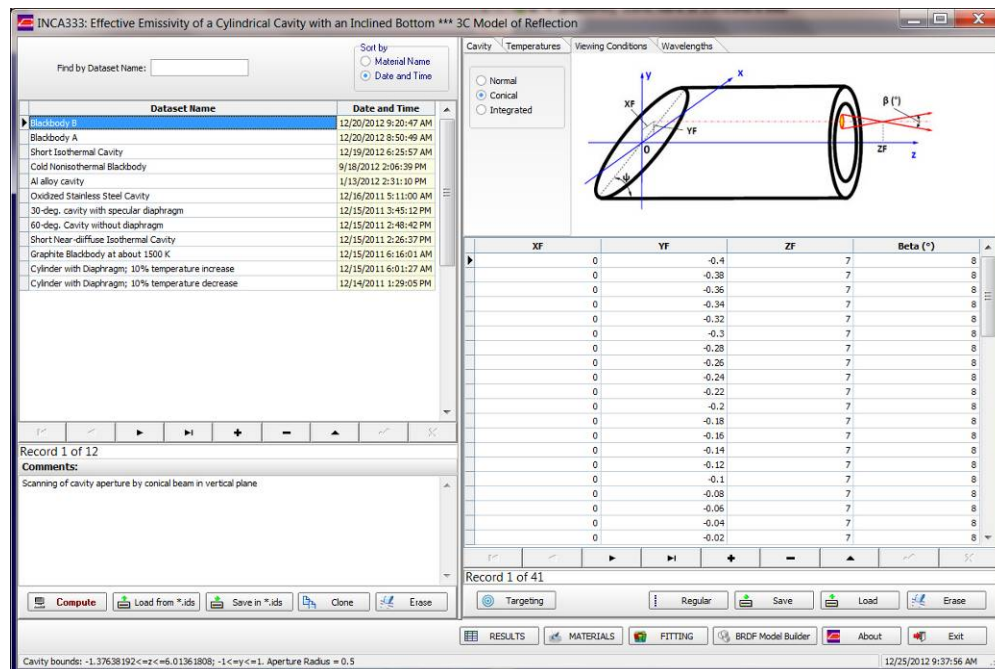


Fig. 67. The tabbed page “Viewing Conditions” of the DATASETS database window.

Viewing Conditions parameters can be loaded from text file using the **Load** button (and saved in text file using the **Save** button). Text file must contain the integer index of viewing conditions (0 is for Normal, 1 is for Conical, and 2 is for Integrated) in the first line, and viewing conditions parameters in next lines; columns must have the same order as in the table for these viewing conditions. A fragment of such a file is shown in Fig. 68. Other examples can be found in **Data\Input\DATASETS\VC** folder.

```

2 // 0 - Normal, 1 - Conical, 2 - Integrated
  XD      YD      HD      RD
0.0000    0.0000    0.0000    0.2500
0.0000    0.0000    0.1000    0.2500
0.0000    0.0000    0.2000    0.2500
-----
0.0000    0.0000    0.9000    0.2500
0.0000    0.0000    1.0000    0.2500
0.0000    0.0000    1.1000    0.2500
0.0000    0.0000    1.2000    0.2500
-----
0.0000    0.0000    10.0000    0.2500
0.0000    0.0000    12.0000    0.2500
-----
0.0000    0.0000    38.0000    0.2500
0.0000    0.0000    40.0000    0.2500
0.0000    0.0000    42.0000    0.2500
0.0000    0.0000    44.0000    0.2500
0.0000    0.0000    46.0000    0.2500
0.0000    0.0000    48.0000    0.2500
0.0000    0.0000    50.0000    0.2500

```

Fig. 68. A fragment of text file, which contains parameters of Integrated VC.

Regular viewing conditions correspond to a case when one of the geometrical parameters defining viewing conditions, changes incrementally, i.e., with constant step. After clicking the **Regular** button, the window like that shown in Fig. 69 will appear.

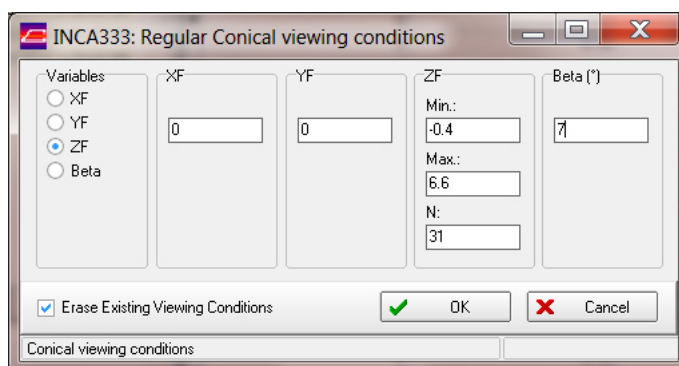


Fig. 69. Defining Regular Conical VC.

Using the switches **Variables** one can choose a parameter that will change incrementally, enter values of constant parameters, then enter minimal and maximal values for the variable parameter, as well as the number N of its values, then click **OK**. To add new viewing conditions parameters to those previously entered into the table, uncheck the checkbox **Erase Existing Viewing Conditions**. In such a way one can

change more than one parameter throughout the viewing condition parameters set. Manual entering is an alternative for regular viewing conditions and also allows changing more than one geometrical parameter in the table. However, it should be noted that the resulting graphs become in this case useless because they show dependence only upon one variable.

11.5. Targeting

Click **Targeting** in the tabbed page “Viewing Conditions” (Fig. 67) to open the window shown in Fig. 70 that allows to perform initial (until first reflection) ray tracing in order to check the correctness of defining the viewing conditions. The results of preliminary ray tracing are shown for two orthogonal planes YZ and XZ (it is supposed that the coordinate system XYZ has the right-handed orientation, i.e., in the left-hand screenshot in Fig. 70, the X axis is directed behind the plane of the graph).

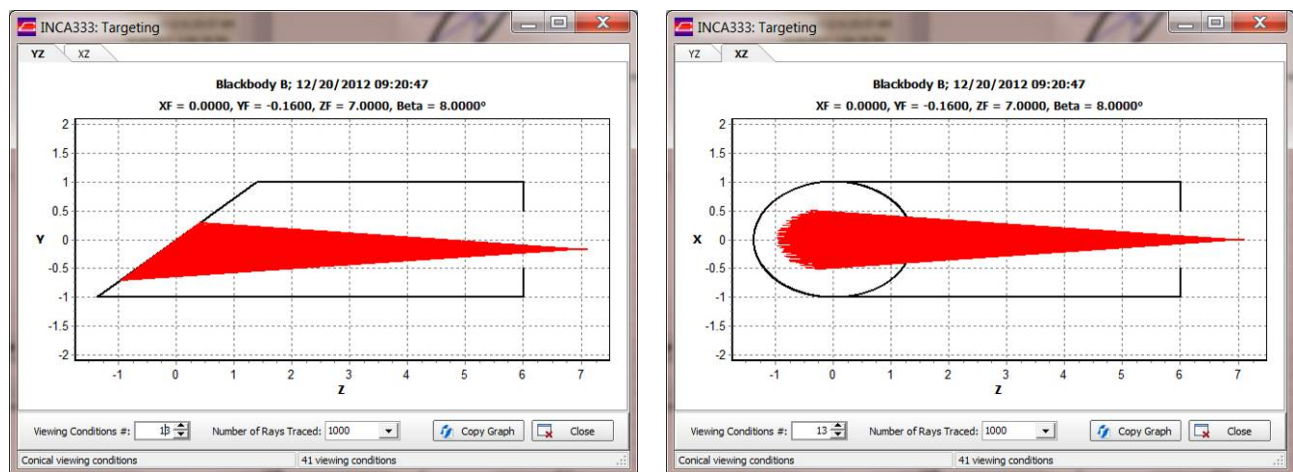


Fig. 70. Targeting (initial ray tracing).

As soon as **Targeting** window is open, ray tracing for the first set of viewing condition parameters is performed and displayed. By default, the number of rays traced is 1000. One can change this value on 100, 10,000, or 100,000. Ray tracing and drawing will start automatically. After changing the viewing conditions number (i.e., number of a set for viewing conditions parameters) in the **Viewing Conditions #** input field, ray tracing will be performed and redrawn automatically. If a traced ray is directed out of a cavity aperture, ray tracing will be stopped, and blinking text “OUT OF CAVITY APERTURE” will appear below the graph.

11.6. Entering Wavelengths and Performing Spectral Interpolation

Since spectral reflectance of different materials assigned to different surfaces forming a cavity may be defined over different sets of wavelengths, INCA333 uses interpolation and extrapolation of all spectral data for the joint wavelength set (i.e., wavelengths for which spectral effective emissivities and radiance temperatures will be computed). These wavelengths have to be entered in the table on the tabbed page “Wavelengths” (Fig. 71).

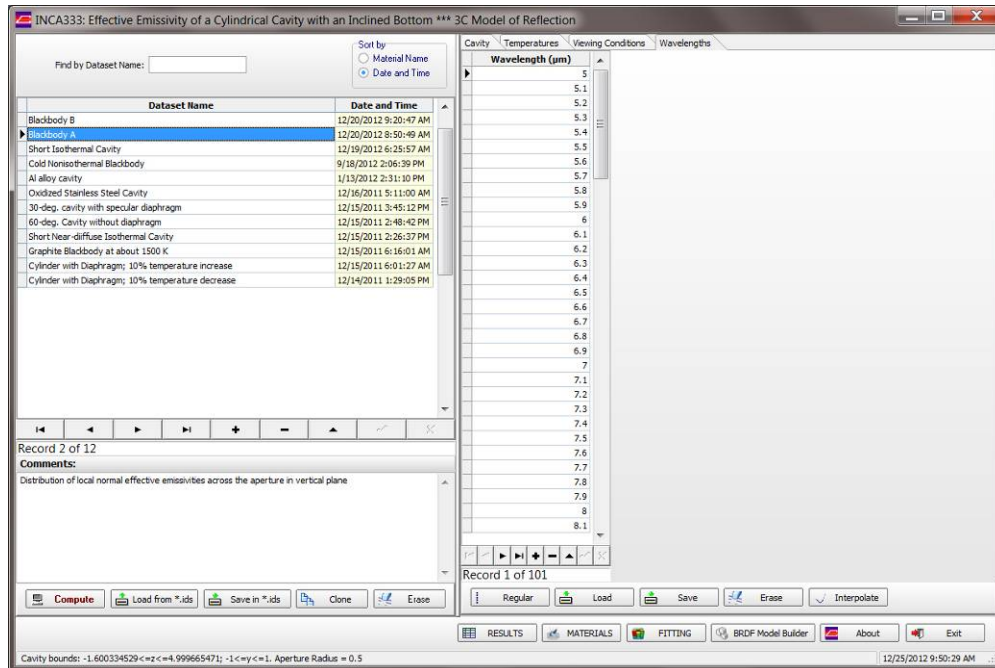
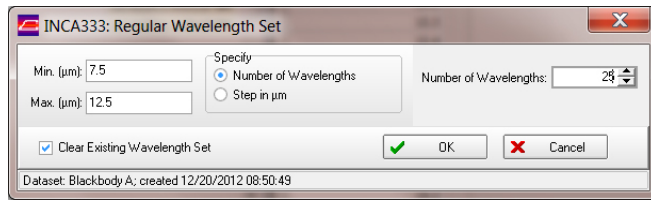


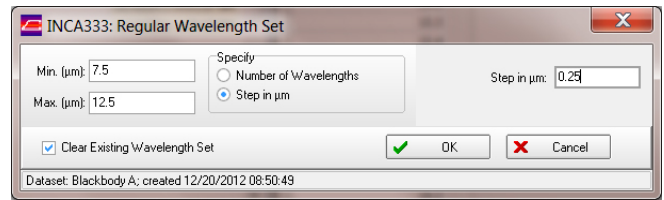
Fig. 71. The tabbed page “Wavelengths”.

Wavelength can be entered manually, value-by-value, or loaded from (and saved in) text file using **Load** (and **Save**) button. These files have simplest structure; several examples can be found in **Data\Input\DATASETS\WL** folder.

Click **Regular** button to define the set of wavelengths uniformly distributed from minimal to maximal value. In the window shown in Fig. 72, one can specify number of wavelengths or constant wavelength step. After clicking **OK**, the equidistant wavelength set will replace the existing one if the checkbox **Clear Existing Wavelength Set** is checked. Otherwise, it will be added to the existing wavelength set; duplicated wavelength will be rejected.



Number of wavelengths is specified



Wavelength step is specified

Fig. 72. Two cases of the regular wavelength set defining.

The **Interpolate** button can be used for visual evaluation of interpolation/extrapolation quality. INCA333 uses linear interpolation for calculation of spectral values between points extracted from the MATERIALS database and holds the constant values outside the spectral range of data extracted from the MATERIALS database. Fig. 73 illustrates interpolation and extrapolation rules used in INCA333.

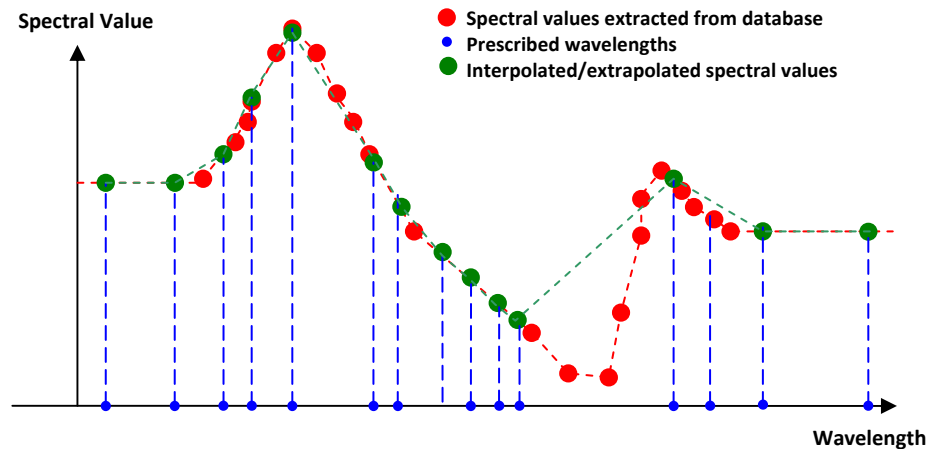


Fig. 73. Interpolation and extrapolation rules for spectral values used in INCA333.

After clicking **Interpolate**, both SPRs extracted from MATERIALS database and interpolated/extrapolated values of R_d , R_{qs} , and R_g will be plotted in the graph for each cavity surface (see Fig. 74). Surface number can be changed using the input field **Surface #**.

It is recommended to check the quality of spectral interpolation/extrapolation before Monte Carlo modeling to be ensured that spectral ranges of the joint wavelength set matches well those of data extracted from database and that interpolated spectral dependences adequately reproduce all features of dependences stored in the **MATERIALS** database.

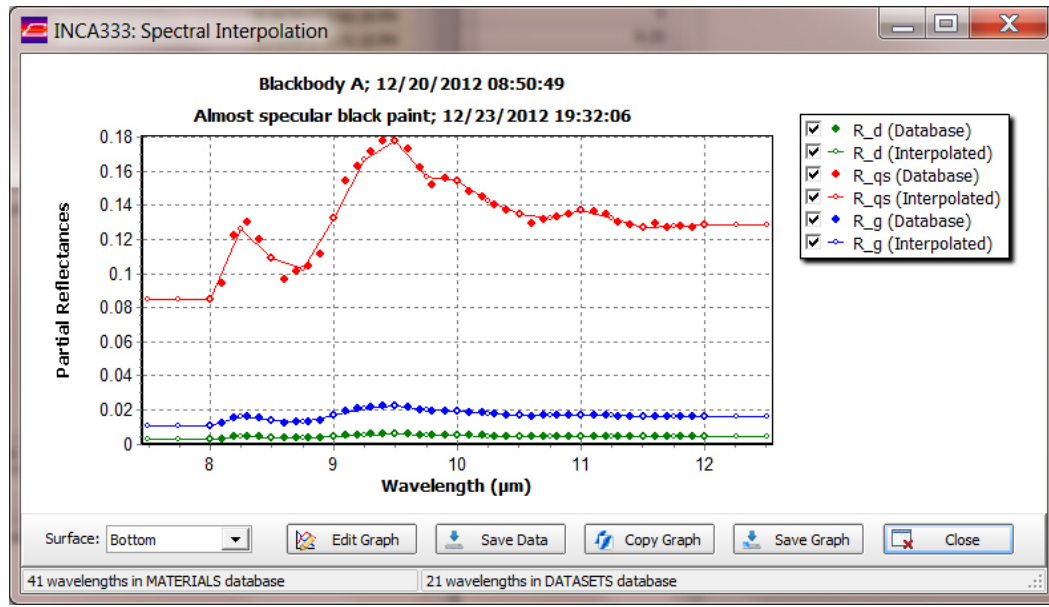


Fig. 74. The **Spectral Interpolation** window.

12. Monte Carlo Calculations

Now, when all the initial data are prepared, one can start MCRT calculations by clicking **Compute**. If the dataset from contains materials which are absent in the **MATERIALS** database, INCA333 before calculations will show the notification (Fig. 75) and cancel the Monte Carlo modeling. Another material instead of absent one should be assigned.

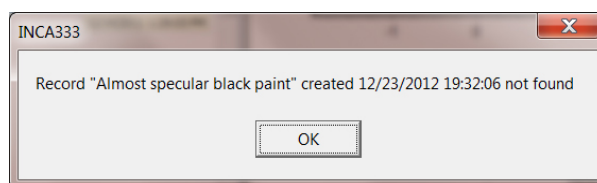


Fig. 75. Notification about absence of the material in the MATERIALS database.

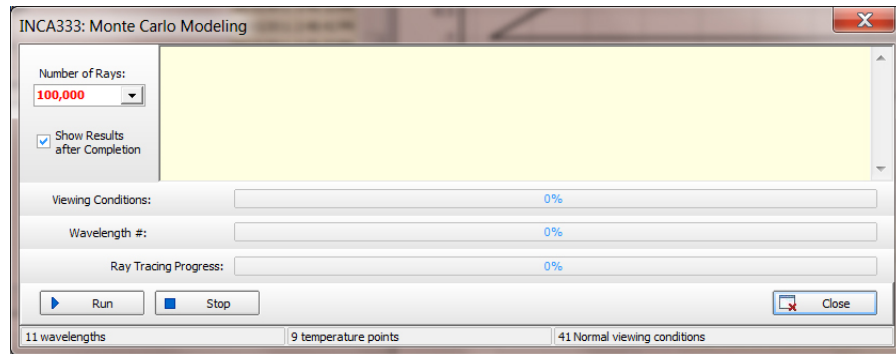
If checking test is passed, the window **Compute** will appear (Fig. 76, the upper screenshot). Enter the number N of rays that will be traced. This parameter defines the random component of uncertainty for EEs and RTs calculations. Due to stochastic character of the algorithm used in INCA333, the random uncertainty of calculations varies in inverse proportion of \sqrt{N} . The choice of N to a great extent depends on cavity blackness, i.e. deviation of effective emissivity from the unity. Probably, the best way is to evaluate the required values of N from numerical experiments. We recommend to begin with $N = 10,000$. This also allows to evaluate the total time needed for final modeling. Usually, for modeling a cavity with effective emissivity from 0.995 than 0.9999 for isothermal condition, $N = 100,000$ is enough for any realistic temperature distribution.

Click **Run** to start the Monte Carlo modeling. It can be interrupted by clicking **Stop** at any time.

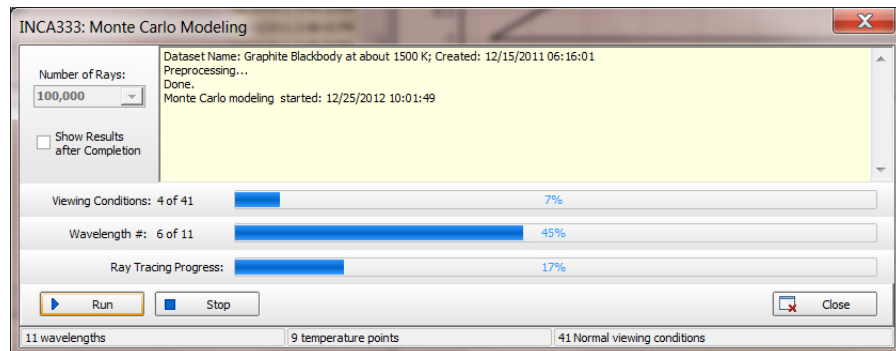
First, the initial data preprocessing will be performed, including spectral interpolation for the diffuse, quasi-specular, and glossy SPRs for each surface forming the cavity. Then INCA333 will perform Monte Carlo calculations successively, wavelength-by-wavelength and for each set of viewing conditions parameters (see the second screenshot in Fig. 76).

If the checkbox **Show Results after Completion** is checked, the window **Compute** will be closed automatically after successful modeling and the **RESULTS** database window will be opened. Otherwise, it is necessary to close the Compute window by clicking **Close** (see the third screenshot in Fig. 76) then **RESULTS** on the lower panel of the INCA333 main window in to browse results of calculations.

Before modeling



Modeling in progress



Modeling is completed

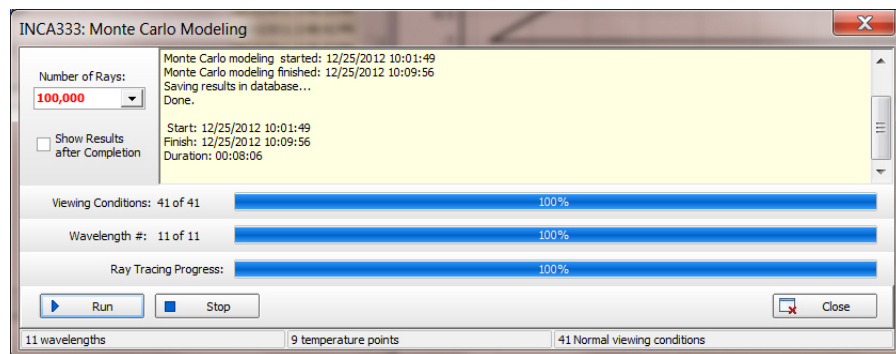


Fig. 76. Three stages of the MCRT calculations (the **Compute** window).

13. The RESULTS Database

13.1. Viewing Results

The screenshot of the **RESULTS** database window is shown in Fig. 77. All fields in both tables are read-only. After completing MCRT calculations, the text field “Comments” contains the copy of the similar field from the **DATASETS** database. This field is editable; user can add some information after analysis of results.

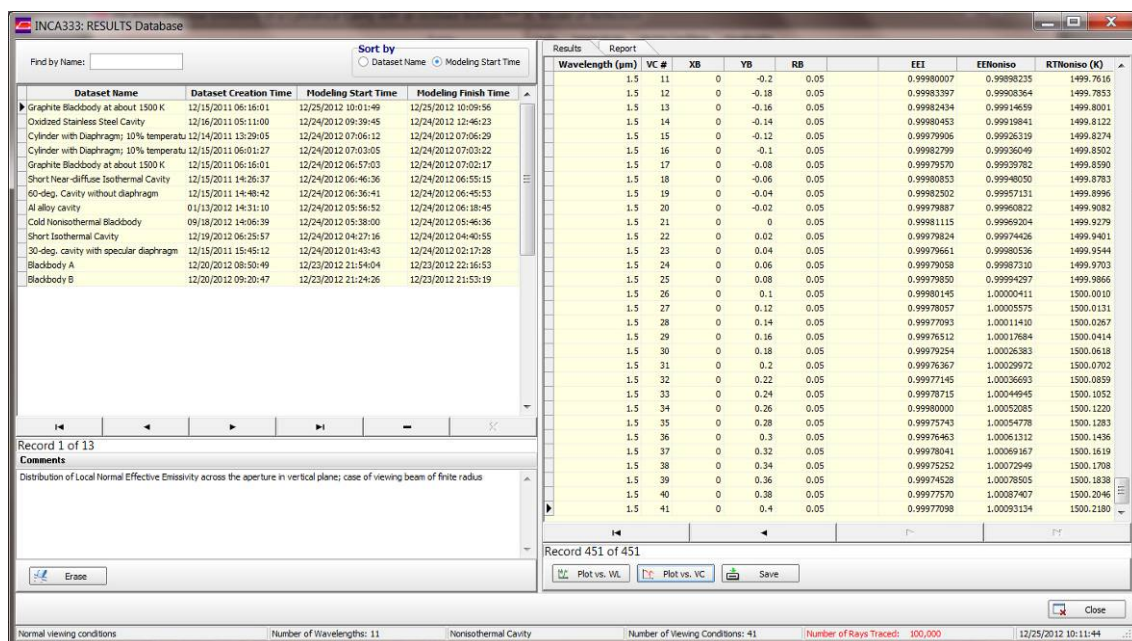


Fig. 77. The **RESULTS** database window.

Columns of the table on the tabbed page “Results” present: the wavelength (in μm); viewing conditions number (VC #); viewing conditions parameters in the next columns; effective emissivity for the isothermal case (EEIso), then – the EE and RT (in K) for the nonisothermal cavity. Clicking **Save** allows to save all results of calculations in the text file (for instance, to import them into MS Excel or some other software for further processing). Examples of such text files can be found in the folder **Data\OUTPUT\Results**.

13.2. Plotting Graphs

The buttons **Plot vs. WL** and **Plot vs. VC** open windows where EEs and RTs are plotted against wavelength (Fig. 78) and against variable parameter of viewing conditions (Fig. 79), respectively. In the first case, to plot these dependences for different viewing conditions number in the input field **Viewing Conditions #**. In the second case, select the variable parameter using drop-down list **Viewing Conditions Variable Parameter** (if it should be changed). To plot dependences of monochromatic EEs and RTs on the viewing condition parameter for different wavelengths, change wavelength number in the field **Wavelength #**.

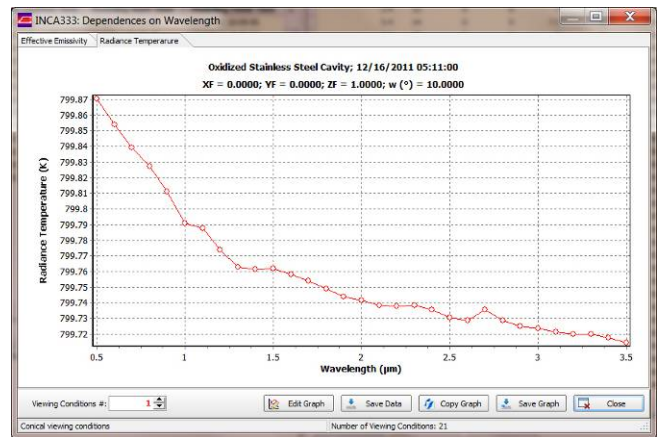
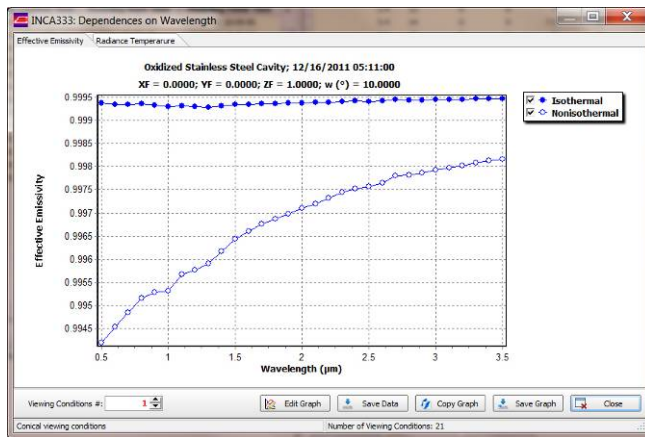


Fig. 78. Plots of spectral effective emissivities and radiance temperatures against wavelength.

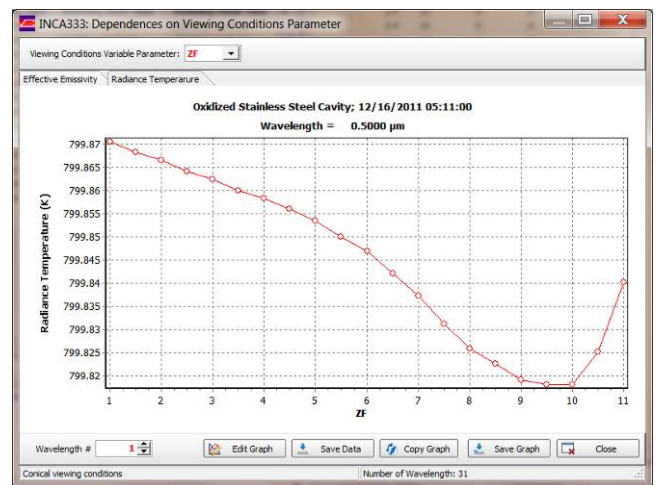
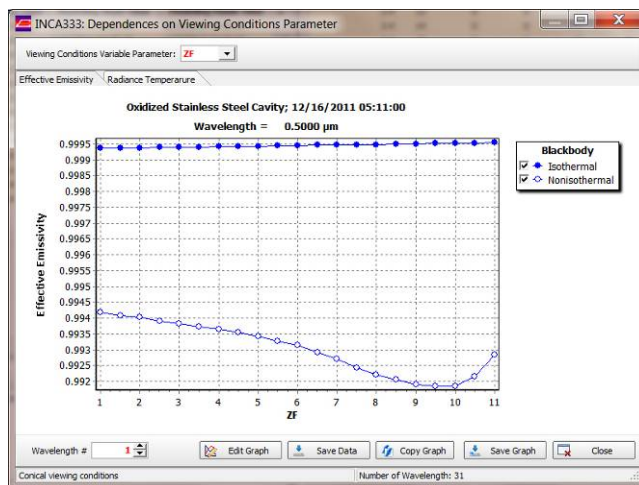


Fig. 79. Plots of monochromatic effective emissivity and radiance temperature against the variable parameter of viewing conditions.

13.3. MCRT Calculation Report

The tabbed page “Report” contains the report on MCRT calculations. It consists of initial data together with results of modeling (see Fig. 80). To edit the report, uncheck the **Read Only** checkbox.

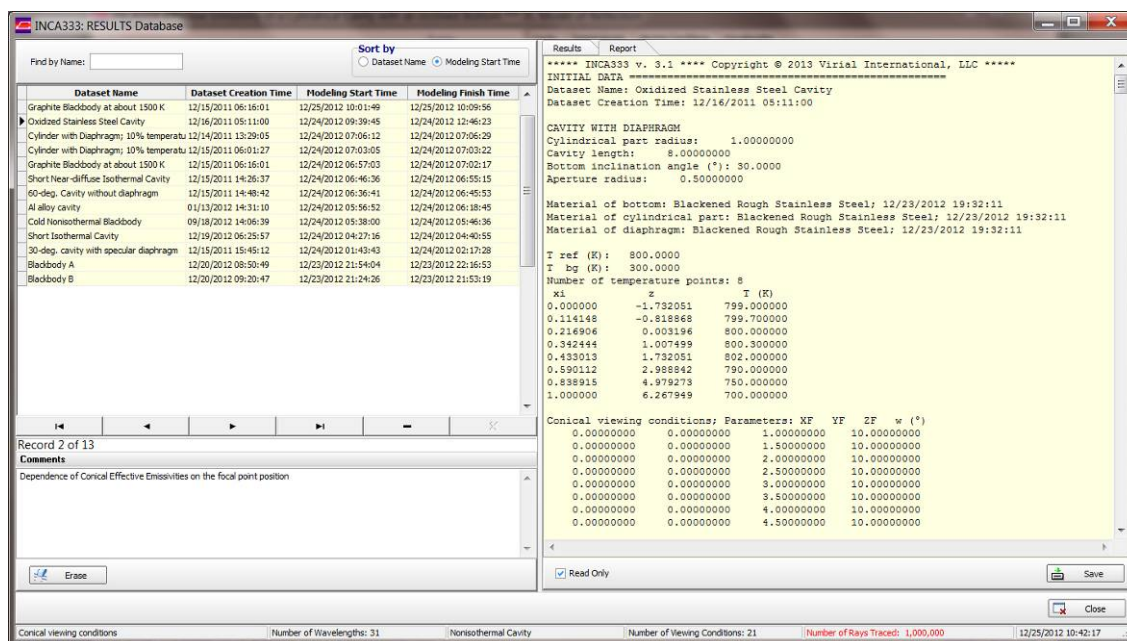


Fig. 80. MCRT calculations report.

Report can be saved as a separate text file by clicking **Save** button below the Report. Multiple examples of report files can be found in the **Data\Output\RESULTS\Reports** folder.

14. References

1. A. Prokhorov, "Effective emissivities of isothermal blackbody cavities calculated by the Monte Carlo method using the three-component BRDF Model," *Applied Optics* **51**, 2322-2332 (2012).
2. A. Prokhorov and N. I. Prokhorova, "Application of the three-component bidirectional reflectance distribution function model to Monte Carlo calculation of spectral effective emissivities of nonisothermal blackbody cavities," *Applied Optics* **51**, 8003-8012 (2012).
3. U. Mester and P. Winter, "New blackbody calibration source for low temperatures from -20 to +350°C," *Thermosense XXIII, Proceedings of SPIE* **4360**, 372-380 (2001).
4. I. Pušnik, E. van der Ham E, and J. Drnovšek, "Comparison of Blackbody Cavities for Calibration of Infra-Red Ear Thermometers," – in *TEMPMEKO 2004: Proc. 9th Int. Symp. on Temperature and Thermal Measurements in Industry and Science*, 823-826 (Dubrovnik, Croatia, 2004).
5. J. Gröbner, "Operation and investigation of a tilted bottom cavity for pyrogeometer characterizations," *Appl. Opt.* **47**, 4441-4447 (2008).
6. B Gutschwager *et al.*, "Calculable blackbody radiation as a source for the determination of the spectral responsivity of THz detectors," *Metrologia* **46**, S165-S169 (2009).
7. A. Steiger *et al.*, "Optical methods for power measurement of terahertz radiation," *Optics Express* **18**, 21804-21814 (2010).
8. I. Pušnik *et al.*, "Comparison of blackbodies for calibration of infrared ear thermometers," *Int. J. Thermophysics* **32**, (1-2), 127-138 (2011).
9. European Standard EN 12470-5:2003 Clinical Thermometers – Part 5: Performance of Infrared Ear Thermometers (with Maximum Device) CEN TC205, p. 29 (2003).
10. J. M. Houston and J. P. Rice, "NIST Reference Cryogenic Radiometer Designed for Versatile Performance," *Metrologia* **43**, S31-S35 (2006).
11. Y. J. Shen, D. H. Chen, and Z. M. Zhang, "Thermal Model of an Absolute Solar Radiometer Designed for Future Satellite Missions," *J. Solar Energy Engineering (Trans. ASME)* **123**, 50-52 (2001).
12. B. C. Johnson *et al.*, "Heat Transfer Analysis and Modeling of a Cryogenic Laser Radiometer," *J. Thermophys. Heat Transfer* **12**, 575-581 (1998).
13. J. E. Proctor and P. Y. Barnes, "NIST High Accuracy Reference Reflectometer-Spectrophotometer," *J. Res. Natl. Inst. Stand. Technol.* **101**, 619-627 (1996).
14. D. R. White, P. Saunders, S. J. Bonsey, J. van de Ven, and H. Edgar, "Reflectometer for measuring the bidirectional reflectance of rough surfaces," *Appl. Opt.* **37**, 3450-3454 (1998).
15. K. J. Voss, A. Chapin, M. Monti, and H. Zhang, "Instrument to measure the bidirectional reflectance distribution function of surfaces," *Appl. Opt.* **39**, 6197-6208 (2000).
16. K. J. Dana and J. Wang, "Device for convenient measurement of spatially varying bidirectional reflectance," *J. Opt. Soc. Am. A* **21**, 1-12 (2004).
17. C. Hahlweg and H. Rothe, "Design of a semi-hemispherical spectro-radiometer for fast acquisition of BRDF libraries in VIS and NIR," *Proc SPIE* **5546**, 37-48 (2004).
18. M. Barilli, A. Mazzoni, "An equipment for measuring 3D bi-directional scattering distribution function of black painted and differently machined surfaces," *Proc SPIE* **5962**, 59620L-1-12 (2005).

19. D. Hünerhoff, U. Grusemann and A. Höpe, "New robot-based gonireflectometer for measuring spectral diffuse reflection," *Metrologia* **43**, S11-S16 (2006).
20. H. Li, S.-C. Foo, K. E. Torrance, and S. H. Westin, "Automated three-axis gonireflectometer for computer graphics applications," *Opt. Eng.* **45**, 043605, 1-11 (2006).
21. E. Kawate, "Measurement method of optical scatter using a STAR GEM as a scatterometer," *Proc SPIE* **7065**, 706515-1-9 (2008).
22. J. Zeng and L. Hanssen, "An infrared laser-based reflectometer for low reflectance measurements of samples and cavity structures," *Proc. SPIE* **7065**, 70650F,1-12 (2008).
23. D. B. Kim, K. S. Park, K. Y. Kim, M. K. Seo, and K. H. Lee, "High-dynamic-range camera-based bidirectional reflectance distribution function measurement system for isotropic materials," *Opt. Eng.* **48**, 093601, 1-11 (2009).
24. H. W. Yoon, D. W. Allen, G. P. Eppeldauer, and B. K. Tsai, "The Extension of the NIST BRDF Scale from 1100 nm to 2500 nm," *Proc. SPIE* **7452**, 745204-1-12 (2009).
25. G. T. Georgiev, and J. J. Butler, "Progress in BRDF calibration measurements in the SWIR," *Proc SPIE* **7452**, 745205-1-9 (2009).
26. J. Zeng and L. Hanssen, "Development of an infrared optical scattering instrument from 1 μm to 5 μm ," *Proc SPIE* **7453**, 74530Q-1-10 (2009).
27. R. Baribeau, W. S. Neil and É. Côté, "Development of a robot-based gonireflectometer for spectral BRDF measurement," *J. Modern Optics* **56**, 1497–1503 (2009).
28. R. Baribeau and J. Zwinkels, "Comparison of NRC goniometric and integrating sphere methods for realizing an absolute diffuse reflectance scale," *Proc. SPIE* **8495**, 84950A1-84950A10 (2012).
29. A. Höpe, T. Atamas, D. Hünerhoff, S. Teichert, and K.-O. Hauer, "ARGon³: "3D appearance robot-based gonireflectometer" at PTB," *R. Sci. Instrum.* **83**, 045102, 1-8 (2012).
30. A. M. Rabal, A. Ferrero, J. Campos, J. L. Fontecha, A. Pons, A. M. Rubiño, and A. Corróns, "Automatic gonio-spectrophotometer for the absolute measurement of the spectral BRDF at in- and out-of-plane and retroreflection geometries," *Metrologia* **49**, 213-223 (2012).
31. H. J. Patrick, L. M. Hanssen, J. Zeng and T. A. Germer, "BRDF measurements of graphite used in high-temperature fixed point blackbody radiators: a multi-angle study at 405 nm and 658 nm," *Metrologia* **49**, S81-S92 (2012).
32. J. M. Palmer, "Measurement of Transmission, Absorption, Emission, and Reflection," *Handbook of Optics. Vol. II: Design, Fabrication, and Testing; Sources and Detectors; Radiometry and Photometry*, M. Bass, ed., 35.1-35.23, McGraw Hill (2010).
33. A. Springsteen, "Reflectance Spectroscopy: An Overview of Classification and Techniques," *Applied Spectroscopy: A Compact Reference for Practitioners*, J. Workman Jr., A. Springsteen, Eds., 194-224, Academic Press (1998).
34. A. Springsteen, "A Guide to Reflectance Spectroscopy," Labsphere, Inc., North Sutton, NH (1992).
35. K. F. Carr, "A Guide to Integrating Sphere Theory and Applications," Labsphere, Inc., North Sutton, NH (1997).
36. P. J. Mohr, B. N. Taylor, and D. B. Newell, "CODATA recommended values of the fundamental physical constants: 2010," <http://physics.nist.gov/cuu/Constants/Preprints/Isa2010.pdf>.
37. A. V. Prokhorov, L. M. Hanssen, and S. N. Mekhontsev, "Calculation of Radiation Characteristics of Blackbody Radiation Sources," *Radiometric Temperature Measurements*, Volume 42: I. Fundamentals (Experimental Methods in the Physical Sciences), Z. Zhang, B. Tsai, and G. Machin, eds., pp. 181-240 (Academic, 2009).

38. R.E. Bedford. "Calculation of Effective Emissivities of Cavity Sources of Thermal Radiation," *Theory and Practice of Radiation Thermometry*, D. P. DeWitt and G. D. Nutter, eds., pp. 653-772 (Wiley, 1988).
39. R. E. Bedford. "Effective Emissivities of Blackbody Cavities – A Review," *Temperature, Its Measurement and Control in Science and Industry*, Vol. 4, Part 1, H.H. Plumb, ed., pp. 425-434, (Instrument Society of America, Pittsburg, 1972).
40. R. E. Bedford and C. K. Ma, Emissivities of diffuse cavities: Isothermal and nonisothermal cones and cylinders, *J. Opt. Soc. America* **64**, pp. 339–349 (1974).
41. R. E. Bedford and C. K. Ma, Emissivities of diffuse cavities, II: Isothermal and nonisothermal cylindrocones, *J. Opt. Soc. America* **65**, pp. 565–572 (1975).
42. R. E. Bedford and C. K. Ma, Emissivities of diffuse cavities, III: Isothermal and nonisothermal double cones, *J. Opt. Soc. America* **66**, 724–730 (1976).
43. A. Ono, "Calculation of the Directional Emissivities of the Cavities by the Monte Carlo Method," *J. Opt. Soc. Am.* **70**, 547–554 (1980).
44. A. Ono, "Apparent Emissivities of Cylindrical Cavities with Partially Specular Conical Bottoms," *Temperature: Its Measurement and Control in Science and Industry*, J. F. Schooley, ed., Vol. 5, pp. 513-516 (AIP, 1982).
45. Z. Chu, J. Dai, and R. E. Bedford, "Monte Carlo Solution for the Directional Effective Emissivity of a Cylindro-Inner Cone," *Temperature: Its Measurement and Control in Science and Industry*, J. F. Schooley, ed., Vol. 6, pp. 907-912 (AIP, 1992).
46. A. V. Prokhorov, "Monte Carlo method in optical radiometry," *Metrologia* **35**, 465-471 (1998).
47. V. I. Sapritsky and A. V. Prokhorov, "Calculation of the Effective Emissivities of Specular-Diffuse Cavities by the Monte Carlo Method," *Metrologia* **29**, 9-14 (1992).
48. V. I. Sapritsky and A. V. Prokhorov, "Spectral Effective Emissivities of Nonisothermal Cavities Calculated by the Monte Carlo Method," *App. Opt.* **34**, 5645-5652 (1995).
49. M. J. Ballico, "Modeling of the Effective Emissivity of a Graphite Tube Black Body," *Metrologia* **32**, 259–265 (1995/ 1996).
50. J. Ishii, M. Kobayashi, and F. Sakuma, "Effective Emissivities of Black-Body Cavities with Grooved Cylinders," *Metrologia* **35**, 175-180 (1998).
51. A. V. Prokhorov and L. M. Hanssen, "Effective Emissivity of a Cylindrical Cavity with an Inclined Bottom: I. Isothermal Cavity," *Metrologia* **41**, 421-431 (2004).
52. A. V. Prokhorov and L. M. Hanssen, "Effective Emissivity of a Cylindrical Cavity with an Inclined Bottom: II. Non-isothermal Cavity," *Metrologia* **47**, 33-46 (2010).
53. J. Hollandt, J. Seidel, R. Klein, G. Ulm, A. Migdall, and M. Ware, "Primary Sources for Use in Radiometry," *Optical Radiometry*, A. C. Parr, R. U. Datla, and J. L. Gardner, eds. (Academic, 2005), pp. 213–290.
54. Z. J. Hartmann, J. Hollandt, B. Khlevnoy, S. Morozova, S. Ogarev, and F. Sakuma, "Blackbody and Other Calibration Sources," *Radiometric Temperature Measurements. I. Fundamentals*, Z. M. Zhang, B. K. Tsai, and G. Machin, eds., 241–295 (Academic, 2010).
55. F. E. Nicodemus *et al.* *Geometrical considerations and nomenclature for reflectance*, NBS Monograph 160 (US Dept. of Commerce, NBS, 1977).
56. E. M. Sparrow and S. L. Lin, "Radiation Heat Transfer at a Surface Having Both Specular and Diffuse Reflectance Components," *Int. J. Heat Mass Transfer* **8**, 769-779 (1965).
57. K. A. Snail *et al.*, "Optical Characterization of Black Appliqués," *Proc. SPIE* **2864**, 465-474 (1996).

58. M. J. Persky, "Review of black surfaces for space-borne infrared systems," *Rev. Sci. Instrum.* **70**, 2193-2217 (1999).
59. S. R. Meier, "Characterization of highly absorbing black appliquéés in the infrared," *Appl. Opt.* **40**, 2788-2795 (2001).
60. S. R. Meier, "Reflectance and Scattering Properties of Highly Absorbing Black Appliquéés over a Broadband Spectral Region," *Appl. Opt.* **40**, 6260-6264 (2001).
61. J. Zeng and L. Hanssen, "Development of an infrared optical scattering instrument from 1 μm to 5 μm ," *Proc. SPIE* **7453**, 7453Q1-7453Q10 (2009).
62. L. M. Hanssen and A. V. Prokhorov, "Stochastic modeling of non-Lambertian surfaces for Monte Carlo computations in optical radiometry," *Proc. SPIE* **7427**, 742707-1–742707-8 (2009).
63. J. Hartmann, "High-Temperature Measurement Techniques for the Application in Photometry, Radiometry and Thermometry," *Phys. Rep.* **469**, 205-269 (2009).
64. H. J. Patrick, L. M. Hanssen, J. Zeng, and T. A. Germer, "BRDF measurements of graphite used in high-temperature fixed point blackbody radiators: a multi-angle study at 405 nm and 658 nm," *Metrologia* **49**, S81-S92 (2012).
65. A. S. Glassner, *Principles of Digital Image Synthesis*. Volume II (Morgan Kaufmann, 1995).
66. P. Shirley, *Fundamentals of Computer Graphics* (A K Peters, 2002).
67. P. Dutré, P. Bekaert, and K. Bala, *Advanced Global Illumination* (A K Peters, 2003).
68. M. Pharr and C. Humphreys, *Physically Based Rendering: from Theory to Implementation* (Morgan Kaufmann, 2010).
69. M. Kurt, D. Edwards, "A survey of BRDF models for computer graphics," *Computer Graphics* **43**, Article No. 4 (2009).
70. K. Schwenk, "A Survey of Shading Models for Real-time Rendering," URL: http://www.karsten-schwenk.de/downloads/a_survey_of_shading_models.pdf (2011).
71. S. Liang, *Quantitative remote sensing of land surfaces* (Wiley, 2004).
72. D. L. B. Jupp, "A compendium of kernel & other (semi-)empirical BRDF Models" (CSIRO Office of Space Science Applications, 2000) - Earth Observation Centre), URL: http://www.eoc.csiro.au/tasks/brdf/k_summ.pdf
73. D. Geisler-Moroder and A. Dür, "A New Ward BRDF Model with Bounded Albedo," *Computer Graphics Forum* **29**, 1391-1398 (2010).
74. K. E. Torrance and E. M. Sparrow, "Theory for Off-Specular Reflection from Roughened Surfaces," *J. Opt. Soc. Am.* **57**, 1105-1114 (1967).
75. C. Schlick, "An Inexpensive BRDF Model for Physically-based Rendering," *Computer Graphics Forum* **13**, 233–246 (1994).
76. M. Clerc, *Particle Swarm Optimization* (ISTE, 2006).
77. M. Clerc and J. Kennedy, "The particle swarm – explosion, stability, and convergence in a multidimensional complex space," *IEEE Trans. Evolutionary Computation* **6**, 58–73 (2002).
78. R. P. Brent, "An algorithm with guaranteed convergence for finding a zero of a function," *Comp. J.* **14**, 422-25 (1971).
79. P. van Dooren and L. de Ridder, "An Adaptive Algorithm for Numerical Integration over an n-Dimensional Cube," *J. Comp. Appl. Math.* **2**, 207–217 (1976).
80. F. J. Kelly, "On Kirchhoffs Law and Its Generalized Application to Absorption and Emission by Cavities," *J. Res. Natl. Bur. Stand.* **69B**, 165–171 (1965).

81. A. S. Glassner, "An Overview of Ray Tracing," *An Introduction to Ray Tracing*, A. S. Glassner, ed., pp. 1–32 (Academic, 1993).
82. G. S. Fishman, *Monte Carlo Concepts, Algorithms, and Applications* (Springer, 1996).
83. E. M. Sparrow and R. D. Cess, *Radiation Heat Transfer* (Hemisphere, 1978).

15. Appendix. INCA333 Software License Agreement

License

1. Under this Software License Agreement (the "Agreement"), Virial International, LLC (the "Vendor") grants to the user (the "Licensee") a non-exclusive and non-transferable license (the "License") to use INCA333 (the "Software").
2. "Software" includes the executable computer programs, related electronic documentation and any other files that accompany the product.
3. Title, copyright, intellectual property rights and distribution rights of the Software remain exclusively with the Vendor. Intellectual property rights include the look and feel of the Software. This Agreement constitutes a license for use only and is not in any way a transfer of ownership rights to the Software.
4. The Software may be loaded onto no more than three computers. A single copy may be made for backup purposes only.
5. The rights and obligations of this Agreement are personal rights granted to the Licensee only. The Licensee may not transfer or assign any of the rights or obligations granted under this Agreement to any other person or legal entity. The Licensee may not make available the Software for use by one or more third parties.
6. The Software may not be modified, reverse-engineered, or de-compiled in any manner through current or future available technologies.
7. Failure to comply with any of the terms under the License section will be considered a material breach of this Agreement.

License Fee

8. The original purchase price paid by the Licensee will constitute the entire license fee and is the full consideration for this Agreement.

Limitation of Liability

9. The Software is provided by the Vendor and accepted by the Licensee "as is". Liability of the Vendor will be limited to a maximum of the original purchase price of the Software. The Vendor will not be liable for any general, special, incidental or consequential damages including, but not limited to, loss of production, loss of profits, loss of revenue, loss of data, or any other business or economic disadvantage suffered by the Licensee arising out of the use or failure to use the Software.

10. The Vendor makes no warranty expressed or implied regarding the fitness of the Software for a particular purpose or that the Software will be suitable or appropriate for the specific requirements of the Licensee.

11. The Vendor does not warrant that use of the Software will be uninterrupted or error-free. The Licensee accepts that software in general is prone to bugs and flaws within an acceptable level as determined in the industry.

Warrants and Representations

12. The Vendor warrants and represents that it is the copyright holder of the Software. The Vendor warrants and represents that granting the license to use this Software is not in violation of any other agreement, copyright or applicable statute.

Acceptance

13. All terms, conditions and obligations of this Agreement will be deemed to be accepted by the Licensee ("Acceptance") on installation of the Software.

Term

14. The term of this Agreement will begin on Acceptance and is perpetual.

Termination

15. This Agreement will be terminated and the License forfeited where the Licensee has failed to comply with any of the terms of this Agreement or is in breach of this Agreement. On termination of this Agreement for any reason, the Licensee will promptly destroy the Software or return the Software to the Vendor.

Force Majeure

16. The Vendor will be free of liability to the Licensee where the Vendor is prevented from executing its obligations under this Agreement in whole or in part due to Force Majeure, such as earthquake, typhoon, flood, fire, and war or any other unforeseen and uncontrollable event where the Vendor has taken any and all appropriate action to mitigate such an event.

Governing Law

17. The Parties to this Agreement submit to the jurisdiction of the courts of the State of Maryland for the enforcement of this Agreement or any arbitration award or decision arising from this Agreement. This Agreement will be enforced or construed according to the laws of the State of Maryland.

Miscellaneous

18. This Agreement can only be modified in writing signed by both the Vendor and the Licensee.

19. This Agreement does not create or imply any relationship in agency or partnership between the Vendor and the Licensee.

20. Headings are inserted for the convenience of the parties only and are not to be considered when interpreting this Agreement. Words in the singular mean and include the plural and vice versa. Words in the masculine gender include the feminine gender and vice versa. Words in the neuter gender include the masculine gender and the feminine gender and vice versa.

21. If any term, covenant, condition or provision of this Agreement is held by a court of competent jurisdiction to be invalid, void or unenforceable, it is the parties' intent that such provision be reduced in scope by the court only to the extent deemed necessary by that court to render the provision reasonable and enforceable and the remainder of the provisions of this Agreement will in no way be affected, impaired or invalidated as a result.

22. This Agreement contains the entire agreement between the parties. All understandings have been included in this Agreement. Representations which may have been made by any party to this Agreement may in some way be inconsistent with this final written Agreement. All such statements are declared to be of no value in this Agreement. Only the written terms of this Agreement will bind the parties.

23. This Agreement and the terms and conditions contained in this Agreement apply to and are binding upon the Vendor's successors and assigns.

Notices

24. All notices to the Vendor under this Agreement are to be provided at the following address:

Virial International, LLC
538 Palmspring Dr.,
Gaithersburg, MD 20878-2972
USA